THE USE OF CHEMILUMINESENCE FOR LIGHT-OFF DETECTION OF FLAMES

by

Andrew J. Hamer

Thesis submitted to the Graduate Faculty of Virginia Polytechnic Institute and State University in partial fulfillment of the requirements for the degree of

MASTER OF SCIENCE
in
Mechanical Engineering

APPROVED:

Richard J. Roby,
Chairman

Larry A. Roe

Clinton L. Dancey

September 1989
Blacksburg, Virginia

THE USE OF CHEMILUMINESENCE FOR LIGHT-OFF DETECTION OF FLAMES

by

Andrew J. Hamer
Committee Chairman: Richard J. Roby
Mechanical Engineering

(ABSTRACT)

A fast response method for detection of light-off in gaseous flames and liquid spray flames has been developed. The method used chemiluminescent signals from the $^2\Sigma$ - $^2\Pi$ OH system centered at 309 nm and the $^2\Delta$ - $^2\Pi$ CH system centered at 430 nm to indicate the presence of a flame. Spectral scans (perfomed on gaseous methane, liquid hexane and liquid Jet-A aircraft fuel) from 280 nm to 610 nm indicated that these two species produced the strongest signals available for flame detection. As their light is emitted in the ultraviolet spectrum, using the OH and CH radicals will potentially provide a good signal-to-noise ratio since, in combustion chambers, most of the broadband background emissions are in the infared and visible wavelengths. These scans also showed that the hexane and Jet-A gave OH and CH signals of approximately equal intensity. The transient histories of OH and CH were investigated by performing light-off ignition tests and intermittent light-off ignition tests. These various flame conditions showed that both signals were good indicators of flame presence, showing on average, a response time of better than 3 milliseconds. It was found that when the Hydrogen to Carbon ratio of the fuel was decreased, the CH signal strength increased as a percentage of OH signal intensity. Finally, the ouput signal intensity was found to be sensitive to both the flame image magnification and to the part of the flame observed.

ACKNOWLEDGMENTS

When I first met , my thesis advisor, I didn't know the difference between a photomultiplier tube and a test tube. He taught me the difference, along with a few million other things along the way, and for that, I am very thankful.

I would never have finished this thesis without the help of . We started working on this project together as undergraduates, but now he is on his way to earning the title "Doctor", I wish him well.

I would like to thank and for all their help, advice, opinions, time, donuts, and most of all, their companionship. You guys certainly made my graduate school studies enjoyable.

and are both experts in their fields, and they made my job here a whole lot easier because of it. I would also like to thank and his men, especially , who always had time for my "two" minute jobs that took twenty.

I would like to thank my parents for always giving me the emotional and financial support to pursue any avenue of my choice. (You truly are the greatest parents, ever.) Finally, I would like to thank , my wife to be, for her love, support, and the sunshine she provided on cloudy days.

TABLE OF CONTENTS

LIST OF FIGURES

LIST OF TABLES

NOMENCLATURE

Si	Lens to Image Distance
So	Lens to Object Distance
f	Focal Length of Lens
M	Flame Image Magnification
Σ	Ground Electronic State
Π	First Electronic State
σ_n	Standard Deviation
TAD	Adiabatic Flame Temperature
PHI	Equivalence Ratio

1. INTRODUCTION

1.1 Background and Motivation

As combustion devices become more complex they are expected to operate at higher performance levels, i.e. greater fuel efficiency, greater power/thrust output, lower pollution emissions, etc. In order to monitor these, and other, performance parameters, an increased need for real time combustion diagnostic systems has developed. This thesis investigates the development of one such diagnostic system; a light-off flame detector probe for gas and liquid spray flames based upon chemiluminescent signals of combustion. The successful development and production of such a probe could benefit gas turbine engines, both aircraft and stationary, as well as other internal combustion engines.

The problems associated with afterburner operation in high performance military aircraft are well documented [1-13]. By far, the majority of problems occur during afterburner ignition or shutdown. Pressure waves created by these transient operations may traverse upstream from the afterburner toward the compressor system, leading to compressor stall, or in a bypass engine, fan stall.

To prevent this, ignition or extinction must be sensed quickly so the variable area exit nozzle may be adjusted to the appropriate area suitable for the new volume of the gas stream. Ideally, the exit nozzle would open at the exact moment of afterburner ignition, however, this is not possible as there is an inherent delay in the hydromechanical actuators that control the nozzle geometry [1].

Often, the exit nozzle is opened before ignition is attempted, however, this has two disadvantages: 1) an immediate loss in thrust and 2) an increase in flow velocity in the flame holder region, which may make flame ignition impossible [2]. Vleghert [2] also states

> Preferably the afterburner [AB] should light up on a small amount of fuel, then - once alight - it can be opened smartly to [the] Maximum. Nowadays a delay - and sometimes a ramp function is built in which under normal conditions prevents maximum afterburner fuel flow at light-up. If ignition is delayed, however, a hard light results. Control would be greatly eased with an AB flame detector, which inhibits fuel flow increase until light-up has occurred. So far, however, reliability of such an installation has been a problem.

Today's larger bypass afterburning engines have an additional problem of attempting to ignite cold gases of an unmixed flow [3,4]. According to Bauerfeind [3]

> While the earlier low bypass ratio engines normally employed a gas stream mixer arrangement, the modern high bypass ratio engines [above 0.6] have no such arrangement mainly in order to save structural weight and length. This means that a large portion of the fuel has to be burnt in the cold stream at comparatively low pressure levels. This entails potential problems when lighting the fuel on afterburner selection and when lighting across the individual zones during an "acceleration" of the afterburner towards maximum boost.

Another condition contributing to poor afterburner performance is operation at high altitude. According to Stetson [5], the combustion stability margin of an afterburner significantly decreases at lower atmospheric pressures and temperatures, i.e. high altitude. Also, the fuel scheduling accuracy of the afterburner decreases with altitude. Stetson concludes that these problems can cause large fluctuations in the augmentor combustion temperatures, which when not adjusted for by the nozzle exit area, increase the probability of augmentor induced fan or compressor stall. In order to prevent these problems, an active control system is commonly used to dampen the effects of unstable afterburner operation.

A digital, multivariable control system for the F100 turbofan developed by Skirak, De Hoff and Hall [6], is one of the more successful at suppressing disturbances

caused by an afterburner ignition. While monitoring an afterburner ignition, they found the fuel flow rate increased rapidly, the tail pipe pressure rose sharply, while the fan and core speeds fell off. With their control system, the fan speed error caused the exhaust nozzle area trim integrator to open the nozzle until the fan discharge pressure was back on schedule. Their control system was successful in suppressing afterburner ignition disturbances in six of the eight flight conditions tested. In the two failures (45,000 feet and 50,000 feet, Mach 0.9), the sensed fan pressure did not change enough for the nozzle trim control to suppress the disturbance.

It is apparent from these problems that a faster, more accurate light-off detector probe for feed-back control during afterburner operation is desirable. With such a device, flame ignition and blowout, as well as unstable operation, could be monitored and could provide the information needed for corrective action to be taken. This thesis details work done to develop such a probe.

1.2 Present Combustion Chamber Monitoring Probes

The development of a probe enabling one to monitor the inside of an operating combustor chamber in real time has received a lot of interest [14-21]. Morey, Quentin and Angello [18] recently tested a probe on a G.E. 7001 stationary gas turbine that used a water-cooled fiber-optic image guide to transfer an image from inside one of the ten combustion chambers to remotely located video and film cameras.

Such observations as ignition delays, flame bistabilities and flame detachments from the nozzle were made during field testing of the probe. The flame front was observed to extend into the combustor exit as well. These successful results led the investigators to conclude that such a system could become an important diagnostic tool for maintaining peak performance of gas turbines.

Presently, stationary gas turbines commonly use Geiger-Meuller Phototubes for flame detection. Each tube contains an easily ionized gas which produces a current when ultraviolet radiation from the flame in the combustion chamber enters the tube. The current is used to charge a capacitor to its operating voltage before discharging. The frequency of this charging and discharging cycle is monitored and analyzed. A frequency over 120 Hz is considered the signal of a stable flame. The tube is responsive to radiation in the 180 nm to 260 nm spectral range. Response time, including signal processing, is on the order of 100 milliseconds.

According to Cohen, Gat and Witte [19], reliable sensing of ignition in a diesel engine has long been sought by diesel engine designers to more precisely control fuel injection. They designed an ignition sensing probe containing both an ionization sensor (Langmuir gage) and luminosity sensor to be installed in place of a glow plug for diesel engines. After testing the probe on both an Oldsmobile and Volkswagen diesel engines at various RPM and loading conditions, they concluded

> The noticeable and repeatable delay of the ionization signal which is encountered at higher engine speeds, is accompanied by a variable rate of rise. [However,] the luminosity sensor has an easily characterized and repeatable signal making it a better ignition marker. The luminosity sensor "sees" all radiant emission from the combustion event occurring anywhere in the prechamber and so accurately indicates the start-of-ignition [19].

Such preliminary work led to the successful development of two combustion monitoring probes which will help automobile engines produce more power with greater efficiency. Texas Instruments Incorporated and Hitachi Limited have developed, and are looking to market, two such probes [20]. The Texas Instruments (TI) probe is a pressure sensor which, when mounted into an automobile combustor chamber through the cylinder head, will provide automakers the opportunity to optimize combustion efficiency in each chamber.

The TI probe measures the force transferred from a diaphragm to a piezoelectric transducer which creates a signal proportional to the pressure. With the aid of an onboard computer, peak pressure can be monitored. This information will allow timing adjustments to be made in order to compensate for variations in humidity, octane content, or manufacturing tolerances and wear.

The Hitachi Ltd. probe uses a fiber-optic cable which fits through the center of a standard spark plug. The probe, with its viewing angle of 160 degrees, transmits visible light from the combustion chamber to an engine control unit. If the light detected is shifted toward the red end of the visible spectrum, a low spark energy and low combustion rate are indicated. Conversely, blue light corresponds to a high spark energy and high combustion rate. This information allows fuel or air quantities delivered to each cylinder to be optimized for peak engine performance. The Hitachi probe, which is immune to electromagnetic interference, may increase horsepower 10 percent while reducing noise by 10 decibels.

Since the environment in a combustion chamber is very harsh, the use of a non-intrusive method for flame monitoring is a must. All of these successfully tested probes fulfill that requirement. However, while these probes examine a range of visible and/or ultraviolet light to detect their signal, (except for the TI probe which examines pressure), the probe designed for this thesis only examines a narrow band of wavelengths which are a characteristic of a preselected chemiluminescent species.

1.3 Chemiluminescence

Chemiluminescence is the light given off by excited molecules as they drop down from their combustion induced excited state to their preferred equilibrium ground state. Many studies have documented use of chemiluminescence as a measure of important combustion species such as OH, CH, CO_2 and C_2 [22-33]. By far, one of the best sources for background information on chemiluminescence is Gaydon's The Spectroscopy of Flames [22], where this information was obtained.

Spectra that are emitted from flames are one of three basic types. The first, called line spectra, are emitted by free atoms. Each line corresponds to an electronic transition, i.e., an electron dropping from its excited state to its ground state. For energy to be conserved a quantum of light is released, and thus a chemiluminescent signal is produced.

In the second type of spectra, called banded spectra, the electronic transition of a molecule creates a system. For each different electronic transition, a different system is created. Each system consists of a number of lines that are created by the simultaneous change in the internal vibrational and rotational energy of the molecules. These internal energy changes create the lines that form the band of a system. Bands usually have a wavelength of particularly high intensity, called a "head", which is easily measured.

The third type of spectra, called continuous spectra, have many causes; mainly, emission or absorption by solid particles or liquid droplets, gas-phase processes such as dissociation of molecules, ionization of atoms, or recombination processes.

In flames, band spectra are usually more prominent than line or continuous spectra. The strongest band systems are created by the free radicals CH, OH, C_2 and NH.

The bands of these radicals are usually in the visible or ultraviolet wavelengths because the amount of energy required for a resonance transition from the ground electronic state to the lowest of the excited states is relatively high.

Gaydon suggests that the transient response of a combustion system can be studied by setting a monochromator on a selected spectrum line or band and storing a photomultiplier's output with respect to time with an oscilloscope [22]. This experimental technique has been used to study a wide range of fuels while using a wide range of burners. One such early study was done by Schott [32] in 1960 when he studied OH concentration maxima in a detonating oxygen-hydrogen system. Lyon and Kydd [33] studied C_2, CH and OH absorption as a function of time in acetylene detonations in 1961.

More recently Beyler [23] used chemiluminescent emission measurements of OH, CH and CO_2 to examine the flame structure and mechanism of flame stabilization in a premixed swirl-stabilized combustor. His measurements found that combustion is confined to a spatially well-defined region within the combustor.

Beyler suggests three criteria to allow the use of chemiluminescent emissions as signatures of a combustion reaction zone. First, these measured emissions must result from chemiluminescent reactions involving intermediate species in the combustion process. Secondly, the relaxation of the excited species must be quick enough to allow the location of emissions to be interpreted as the location of excitation. Thirdly, the thermal emissions from these signals at combustion temperatures must be negligible compared to chemiluminescent emissions. Beyler shows these criteria have been met by several investigators [24-31].

1.4 Scope of Thesis

The problems associated with the operation of an afterburner make it apparent that the development of a very fast response light-off detector is desired. Such a probe, as described in this thesis, would detect afterburner ignition, blowout and unstable operation by examining a wavelength specific to a particular chemiluminescent signal.

For example, the formation of the radicals OH and CH is critical to the initial reactions of combustion. Since these reactions occur on the time scale of several hundred microseconds to several milliseconds, monitoring the chemiluminescent emission from one, or both, of these species should provide a very fast flame sensing signal. The recent advent of high quality optical fibers with good transmission properties in the UV makes the use of chemiluminescence as a combustion diagnostic practical.

There are six (6) necessary steps to develop a practical flame sensing probe. The first three (3) steps were performed for this thesis and are discussed below. Possible experimental setups for steps four (4) and five (5), and the future experiments of step six (6), are discussed in Chapter 5.

1) Identify possible species to be used for flame sensing by performing full spectral scans. Narrow the candidate list by performing averaging tests to find the species (and corresponding wavelengths) with the highest signal intensity. Experimental setup consists of a photomultiplier tube and monochromator.

2) Test species' transient signal for light-off ignition test and intermittent light-off ignition test conditions using gaseous and liquid fuels.

3) Investigate effects of flame image magnification and flame position upon species signal intensity.

4) Reduce probe weight, volume and system complexity by replacing the monochromator with a narrow band interference filter and the photomultiplier tube with a photodiode. This step will make the probe more durable and less expensive.

5) Implement fiber optic cable to transport light to remote detector.

6) Perform future experiments to optimize probes effectiveness and practicality.

The successful development of a fiber-optic based probe capable of measuring flame species coupled with real time signal processing has the potential to provide confirmation of flame ignition on a time scale of milliseconds.

2. Experimental Apparatus and Procedure

2.1 Introduction

The basic experimental set-up for this thesis consisted of a burner, an ignition source, an optical system to detect light, and a data acquisition/manipulation system. Two types of burners were investigated, a Bunsen burner to study gaseous fuels, and an air atomizing nozzle for burning liquid fuels.

In order to develop a probe based upon a chemiluminescent signal of combustion, the first step was to determine what signals were available in a steady flame, and what chemical radicals corresponded to those signals. The quantity, proportion, and wavelength corresponding to each species was needed in order to determine which one would provide the fastest, strongest, and most reliable signal for light-off. Initial tests, burning methane, were performed with a monochromator for wavelength selection and a photomultiplier tube for light detection. Full spectra scans were run from 280 nm to 610 nm to identify the possible signatures of flame presence.

Once identified by the full spectral scan, these newly- identified candidates were then tested to examine their transient history during light-off ignition and intermittent light-off ignition test conditions. Once response times were determined, magnification and flame position tests were performed to maximize the output signal.

In order to more realistically model an afterburner, liquid fuels were also investigated to see if the same species were present, and if so, in what concentrations and proportions. Using air as the atomizing gas, full spectral scans were repeated. Then, to create the fuel rich atmosphere of an afterburner, N_2 was used as the atomizing gas for each liquid fuel. The light-off ignition and intermittent light-off ignition tests were

repeated to again examine the species' response times. Magnification and position tests were repeated to confirm the methane results.

2.2. Detection System

In the photomultiplier tube detector, seen in Figure 1, the flame image was projected through a fused silica lens onto the entrance slit of a monochromator. The monochromator optically focused radiant energy at a specified wavelength onto a fast response photomultiplier tube (PMT). The PMT produced a current proportional to the amount of light present. The current was read as a voltage across a load resister by an oscilloscope. This system allowed for investigation of a wide range of discrete wavelengths during the initial research.

The monochromator used was a 0.5 m Fisher Scientific scanning monochromator (Jarrel-Ash Model 82-020) with a 1180 lines/mm grating. A motor and appropriate gearing allowed the monochromator to be used in a scanning mode with a variable scanning speed from 0.2 to 50 nm/min. The resolution of the monochromator was better than 0.1 nm. The adjustable entrance and exit slits of the monochromator were set at their maximums of 10 mm wide and 15 mm high in order to allow the greatest amount of light into, and therefore, out of, the monochromator. Also, because the reflecting mirror focused the selected wavelength to leave the monochromator through the center of the exit slit, by having the slit at its maximum width, a greater band of wavelengths (around the selected wavelength) was allowed to leave the the monochromator as well.

The photomultiplier tube (RCA Model 1P28B) was a nine stage, side-window, reflection mode type. The PMT's approximate spectral range was 200 nm to 660 nm with a rise time of 1.8 nanoseconds. To operate the PMT a high voltage power supply (RCA Model PF 1042) was needed. The PF 1042 required 13.5 volts DC and a variable

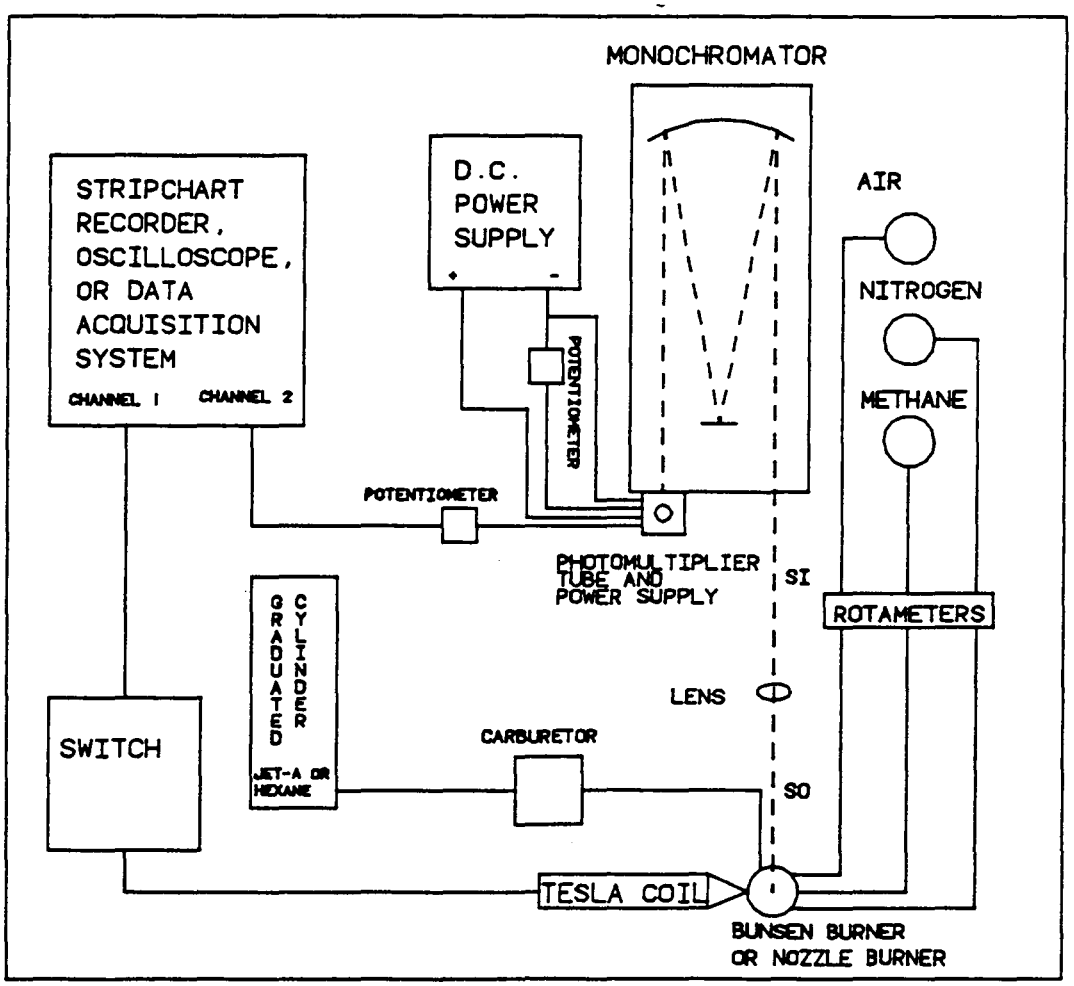

Figure 1. Schematic diagram of the experimental setup.

resister to control its output voltage. By setting the resister at 340 Ω, the PF 1042's voltage into the PMT was -1000 volts.

2.3 Burner and Ignition System Setup

Gaseous fuel was burned in a standard half inch methane Bunsen burner. A laminar premixed methane/air flame was investigated. Flow rates were controlled using Matheson rotameters in the 602 to 604 tube sizes. These rotameters were calibrated with an American Meter Company model 802 gas flow meter [34].

Two liquid fuels were investigated, hexane and Jet-A aircraft fuel. The spray flame nozzle used to burn liquid fuels was a Siphon Type SNA air atomizer (Delavan P/N Nozzle 30609-2 and adaptor P/N 17147). This nozzle provided a vertical solid cone of finely atomized liquid fuel spray. A graduated cylinder was used as a reservoir to enable fuel consumption rates to be calculated. The graduated cylinder fed an automobile carburetor which held the active lift height, and therefore fuel supply pressure, of the nozzle constant. Compressed gas (air and N_2) at 6 psig was used as the atomizing/entraining gas. Figure 2 shows a photograph of a typical air atomized hexane flame. Figure 3 shows a photograph of a typical air atomized Jet-A flame.

The ignition system consisted of a tesla coil and a switch. The tesla coil was used as a high voltage spark ignition source. Because nichrome is not effected by the high temperature of a flame, a nichrome wire was used to transfer the high voltage from the end of the tesla coil to the fuel. The end of the wire was positioned three centimeters above the top of the burner, just on the edge of the unignited gas stream of the fuel.

As the switch was turned on, power was supplied to the tesla coil. The telsa coil supplied a high voltage to the fuel, which then ignited. The arc could be seen jumping

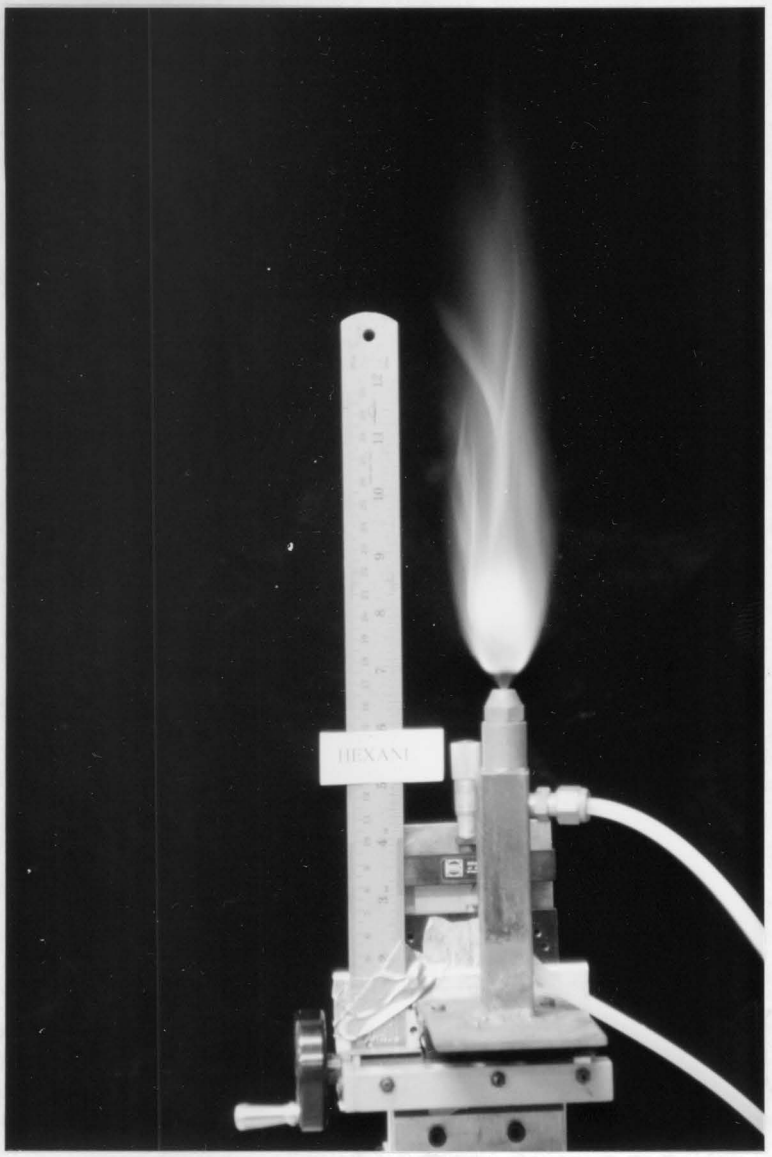

Figure 2. Photograph of a typical air atomized liquid hexane flame.

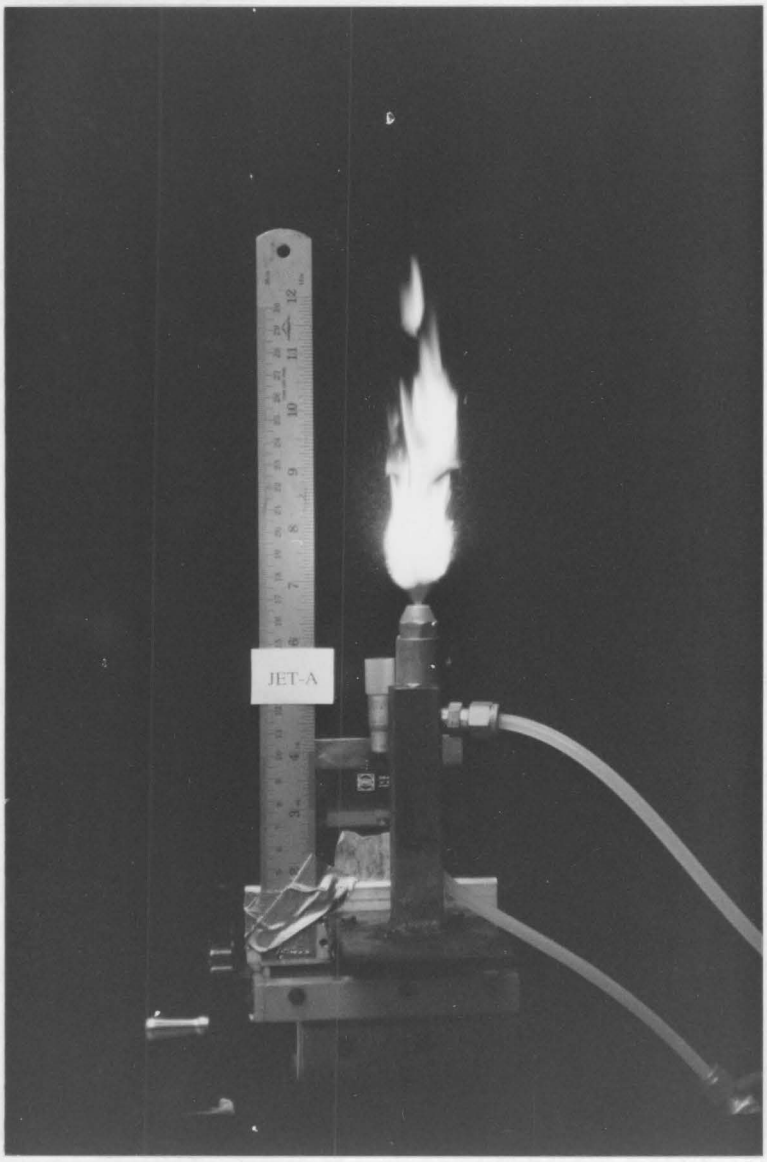

Figure 3. Photograph of a typical air atomized liquid Jet-A flame.

from the end of the wire to the top of the burner. The switch also supplied a -1.5 volt DC signal to trigger the oscilloscope on Channel 1. When the switch was turned off the trigger signal returned to zero volts.

2.4 Optical System Parameters

The size of the flame image that was projected onto the front of the detector, i.e., the entrance slit of the monochromator, was controlled by three variables: 1) the focal length of the lens, 2) the distance between the lens and the object (flame), and 3) the distance between the lens and the image projection location (the entrance slit of the monochromator). By varying these parameters, different flame image magnifications were investigated. The correlation between image magnification and lens distances is given in the following equation

$$M=S_i/S_o \qquad [2.1]$$

where M is the flame image magnification.
S_i is the lens to image distance.
S_o is the lens to object distance.

Assuming the lens is thin, the correlation between lens distances and focal length of the lens is given by the Gaussian lens formula

$$1/f = \{1/S_i + 1/S_o\} \qquad [2.2]$$

where f is the lens focal length.

Table 1. shows the distance and magnification parameters used for this thesis.

The 1.5 inch diameter fused silica Bi-convex lens (Oriel 41370) had a 150 mm focal length. The lens was mounted on an Oriel 11612 table slide. For a set detector

Table 1. Lens and Object Distances for f = 150 mm.

Magnification	S_i (mm)	S_o (mm)
0.33	200	600
0.50	225	450
0.67	251	374
0.75	263	350
1.0	300	300
1.5	375	250
2.0	225	450
3.0	200	600

position, this slide allowed the distance between the lens and the entrance slit (S_i) to be changed easily and accurately.

The stand used to house the burners was mounted on a tri-axis slide which enabled positioning control in three directions. The burner stand was also mounted on an Oriel 11612 table slide. This slide enabled the distance between the lens and the burner (S_o) to be changed easily and accurately. By controlling the placement of the lens and the burner (and therefore S_i and S_o), different flame image magnifications were projected onto the entrance of the detector. With this capability, signal intensity was studied as a function of flame image magnification. Variations in this direction were denoted as changes in the X axis, with X = 0 cm being the plane of the monochromator entrance slit. A top view and a side view of the coordinate axis system is shown in Figure 4.

A second Oriel slide on the burner stand was used to control the burner height above the table. This direction was denoted as the Y axis, with Y = 0 cm being the top of the optical table. The center of the monochromator entrance slit and the center of the lens were positioned at Y = 26.6 cm. The height of the burner was adjusted for each magnification so the base of the inverted flame image always projected onto the top of the monochromator entrance slit. A third slide attached to the burner stand allowed a flame to be scanned across its complete width. With this capability, signal intensity was studied as a function of width across the flame. This direction was denoted as the Z axis, with Z = 0 mm being the centerline of the burner.

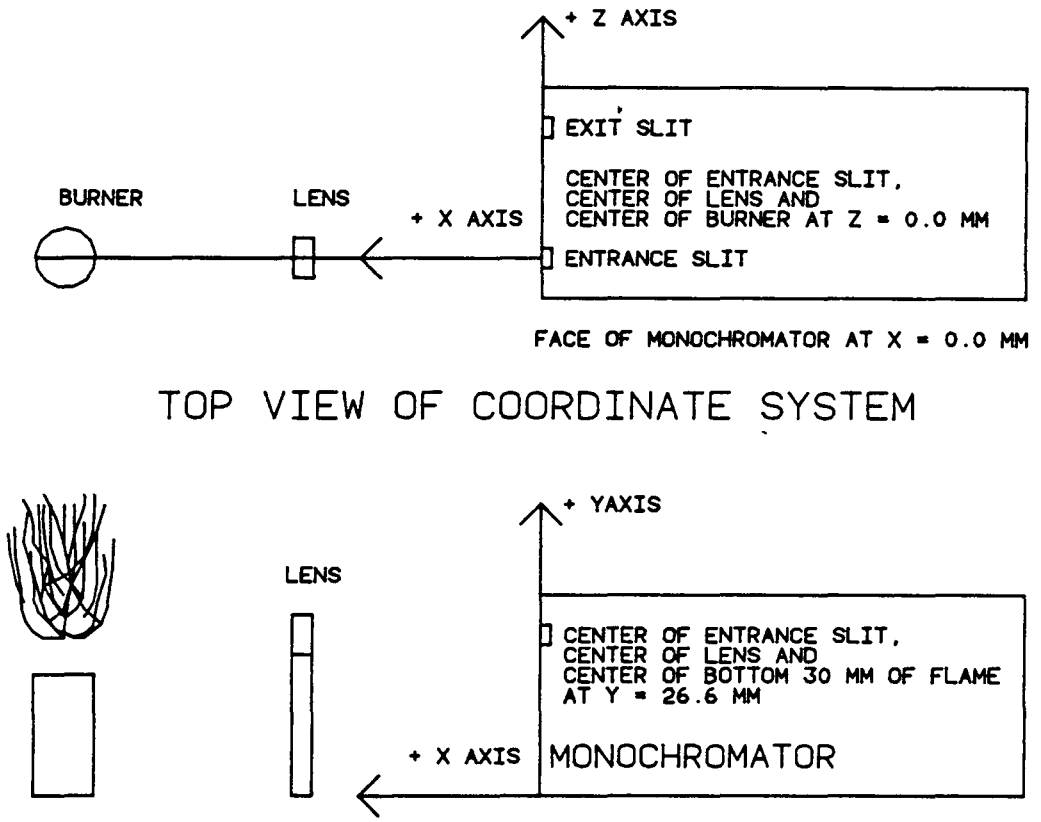

Figure 4. Schematic diagram of the experimental setup's coordinate system.

2.5 Data Acquisition System Setup

The current produced by the photomultiplier tube was fed to a 167 kΩ load resistor and the load voltage was measured by a Nicolet 4094C Digital Oscilloscope. The Nicolet Oscilloscope had an XF-44 Disk Recorder which allowed the storing and retrieving of recorded waveforms. Also included with the Disk Recorder was a set of manufacturer written programs that enabled the operator to perform arithmetic operations on waveforms, and then display the manipulated waveforms on the oscilloscope. To record a waveform, the Nicolet digital oscilloscope records 15,872 voltages at an operator selected sampling speed.

2.6 Experimental Procedure

2.6.1 Full Spectral Scan Test

In an attempt to identify possible signatures of flame ignition, emission spectra in a premixed methane air flame were investigated. By adjusting the Bunsen burner's air inlet and setting the methane flow rate to 12.8 cc/s, a 30 mm inner luminous cone was achieved. This 30 mm high flame was used in all of the steady-state Bunsen burner experiments.

With the oscilloscope sampling data points at 50 millisecond intervals, emission spectra of the methane flame were recorded while the monochromator was advanced in wavelength from 280 nm to 610 nm at 25 nm/min.

To more realistically model an afterburner, liquid fuels were investigated. Full scans were repeated using atomized hexane and Jet-A to determine if the same radicals were present in liquid fuels, and if so, in what concentrations and proportions. Air was initially used as the atomizing gas, but to model the fuel rich atmosphere of an

afterburner, N_2 was also used for each fuel. All full spectral scans were performed with a magnification of 1.0 on an inner cone peak (Z = -4.0 mm).

2.6.2 Determination of Peak Signal Intensities

In order to more exactly determine the wavelength corresponding to the "head" of a system, (and also the strongest signal of the system), an averaging experiment was performed. With the monochromator set on one wavelength, a full waveform was recorded by the oscilloscope at 20 microseconds per point. These 15,872 voltages were averaged using a program supplied with the oscilloscope disk recorder. Two more waveforms were recorded and averaged. These three averages were themselves averaged and recorded. Next, the wavelength of the monochromator was advanced by 1 nm. This averaging process was repeated until the wavelength corresponding to the peak intensity was found.

2.6.3 Light-Off Ignition Test

A number of light-off ignition tests were performed. In the gaseous fuel test, methane flowed through the Bunsen burner unignited until the tesla coil was activated. The nichrome wire of the tesla coil was positioned three millimeters above the top of the burner on the edge of the gas stream. As the tesla coil was turned on, the oscilloscope was triggered on Channel 1 to start recording the waveforms. With the high voltage being applied to the fuel by the tesla coil, the methane ignited and the PMT's transient response was recorded on Channel 2. Bunsen burner tests were run at a magnification of 0.67, flow rate of 12.8 cc/s, methane pressure of 40 psig, and an oscilloscope sampling speed of 10 microseconds per point. The burner Z position was three millimeters off of the burner centerline at Z = -3.0 mm.

In the liquid fuel test, atomized fuel (hexane and Jet-A) flowed through the nozzle unignited until the tesla coil was activated. Nozzle tests were performed at a

magnification of 1.0, atomizing gas flow rate of 115 cc/sec and pressure of 6 psig. To provided a constant pressure, a lift height of 18.3 cm was used. The nozzle Z position was always set on the peak of a luminous cone. The oscilloscope sampling speed was 10 microseconds per point.

2.6.4 Intermittent Light-Off Ignition Test

A number of intermittent light-off ignition tests were performed. In the gaseous fuel test, the methane flow rate was increased to 0.067 L/sec. This caused the velocity of the fuel to become higher than the local turbulent flame speed, which resulted in the flame blowing-off. When the tesla coil was turned on, the high voltage caused the flame to ignite only intermittently.

In the liquid fuel test, the atomizing gas flow rate was decreased to 100 cc/sec, which prevented the fuel from becoming completely atomized or entrained. In addition, the nichrome wire of the tesla coil was positioned so the high voltage was initially applied to the partially atomized mixture further downstream than in the light-off ignition test. Therefore, the flame did not always ignite, and if it did ignite, the flame was not sustained. With the high voltage being applied by the tesla coil, the fuel sporadically ignited, and the PMT's transient response was recorded on Channel 2.

Nozzle tests were performed with a magnification of 1.0, a pressure of 6 psig, and a lift height of 18.3 cm. The nozzle Z position was always set on a peak of a luminous cone, and the oscilloscope recorded data at 10 microseconds per point.

2.6.5 Magnification and Location Tests

Because the Bunsen burner and spray flame nozzles were mounted on a tri-axis slide, different size flame images and different flame locations were able to be investigated. This was done in order to find the magnification and position that provided the strongest signal for light-off detection.

With the monochromator set on the wavelength corresponding to the desired species, the three-waveform averaging procedure described in 2.6.2 was performed. Once a three point average for a set Z position was obtained, the burner was advanced across the front of the fused silica lens. A new three-point average was obtained for this new position. This procedure was repeated until the complete flame width had been scanned. The monochromator wavelength was adjusted to investigate a new species and the scanning process was repeated. Once a scan across the entire flame was completed, appropriate adjustments were made to the lens distances (S_i and S_o) and burner height (Y position), and a new magnification was investigated.

3 EXPERIMENTAL RESULTS

3.1 Introduction

This chapter presents the results for the four basic experiments performed: full spectral scan tests, light-off ignition tests, intermittent light-off ignition tests, and magnification/position tests. Tests were performed on three fuels: methane, hexane and Jet-A aircraft fuel. Two species were investigated, the OH radical at 309 nm, and the CH radical at 430 nm.

3.2 Full Spectral Scan Results

In the full spectral scan tests the monochromator advanced in wavelength while the photomultiplier tube (PMT) recorded the amount of light present at each wavelength. Results of a methane full spectral scan are shown in Figure 5. The 306.4 nm OH system, with its "head" at about 309 nm, can be seen by the very high PMT output voltage. The "head" of the 431.5 nm CH system can be seen by the high PMT voltage at about 430 nm. A second, weaker CH band, (called the 390 nm system), is barely visible with its "head" at about 390 nm. Two weak C_2 systems (473.7 nm and 516.5 nm) can also be seen in the figure. The stronger CH signal was about 40 % the intensity of the OH signal. The C_2 peaks were about 10 % the intensity of the OH signal.

Results of an air atomized hexane full spectral scan are shown in Figure 6. The CH signal produced by the 431.5 nm system was about 80 % the intensity of the OH system's signal. The smaller 390 nm CH system was more pronounced when hexane was burned. The 516.5 nm C_2 system's intensity increased to 45 % of the OH system's intensity, while the 473.7 nm C_2 system only increased to 20 %.

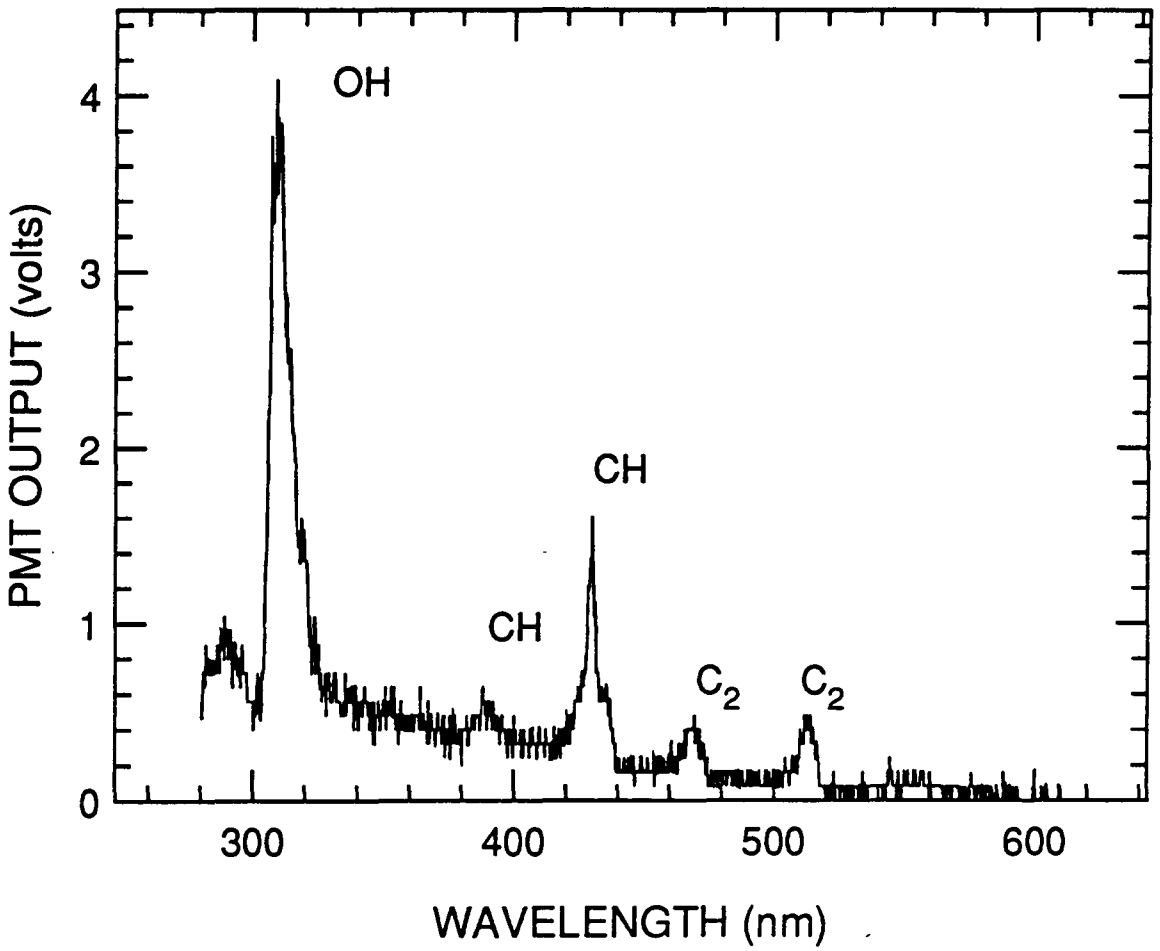

Figure 5. Results of a methane full spectral scan, magnification = 1.0.

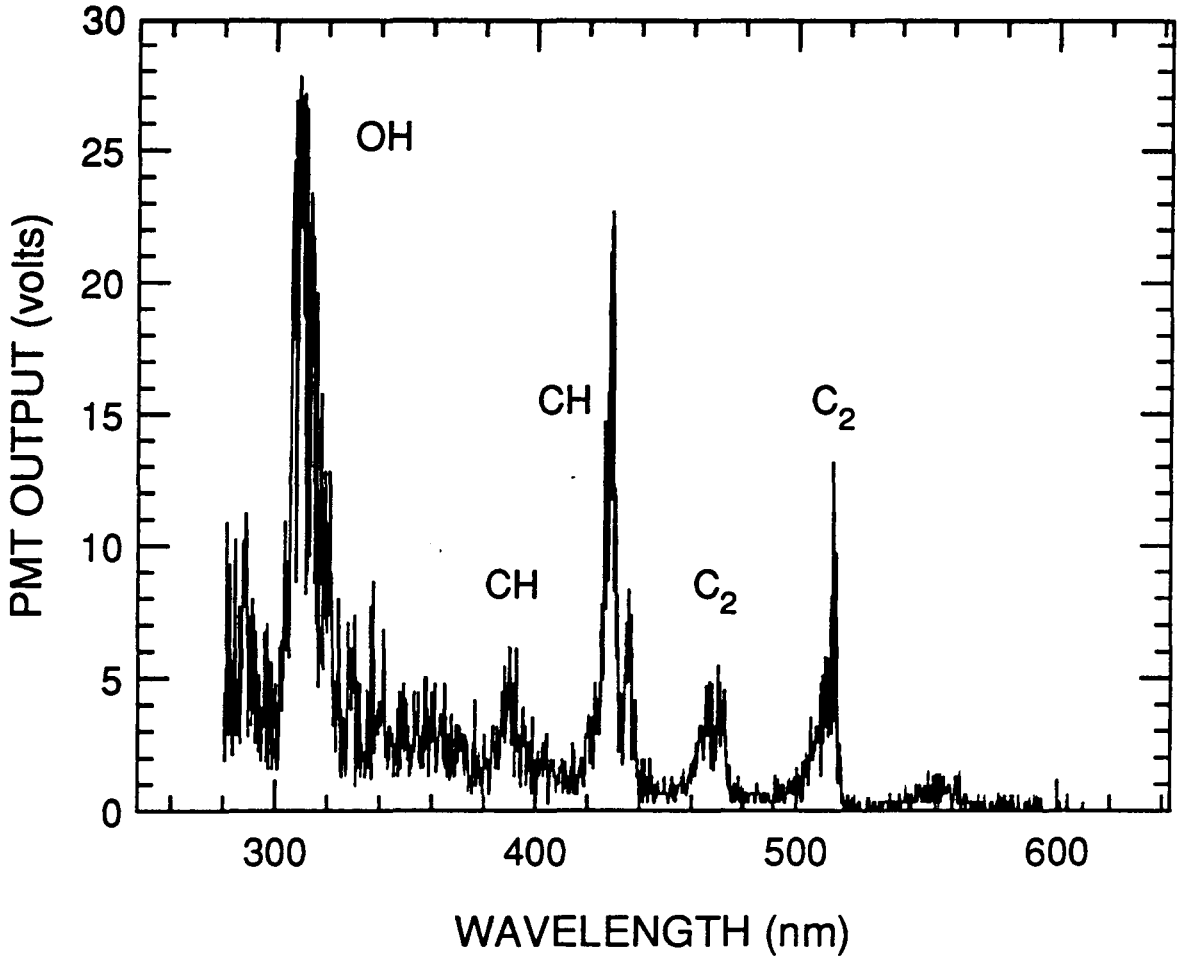

Figure 6. Results of an air atomized hexane full spectral scan, magnification = 1.0.

Results of an air atomized Jet-A full spectral scan are shown in Figure 7. The CH signal produced by the 431.5 nm system was about 115 % the intensity of the OH system's signal. The smaller 390 nm CH system was even more pronounced for the Jet-A case compared to both the hexane and methane tests. The 516.5 nm C_2 system's intensity increased to 50 % of the OH system's intensity, while the 473.7 nm system increased to 40 %. The figure revealed that Jet-A fuel produced more light in the visible spectrum (400 nm to 700 nm), particularly from 450 nm to 600 nm than the hexane. Methane produced very little light at these wavelengths.

Because an afterburner is typically fuel-rich, nitrogen was tested in place of air as the atomizing gas to represent more realistically the conditions in an afterburner. Results of a N_2 atomized hexane full spectral scan are shown in Figure 8. The CH signal produced by the 431.5 nm system decreased to about 70 % the intensity of the OH system's signal. When N_2 was used as the atomizing gas, the overall peak intensity of OH dropped 20 % compared to the air atomizing case, while the CH dropped 35 %.

Results of a N_2 atomized Jet-A full spectral scan are shown in Figure 9. When N_2 was used as the atomizing gas, neither the ratio of the OH to CH peak heights, nor the overall peak intensities changed significantly. Once again, the Jet-A fuel produced more light in the visible spectrum than the hexane or methane.

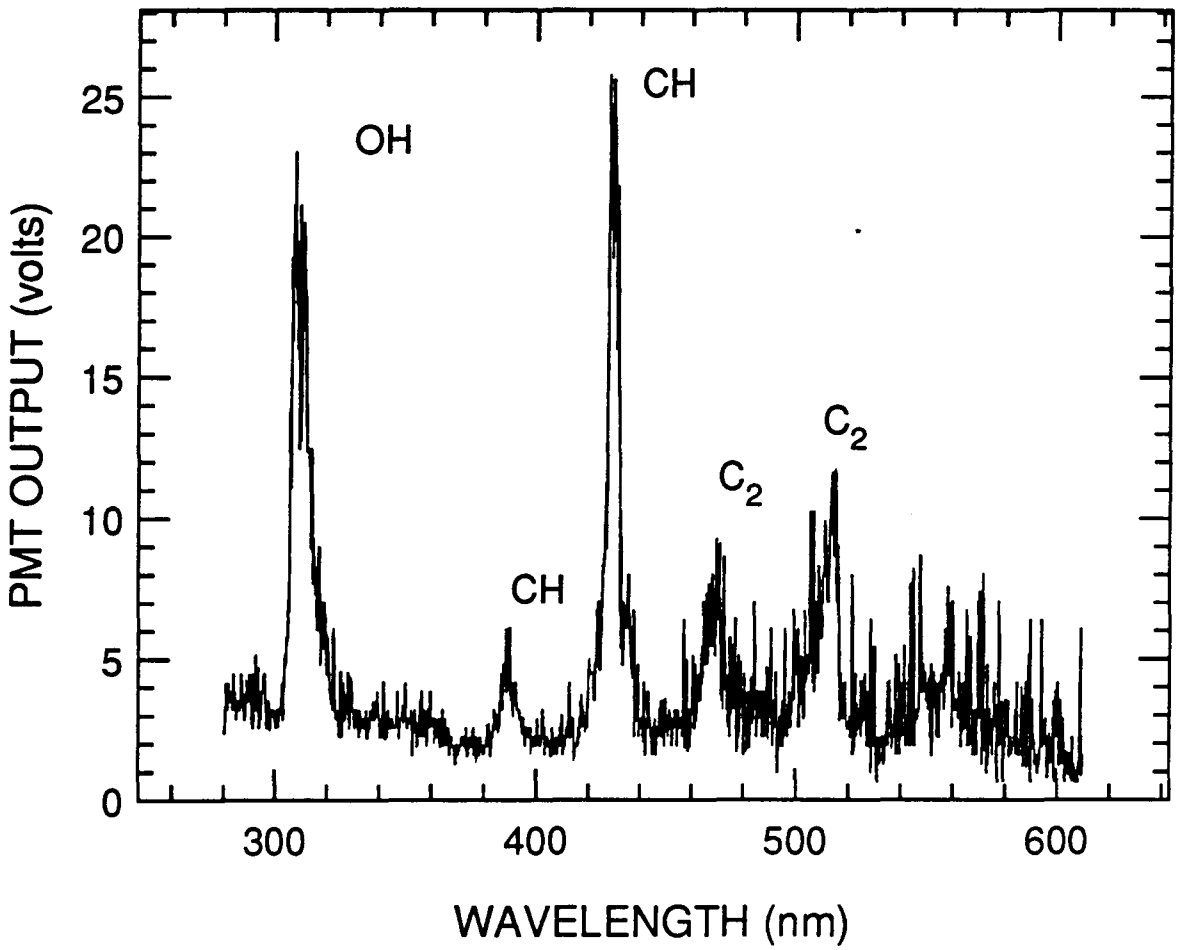

Figure 7. Results of an air atomized Jet-A full spectral scan, magnification = 1.0.

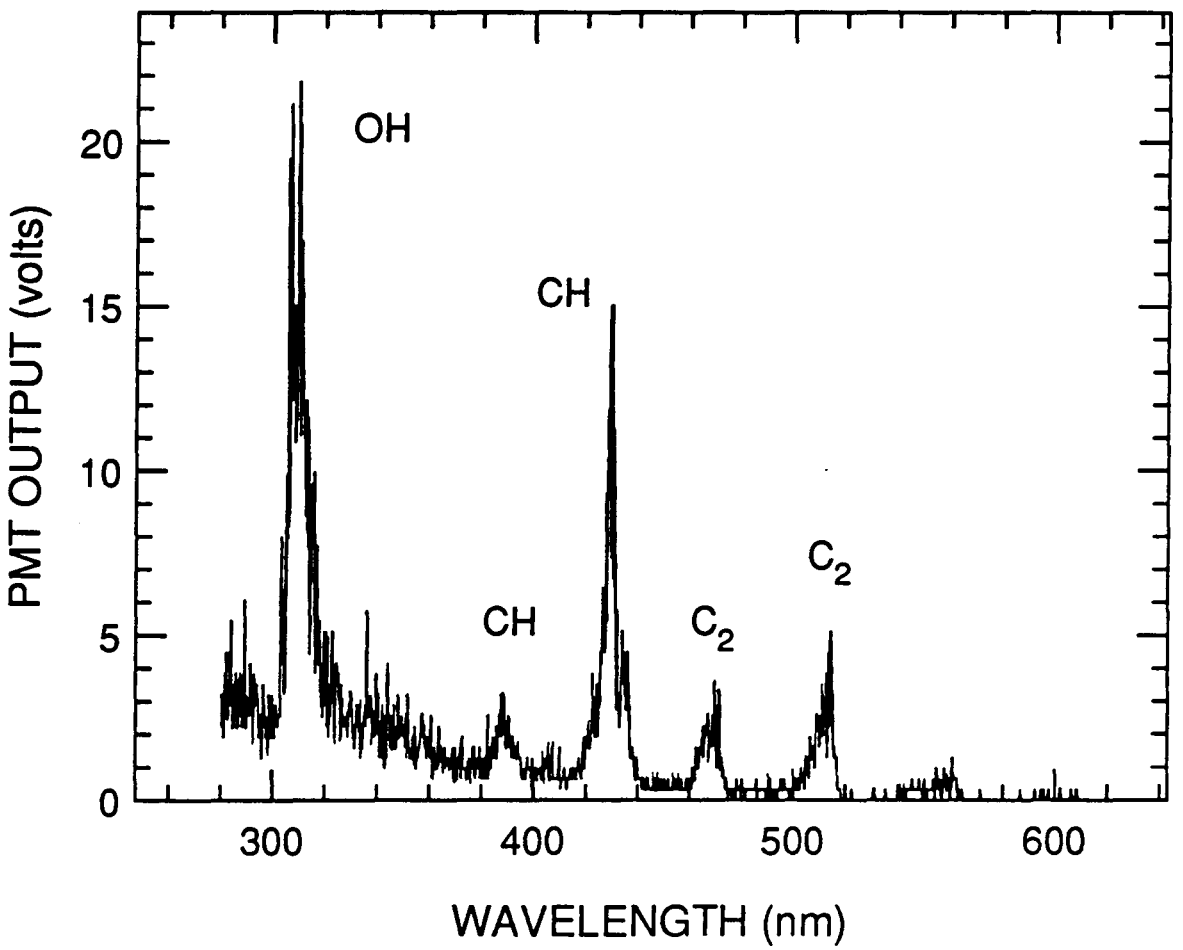

Figure 8. Results of a N_2 atomized hexane full spectral scan, magnification = 1.0.

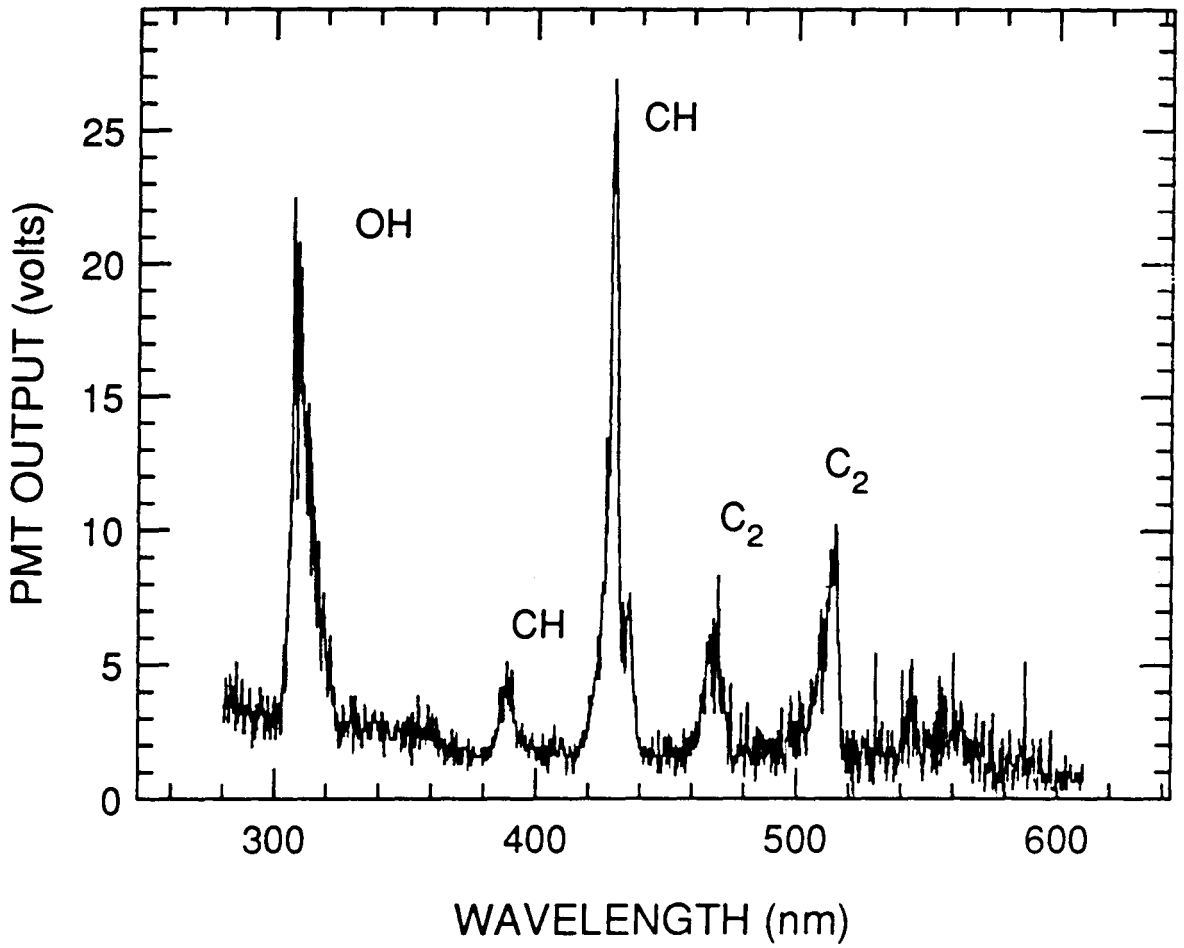

Figure 9. Results of a N_2 atomized Jet-A full spectral scan, magnification = 1.0.

3.3 Determination of Peak Signal Intensities

The wavelengths corresponding to a species maximum signal intensity are summarized in Tables 2-5. Four systems were investigated, the 306.4 nm OH system, the 431.5 nm CH system, the 470 nm C_2 system, and the 515 nm C_2 system, because they had the strongest signals in the full spectral scan tests. Their maximum signals were found to be at 309 nm, 430 nm, 470 nm and 515 nm, respectively.

As the 306.4 nm OH system and the 431.5 nm CH system were the two strongest signals available, they were chosen for continued investigation. To identify the 306.4 nm system with the OH radical Gaydon states [22]

> Detailed analysis of the rotational structure shows the bands are due to a $^2\Sigma$ - $^2\Pi$ transition in a diatomic molecule with a small moment of inertia. This at once limits us to a hydride with an odd number of electrons and the hydroxyl radical is the only possibility.

To identify the 431.5 nm system with the CH radical, Gaydon states [22]

> Three systems of CH are observed in flames, all having a common $^2\Pi$ final level. The systems all show that the open rotational structure characteristic of a diatomic hydride, and the branches are double, indicating a molecule with an odd number of electrons. They are also obtained readily from discharges through pure hydrocarbon vapours, and the emitter can only be CH.

3.4 Light-Off Ignition Test Results

Many aspects of the light-off ignition tests were similar for all three fuels tested. OH and CH concentrations, represented as voltages, were recorded versus time. In the figures, the bottom curve indicated power being supplied to the tesla coil. The top curves were the transient responses of the OH or CH radicals. The figures also show that the tesla coil was not needed to maintain each flame, i.e., when the tesla coil was turned off the flames continued to burn. For all three fuels, the OH and CH light-off ignition test

Table 2. Determination of OH Peak

Wavelength (nm)	Voltage (Volts)
305.0	0.897
306.0	1.68
307.0	2.53
308.0	3.12
309.0	3.60
310.0	3.47
311.0	3.42
312.0	2.82
313.0	2.65
314.0	2.55
315.0	2.22

Table 3. Determination of CH Peak

Wavelength (nm)	Voltage (Volts)
425.0	0.524
426.0	0.584
427.0	0.673
428.0	0.830
429.0	1.13
430.0	1.42
431.0	1.40
432.0	1.02
433.0	0.662
434.0	0.511
435.0	0.555

Table 4. Determination of First C_2 peak

Wavelength (nm)	Voltage (Volts)
465.0	0.263
466.0	0.308
467.0	0.351
468.0	0.379
469.0	0.388
470.0	0.385
471.0	0.365
472.0	0.336
473.0	0.305
474.0	0.268
475.0	0.199

Table 5. Determination of Second C_2 Peak

Wavelength (nm)	Voltage (Volts)
510.0	0.260
511.0	0.333
512.0	0.366
513.0	0.377
514.0	0.417
515.0	0.449
516.0	0.420
517.0	0.306
518.0	0.182
519.0	0.098
520.0	0.073

results agreed with the visual observation of the fuel igniting and then burning in a steady-state mode.

3.4.1 Methane Test Results

Figure 10 shows the results of a typical light-off ignition test while burning a premixed methane/air fuel and recording the transient history of the OH radical. The presence of OH, indicative of the flame, is initially detected at about 12 milliseconds. The large presence of OH radicals at about 25 milliseconds is due to the large volume of gas that is suddenly ignited. The tesla coil is turned off at about 54 milliseconds.

Figure 11 shows the results for the same test procedure, but with the CH concentration being recorded. The presence of CH, indicative of the flame, is initially detected at about 10 milliseconds. The steady-state level of CH radicals occurs at about 28 milliseconds. As before, the large volume of gas that suddenly ignites produces a strong CH signal at about 25 milliseconds. The tesla coil is turned off at about 54 milliseconds. In agreement with the methane full scan test, Figures 10 and 11 show that the OH signal is significantly stronger than the CH signal.

3.4.2 Hexane Test Results

Figure 12 shows the results of a typical light-off ignition test while burning air atomized hexane fuel. The presence of OH, indicative of the flame, is initially detected at about 16 ms, while the steady-state level of OH radicals occurs at about 18 ms. The tesla coil is turned off at about 56 milliseconds.

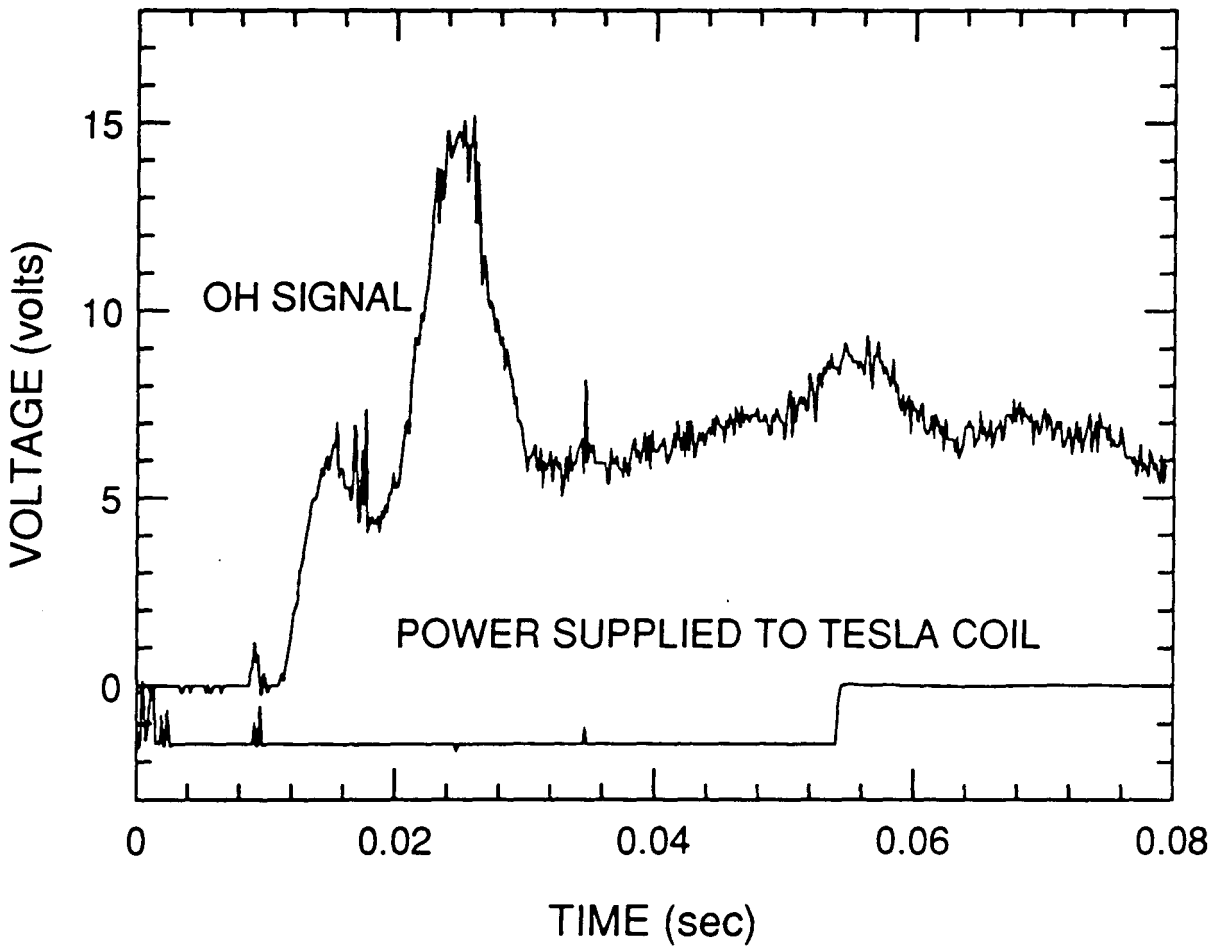

Figure 10. OH measurements in a methane fueled light-off ignition test.

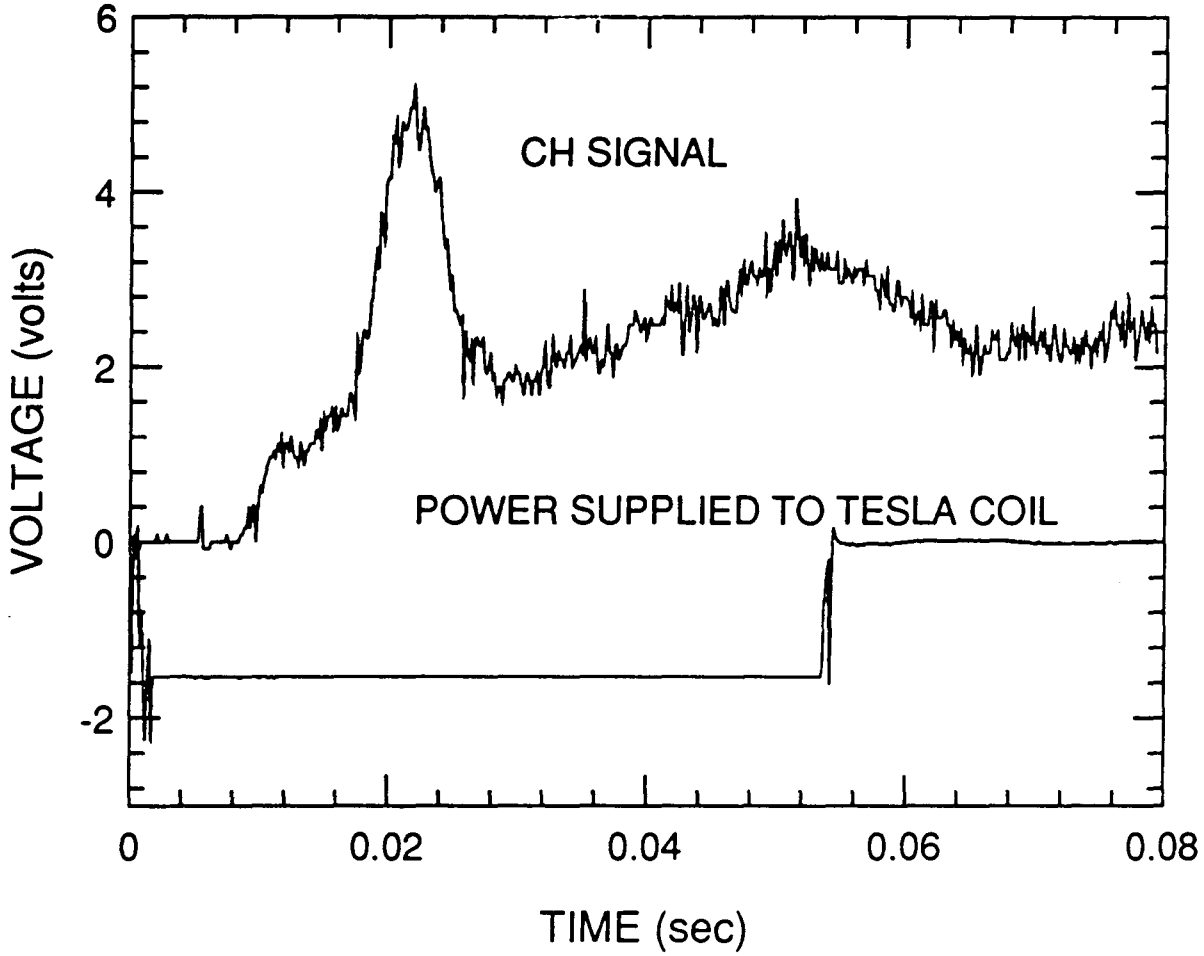

Figure 11. CH measurements in a methane fueled light-off ignition test.

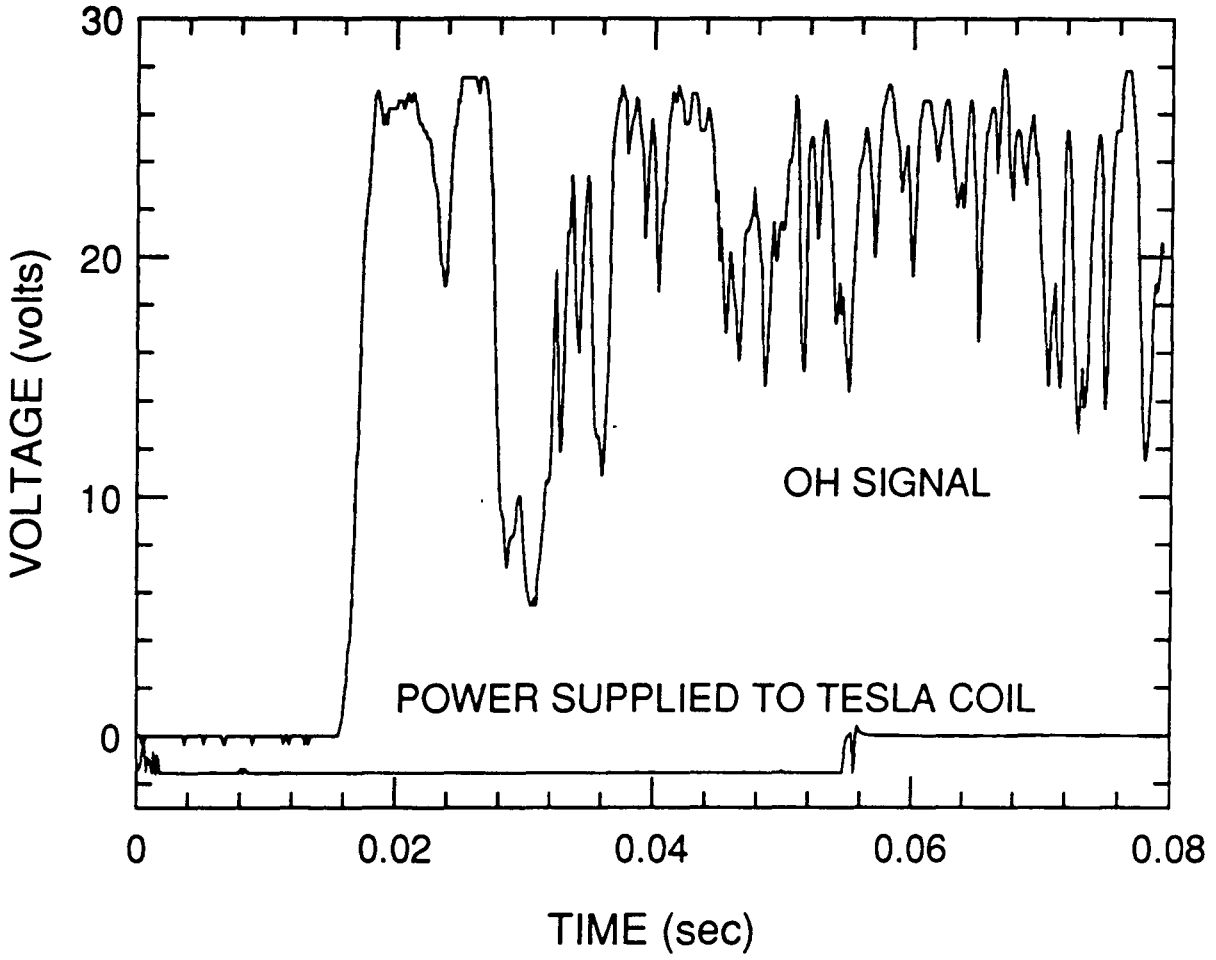

Figure 12. OH measurements in an hexane fueled light-off ignition test.

Figure 13 is the same test procedure, but the CH signal is being recorded. The presence of CH, indicative of the flame, is initially detected at about 29 ms. At about 32 ms the steady-state level of CH radicals is reached. At about 56 milliseconds the tesla coil is turned off.

In agreement with the hexane full spectral scan test, Figures 12 and 13 show that the OH signal is only slightly greater than the CH signal. The turbulent nature of the hexane flame can be seen by comparing the greater fluctuations in the steady-state voltages with those of the laminar methane test.

3.4.3 Jet-A Test Results

The results of a typical light-off ignition test while burning air atomized Jet-A fuel are shown in Figure 14. The presence of OH, indicative of the flame, is initially detected at about 15 ms. The steady-state level of OH radicals occurs at about 18 ms. The tesla coil is turned off at about 57 milliseconds.

With the same test procedure, the CH signal is being recorded in Figure 15. The presence of CH, indicative of the flame, is initially detected at about 23 ms. The steady-state level of CH radicals occurs at about 25 ms. At about 65 milliseconds the tesla coil is turned off.

In agreement with the Jet-A full scan test, Figures 14 and 15 show that the CH signal is now slightly stronger than the OH signal. The turbulent nature of the Jet-A flame can be seen by comparing the greater fluctuations in the steady-state voltages with those of the laminar methane test.

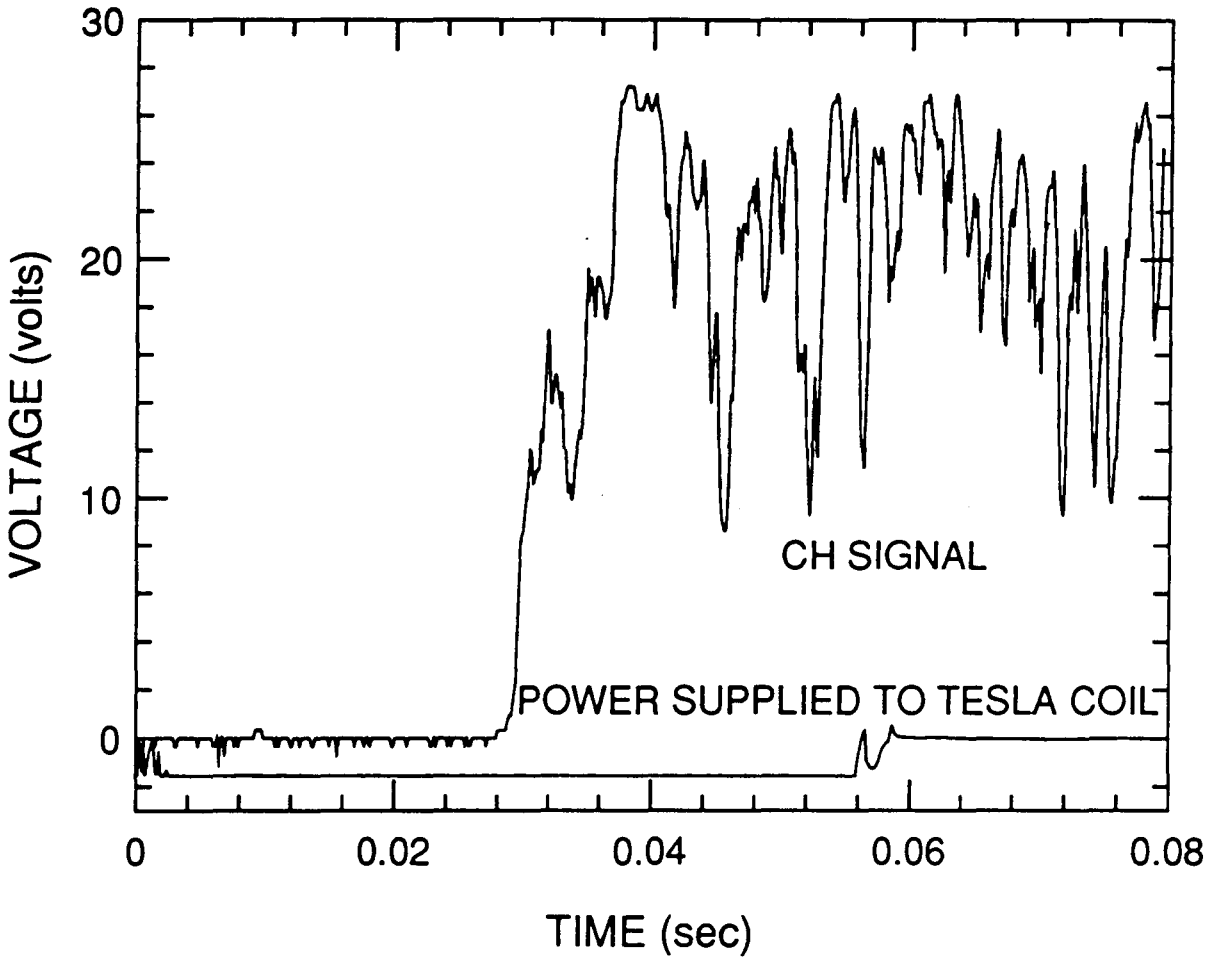

Figure 13. CH measurements in an hexane fueled light-off ignition test.

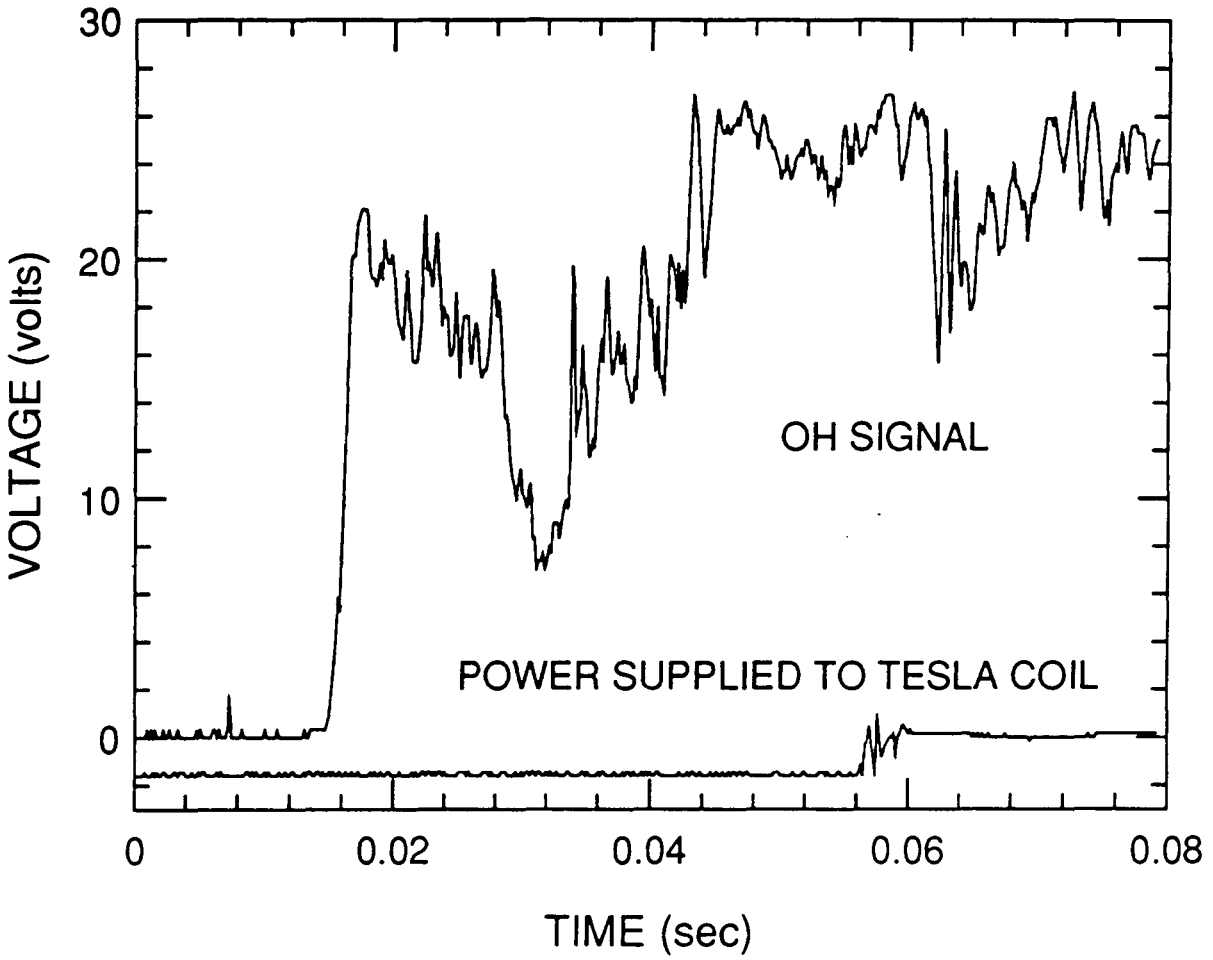

Figure 14. OH measurements in a Jet-A fueled light-off ignition test.

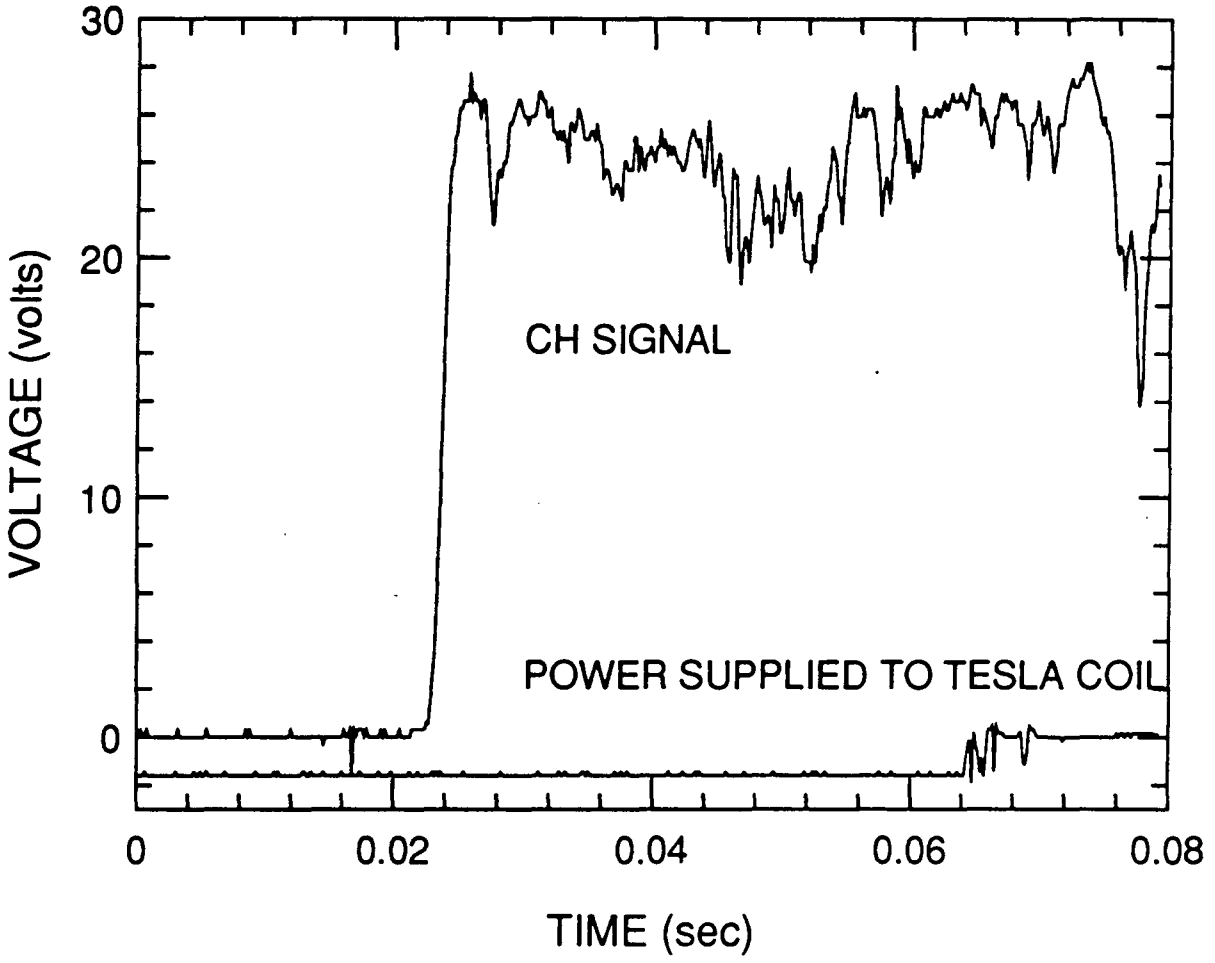

Figure 15. CH measurements in a Jet-A fueled light-off ignition test.

3.5 Intermittent Flame Light-Off Ignition Test Results

Many aspects of the intermittent flame light-off ignition tests were similar for all three fuels tested. OH and CH concentrations, represented as voltages, were recorded versus time. In the figures, the bottom curve indicated power being supplied to the tesla coil. The top curves were the transient responses of the OH and CH radicals. For all three fuels, the OH and CH light-off ignition test results agreed with the visual observation of a brief initial flash of a flame that is not sustained.

3.5.1 Methane Test Results

Figure 16 shows the results of a typical intermittent light-off ignition test while burning a premixed methane/air fuel. The presence of OH, indicative of the flame, is initially detected at about 110 milliseconds. The tesla coil is turned off at about 180 milliseconds, the flame continues to burn briefly, but then extinguishes at 220 milliseconds as it cannot sustain itself.

In Figure 17 the Bunsen burner intermittent light-off ignition test is also performed with the monochromator set on the CH head (430 nm). The presence of CH, indicative of the flame, is initially detected at about 100 milliseconds. The flame burns briefly and then extinguishes at about 240 milliseconds even though the tesla coil is still applying a high voltage to the methane/air mixture.

These figures also show that the OH signal is considerably stronger than the CH signal. This is in agreement with the methane full scan test and the light-off ignition tests.

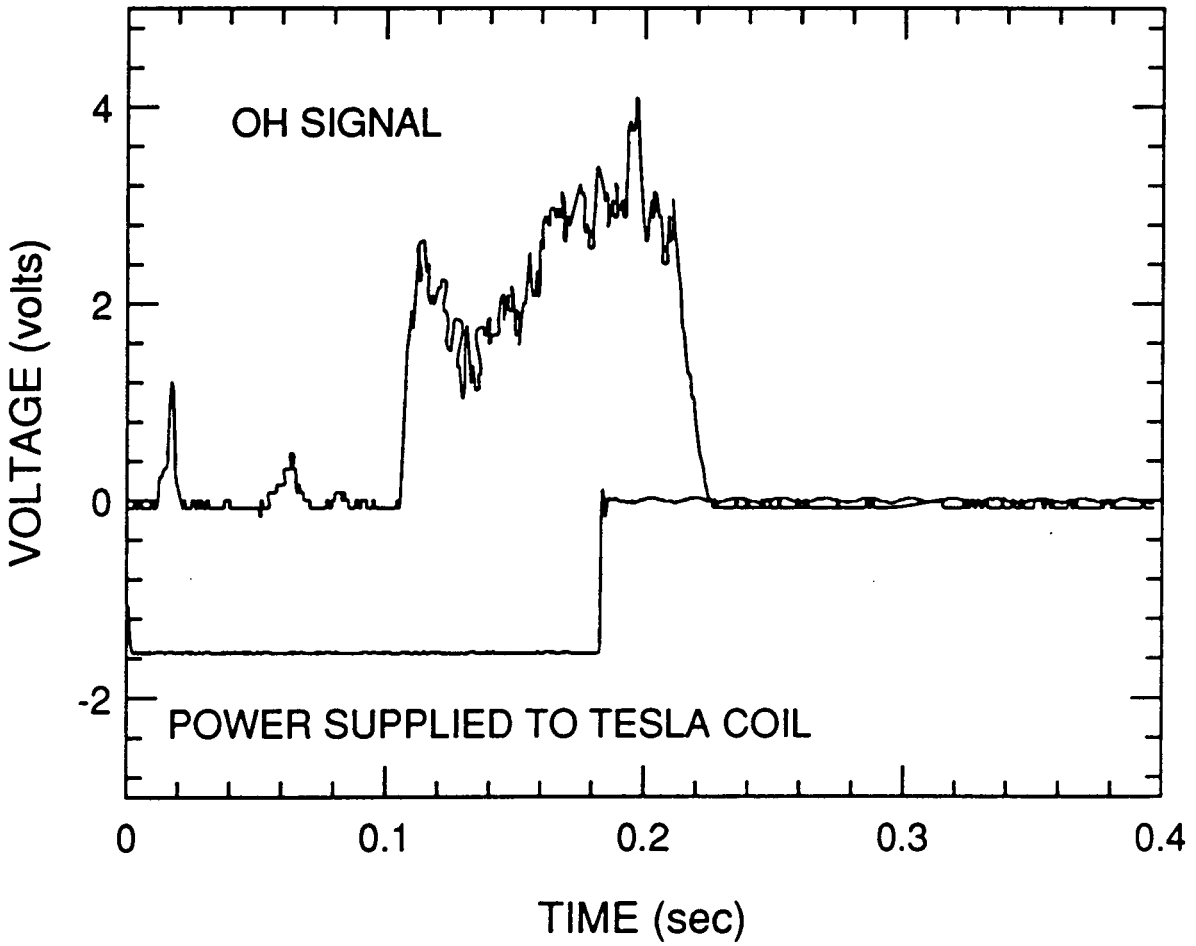

Figure 16. OH measurements in a methane fueled intermittent light-off ignition test.

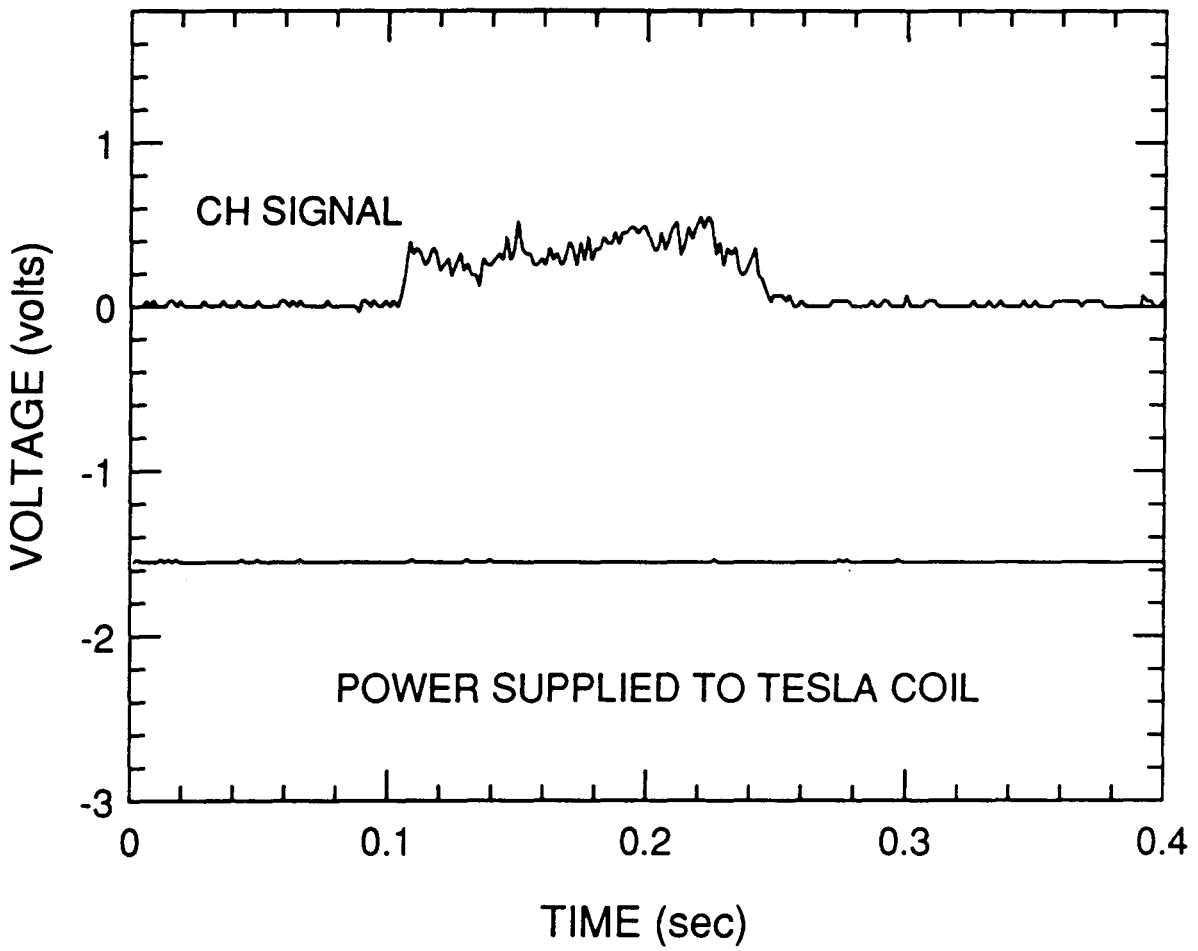

Figure 17. CH measurements in a methane fueled intermittent light-off ignition test.

3.5.2 Hexane Test Results

Figure 18 shows the results of a typical intermittent light-off ignition test while burning hexane fuel. At about 11 ms the presence of OH, indicative of the flame, is initially detected. The flame burns briefly, but then extinguishes at about 58 ms as it cannot sustain itself. Even though the tesla coil is applied to the partially atomized hexane for 8 more milliseconds, the unstable nature of the flame prevents the fuel from igniting again. The tesla coil is turned off at about 66 ms.

Figure 19 is the same test procedure, but the CH signal is being recorded. As seen in the figure, the results are in agreement with the OH intermittent light-off ignition test. The presence of CH, indicative of the flame, is initially detected at about 11 ms. The flame burns briefly, then extinguishes at about 54 ms even though the tesla coil is still applying a high voltage to the partially atomized hexane for about 12 more milliseconds. The tesla coil is turned off at about 68 ms.

Figures 18 and Figure 19 show that the OH signal is slightly stronger than the CH signal. This is in agreement with the hexane full spectral scan test and the light-off ignition tests. The turbulent nature of the hexane flame can be seen by comparing the greater fluctuations in the signal (while the flame was burning) with those of the laminar methane test.

3.5.3 Jet-A Test Results

Figure 20 shows the results of a typical intermittent light-off ignition test while burning Jet-A fuel. The presence of OH, indicative of the flame, is initially detected at about 60 ms. This is also the time the tesla coil is turned off. The flame ignites, burns briefly and then extinguishes at about 130 ms as it cannot sustain itself.

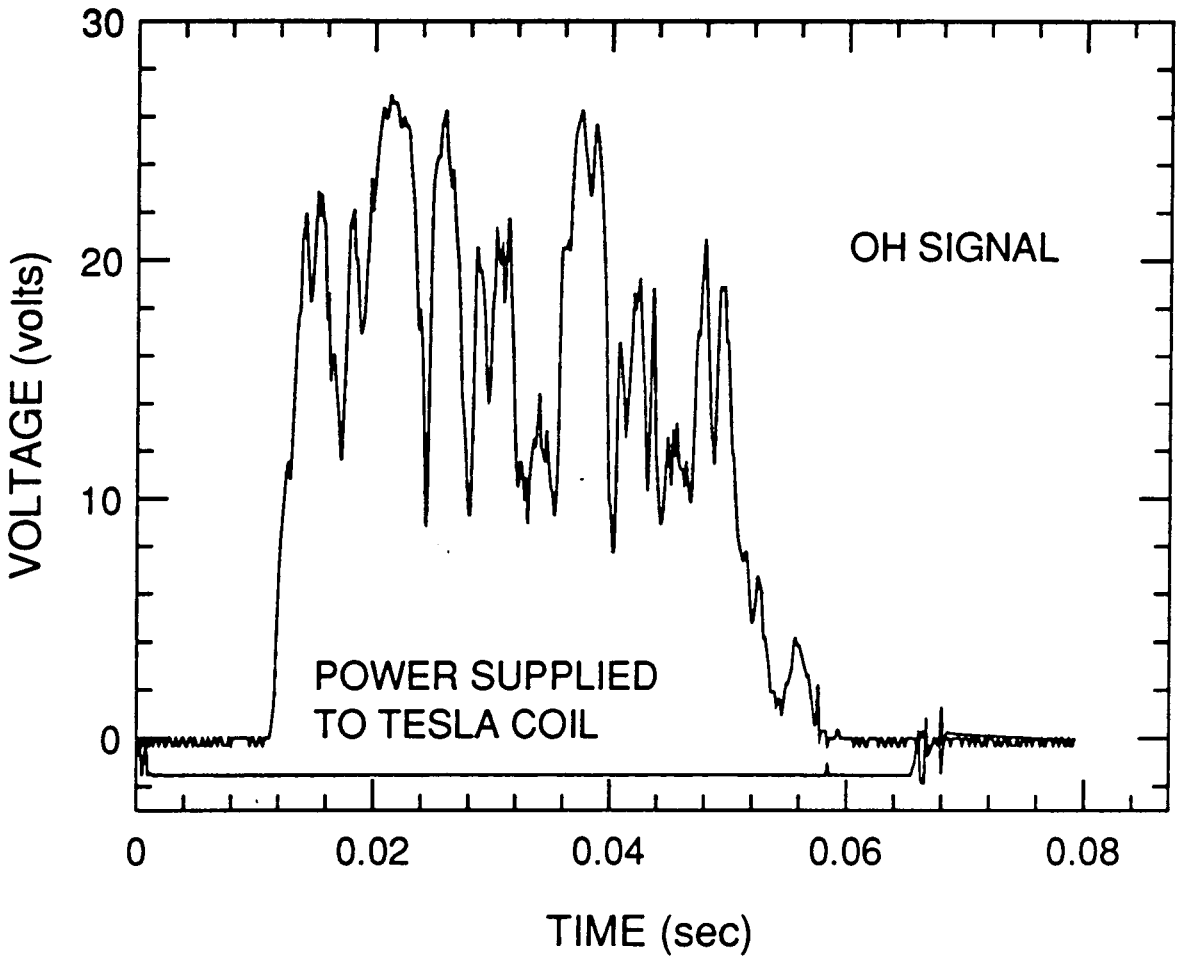

Figure 18. OH measurements in an hexane fueled intermittent light-off ignition test.

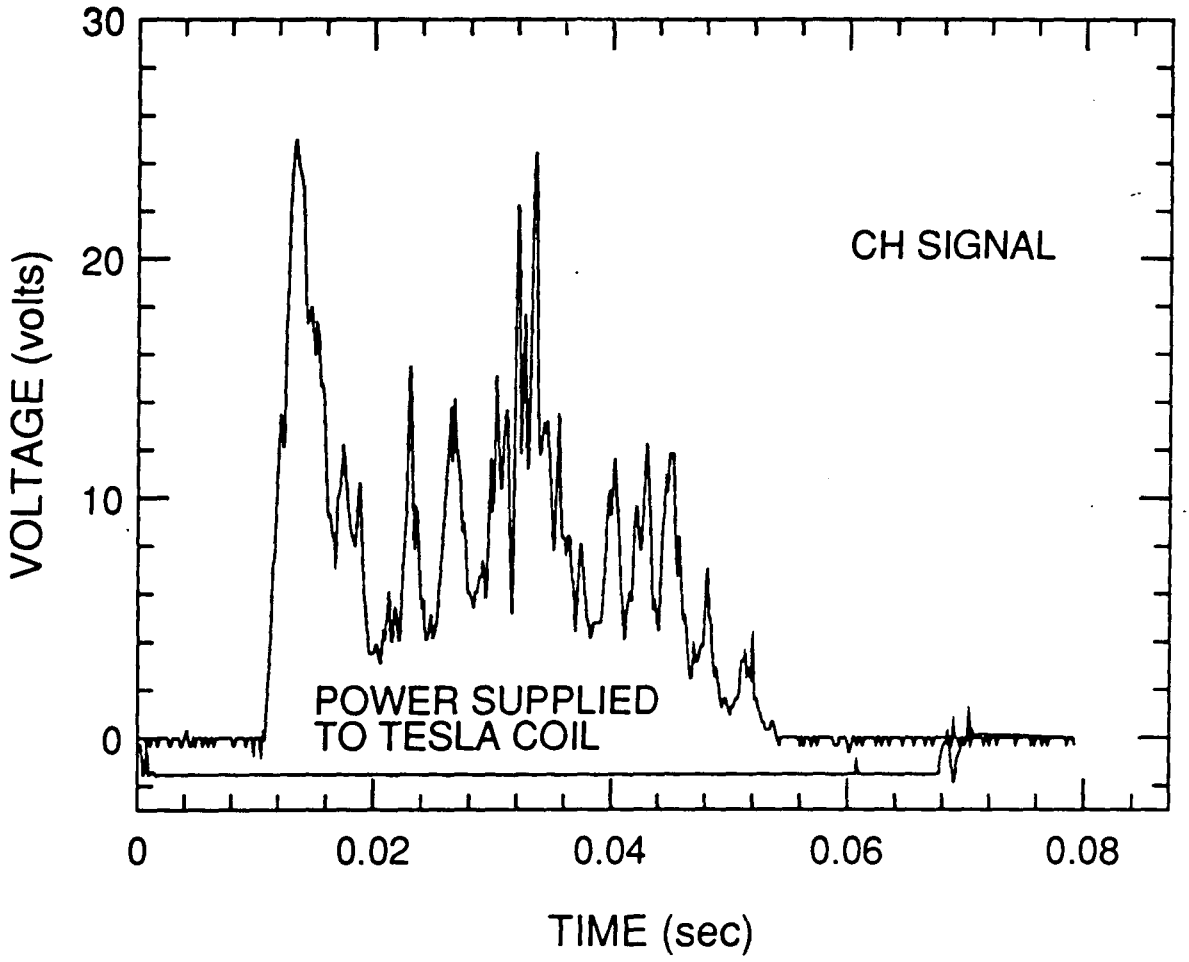

Figure 19. CH measurements in an hexane fueled intermittent light-off ignition test.

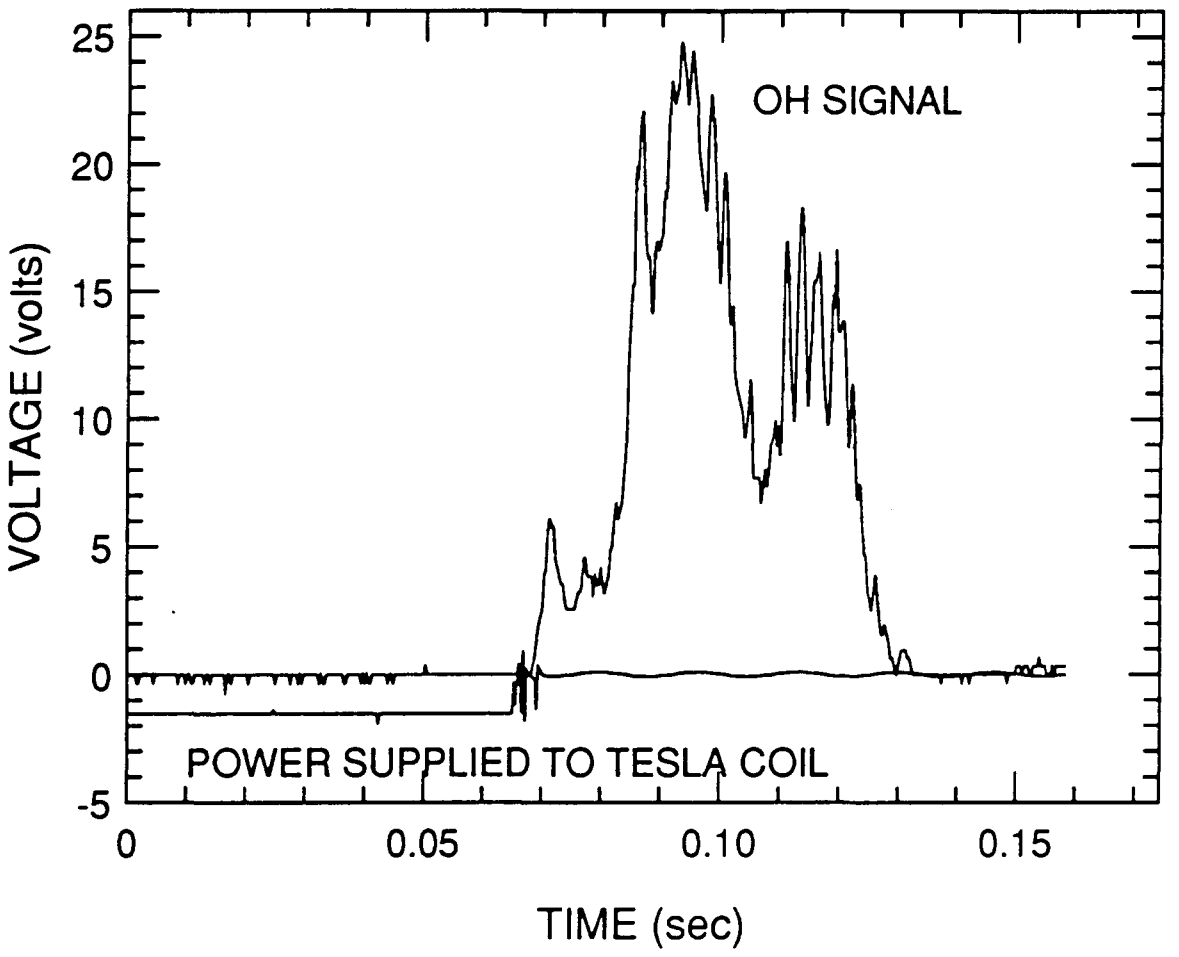

Figure 20. OH measurements in a Jet-A fueled intermittent light-off ignition test.

Figure 21 shows the CH radicals transient response to an intermettent light-off ignition test. As seen in the figure, the results are in agreement with the OH intermittent light-off ignition test. The presence of CH, indicative of the flame, is initially detected at about 45 ms. The flame burns briefly, then extinguishes at about 100 ms even though the tesla coil is still applying a high voltage to the partially atomized Jet-A for about 30 more milliseconds. The tesla coil is turned off at about 100 ms.

Figures 20 and Figure 21 show that the CH signal is now slightly stronger than the OH signal. This is in agreement with the Jet-A full spectral scan test and the light-off ignition tests. The turbulent nature of the Jet-A flame can be seen by comparing the greater fluctuations in the signal (while the flame was burning) with those of the laminar methane test.

3.6 Magnification Test Results

3.6.1 Methane Magnification Test Results

Figure 22 shows the OH and CH radical concentration plotted as the PMT output voltage versus the Z position across the base of a flame. This figure was for a 30 mm premixed methane and air flame of magnification 2.0. This magnification means the size of the flame imaged onto the entrance slit of the monochromator was twice the actual flame size. Therefore, a 30 mm flame height was projected as 60 mm. The entrance slit was set at its maximum height of 15 mm. Therefore, only the bottom 25 percent of the flame image was allowed into the monochromator through the entrance slit. The OH signal intensity was approximately 3.5 times the CH signal intensity.

Figure 23 shows the results for a flame image magnification of 1.5. With this magnification the bottom 33% of the 30 mm flame was allowed into the monochromator.

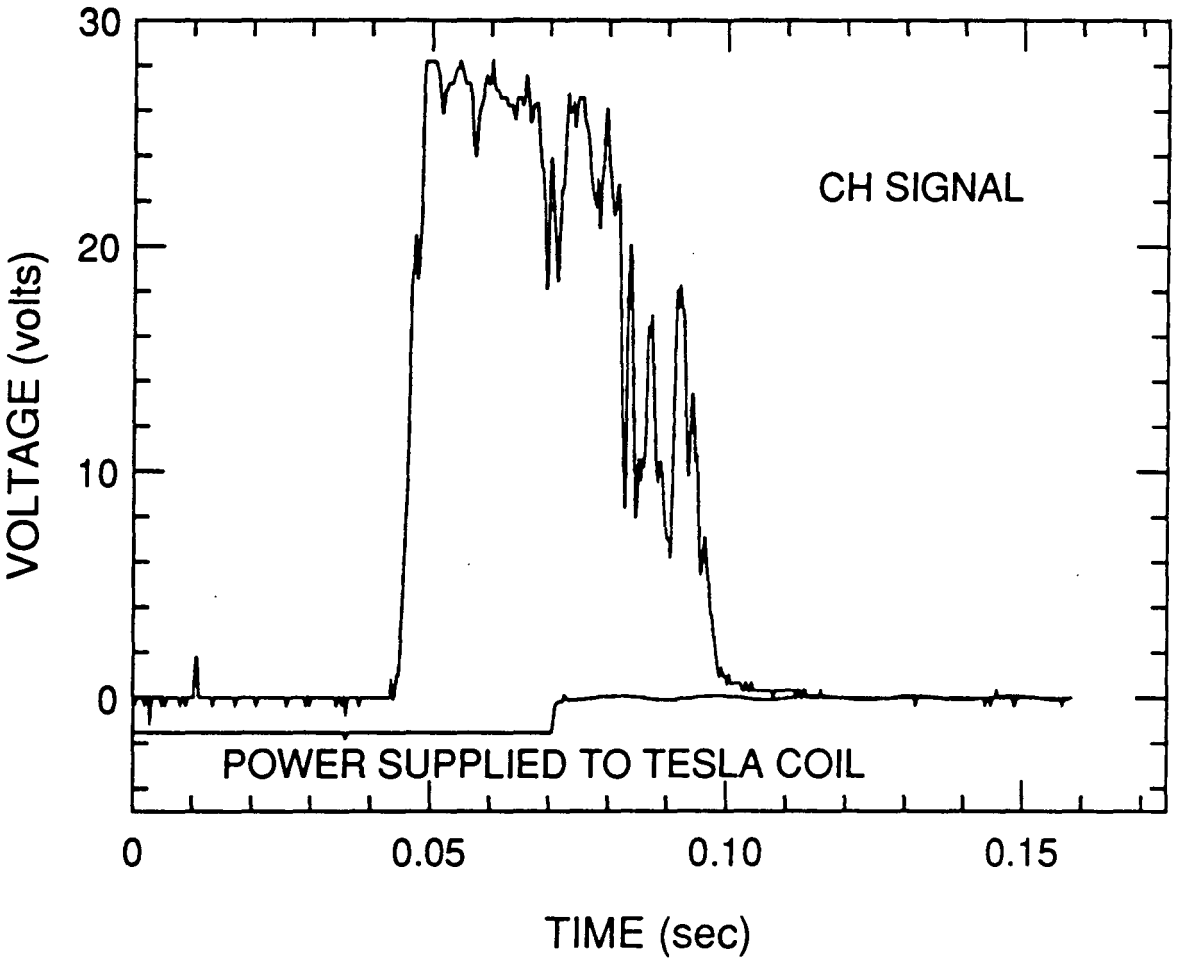

Figure 21. CH measurements in a Jet-A fueled intermittent light-off ignition test.

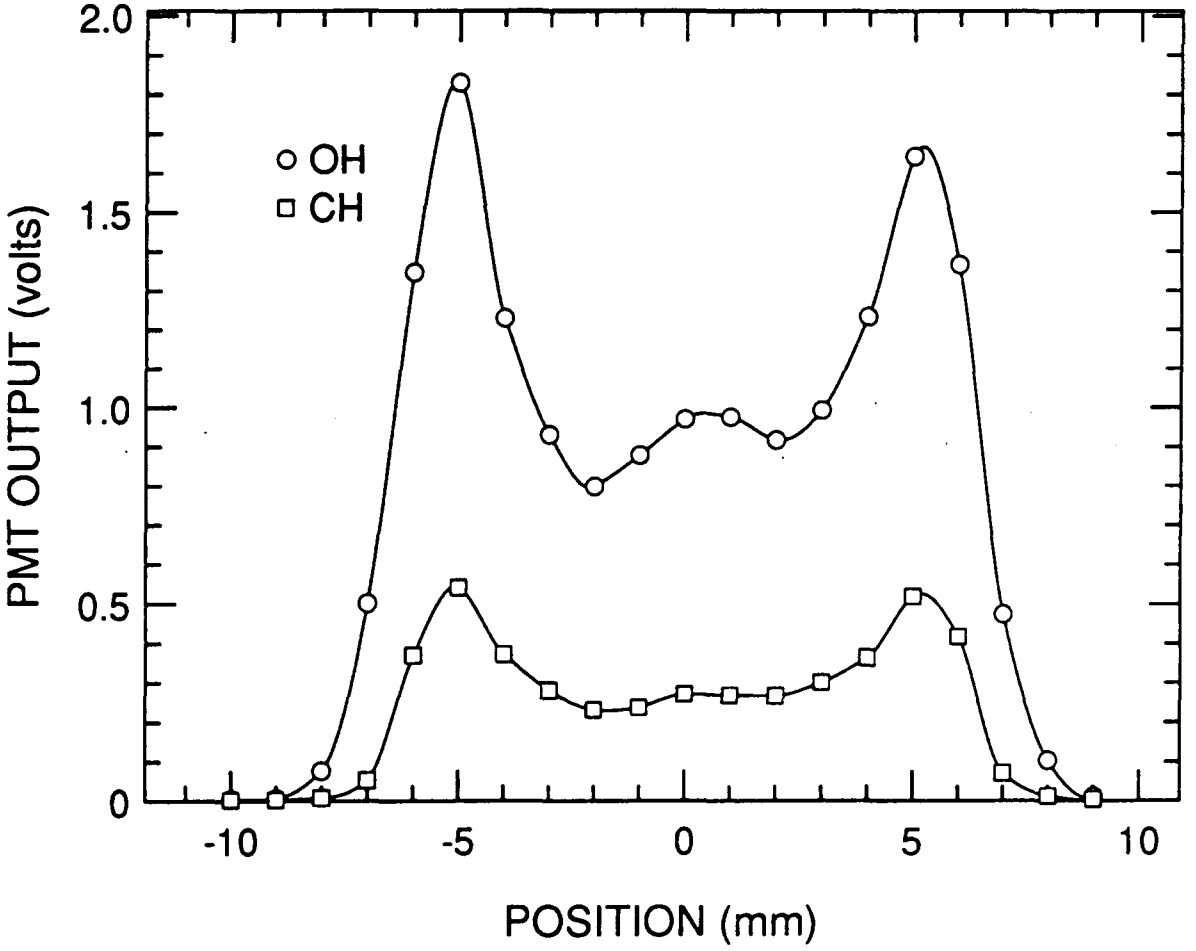

Figure 22. Radical measurements for the methane flame, magnification = 2.0.

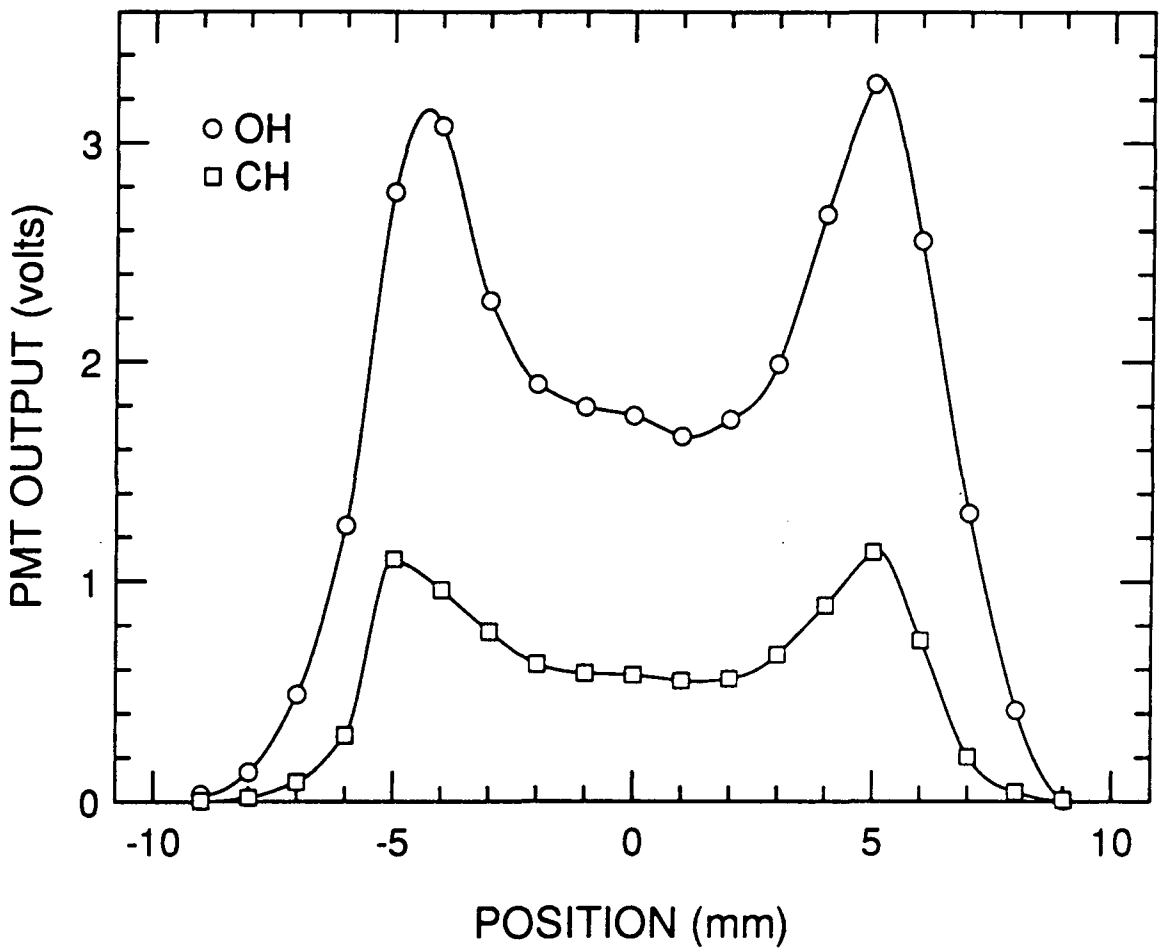

Figure 23. Radical measurements for the methane flame, magnification = 1.5.

The OH signal intensity was approximately 3.0 times the CH signal intensity. For a magnification of 1.0, seen in Figure 24, the bottom 50% of the 30 mm flame was scanned. In this case the OH signal intensity was about 2.5 times the CH signal intensity. Figure 25 shows the results of allowing 75% of the flame image into the monochromator by using a magnification of 0.66. Here, the OH signal intensity was approximately 2.8 times the CH signal intensity. Finally, with a magnification of 0.33, the 30 mm flame image was projected as a 10 mm flame onto the 15 mm entrance slit. These results are shown in Figure 26, where the OH signal intensity was approximately 3.3 times the CH signal intensity.

3.6.2 Hexane Magnification Test Results

Three magnifications were investigated using the air atomized hexane fuel. In the methane experiments the minimum voltages were obtained for the 2.0 magnification. This magnification was repeated for the atomized hexane case with the results seen in Figure 27. Figure 28 shows the result of an intermediate magnification of 1.0. As expected, these voltages were higher than the 2.0 magnification case. Finally, Figure 29 shows the results of the 0.33 magnification test.

In all three of the hexane magnification tests the OH signal intensity was slightly higher than the CH signal intensity. This was in agreement with the full spectral scan test, the light-off ignition tests, and the intermittent light-off ignition tests.

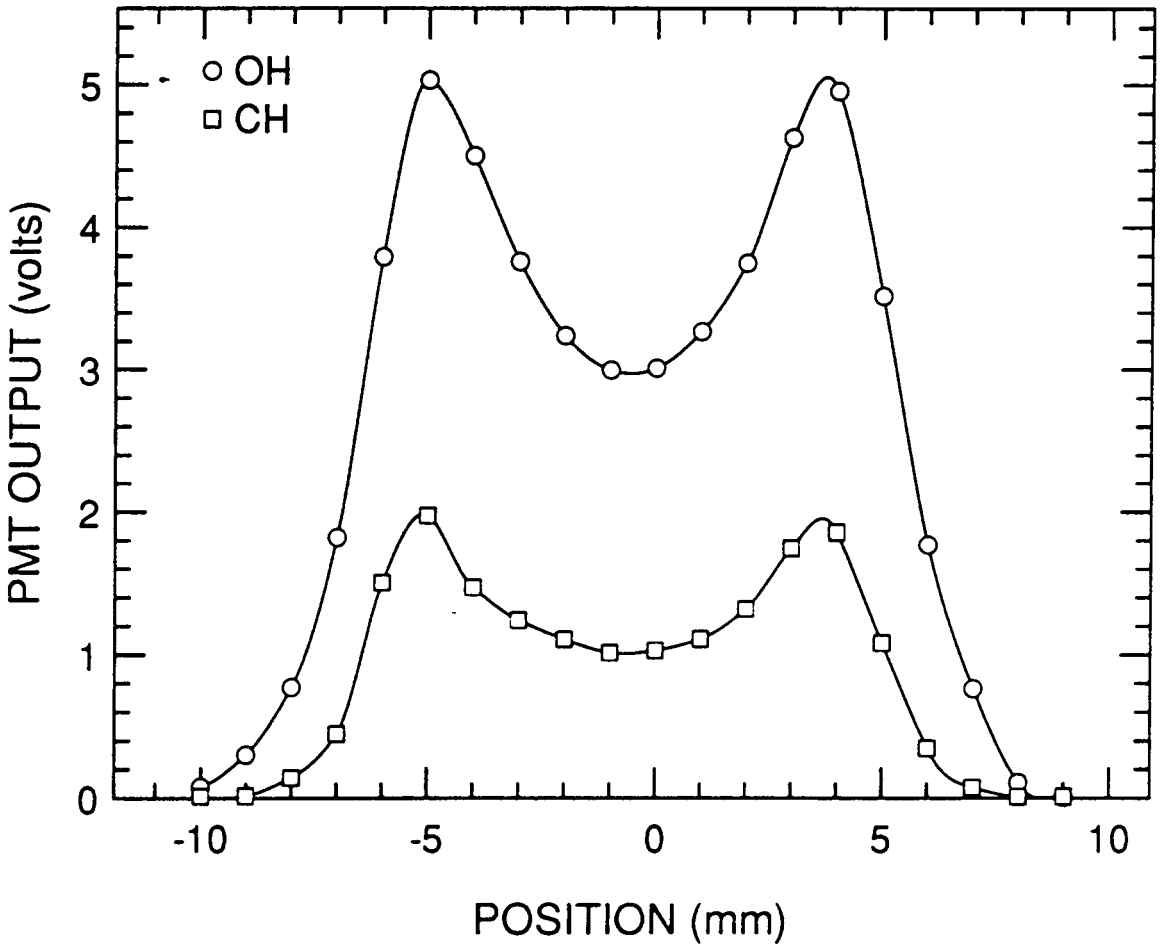

Figure 24. Radical measurements for the methane flame, magnification = 1.0.

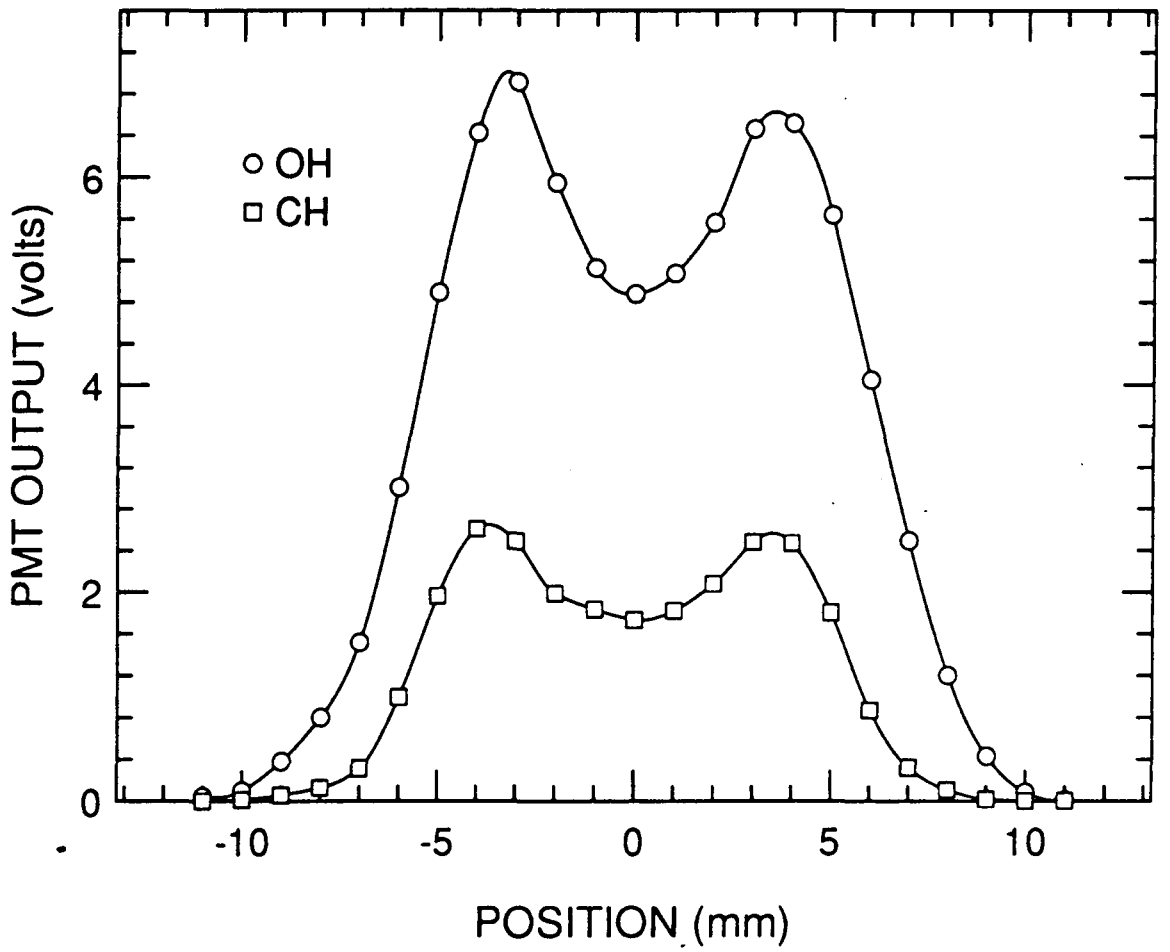

Figure 25. Radical measurements for the methane flame, magnification = 0.67.

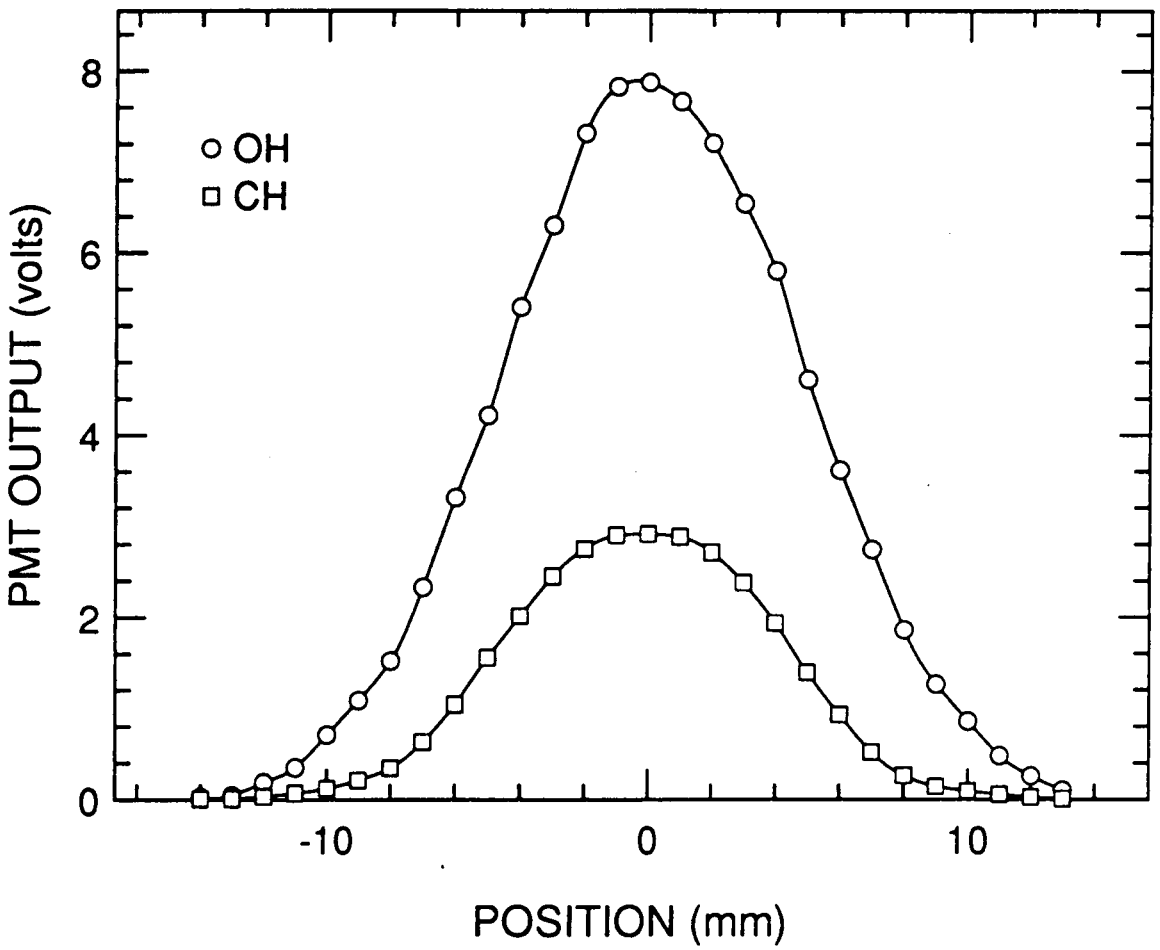

Figure 26. Radical measurements for the methane flame, magnification = 0.33

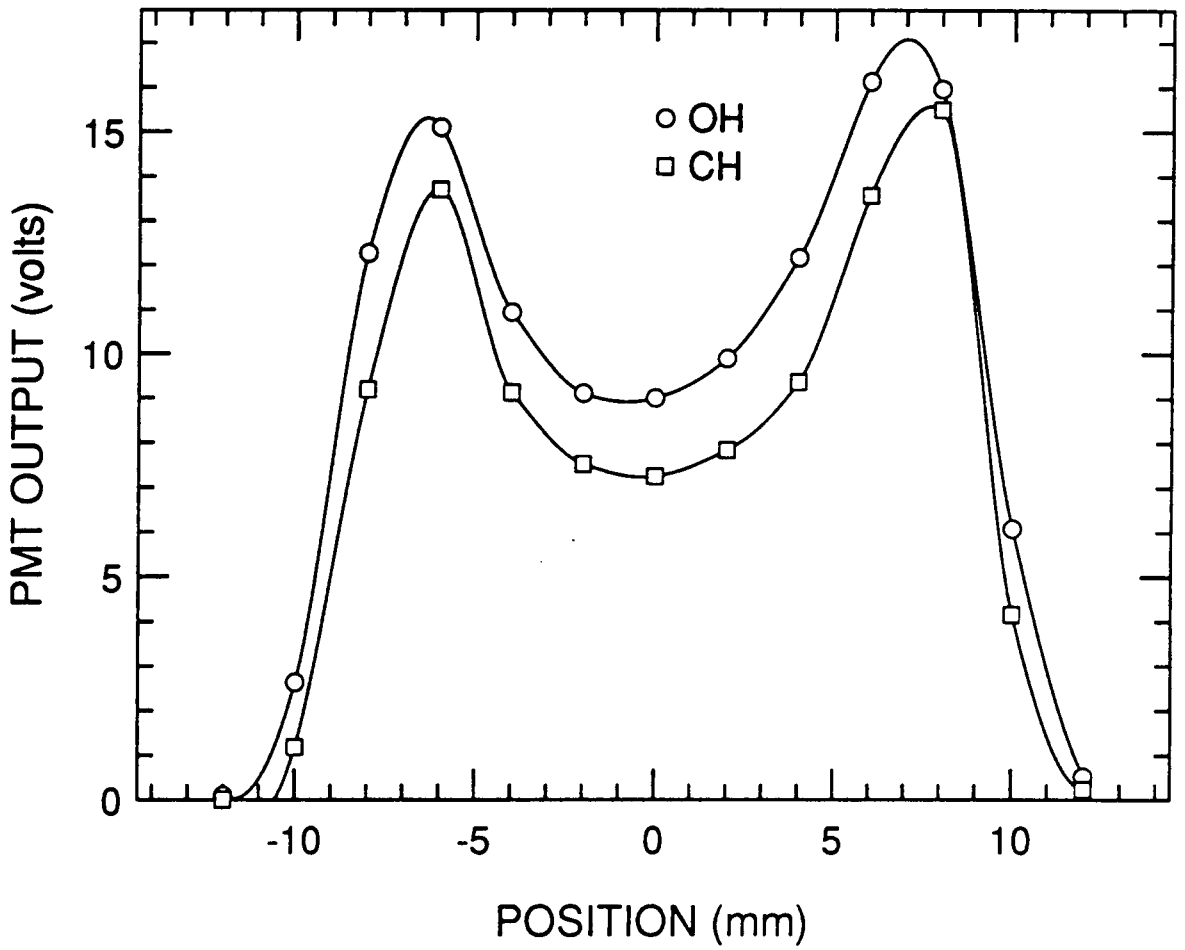

Figure 27. Radical measurements for the air atomized hexane, magnification = 2.0.

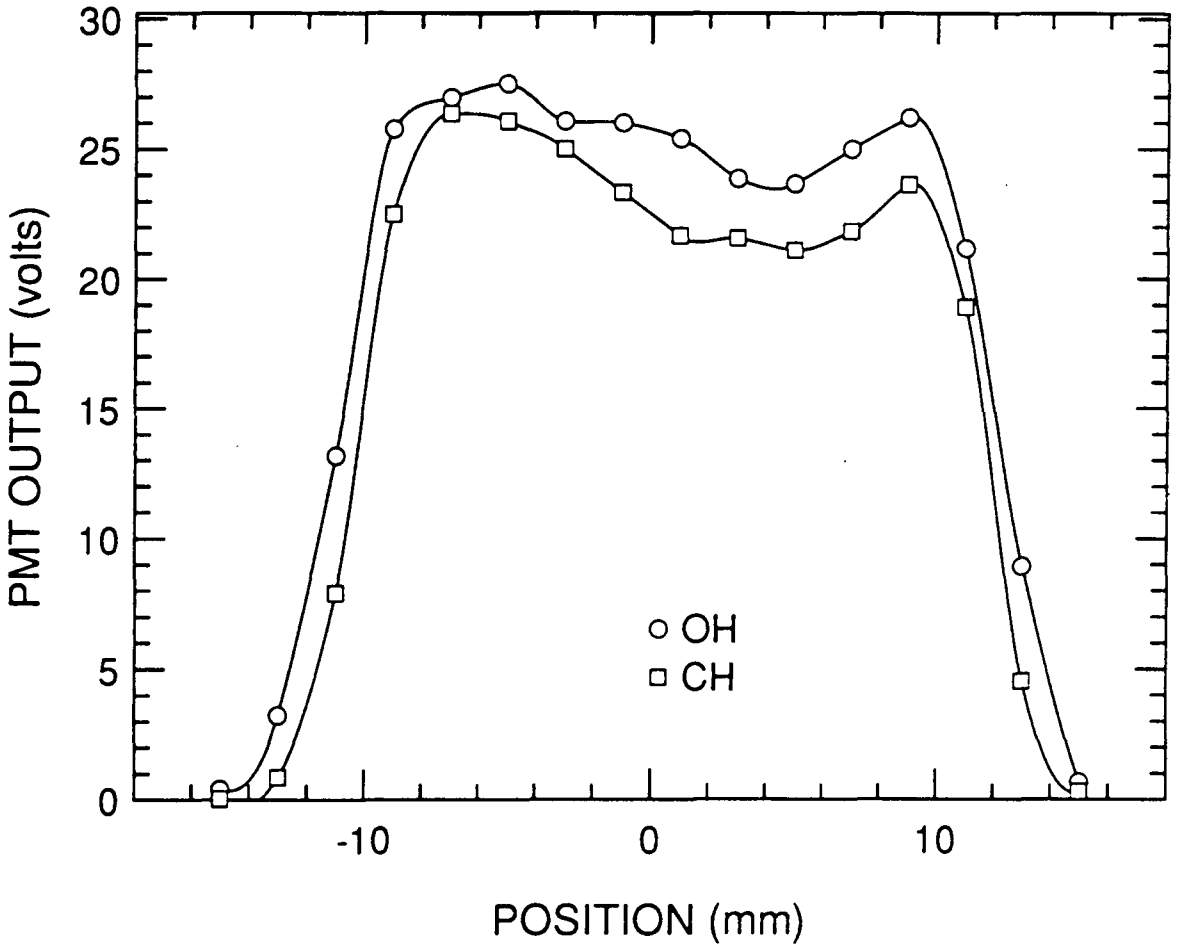

Figure 28. Radical measurements for the air atomized hexane, magnification = 1.0.

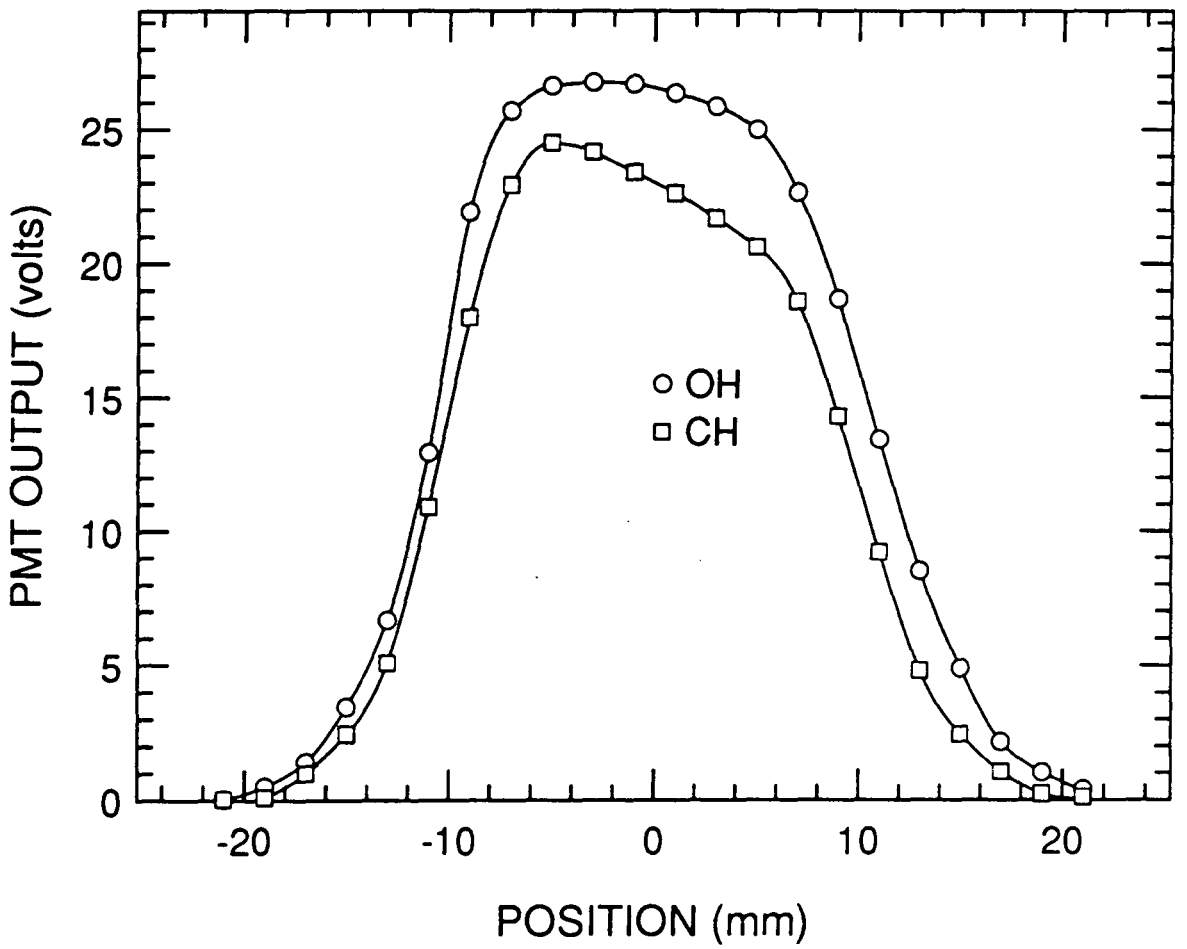

Figure 29. Radical measurements for the air atomized hexane, magnification = 0.33.

3.6.3 Jet-A Magnification Test Results

Three magnifications were also investigated using the air atomized Jet-A fuel. In the methane and hexane experiments the minimum voltages were obtained for the 2.0 magnification. This magnification was repeated for the Jet-A case with the results seen in Figure 30. Figure 31 shows the result of an intermediate magnification of 1.0. As expected, these voltages were higher than the 2.0 magnification case. Finally, the 0.33 magnification, seen in Figure 32, produced the highest voltages.

In all three of the Jet-A magnification tests the CH signal intensity was now slightly higher than the OH signal intensity. This is in agreement with the full spectral scan test, the light-off ignition tests, and the intermittent light-off ignition tests.

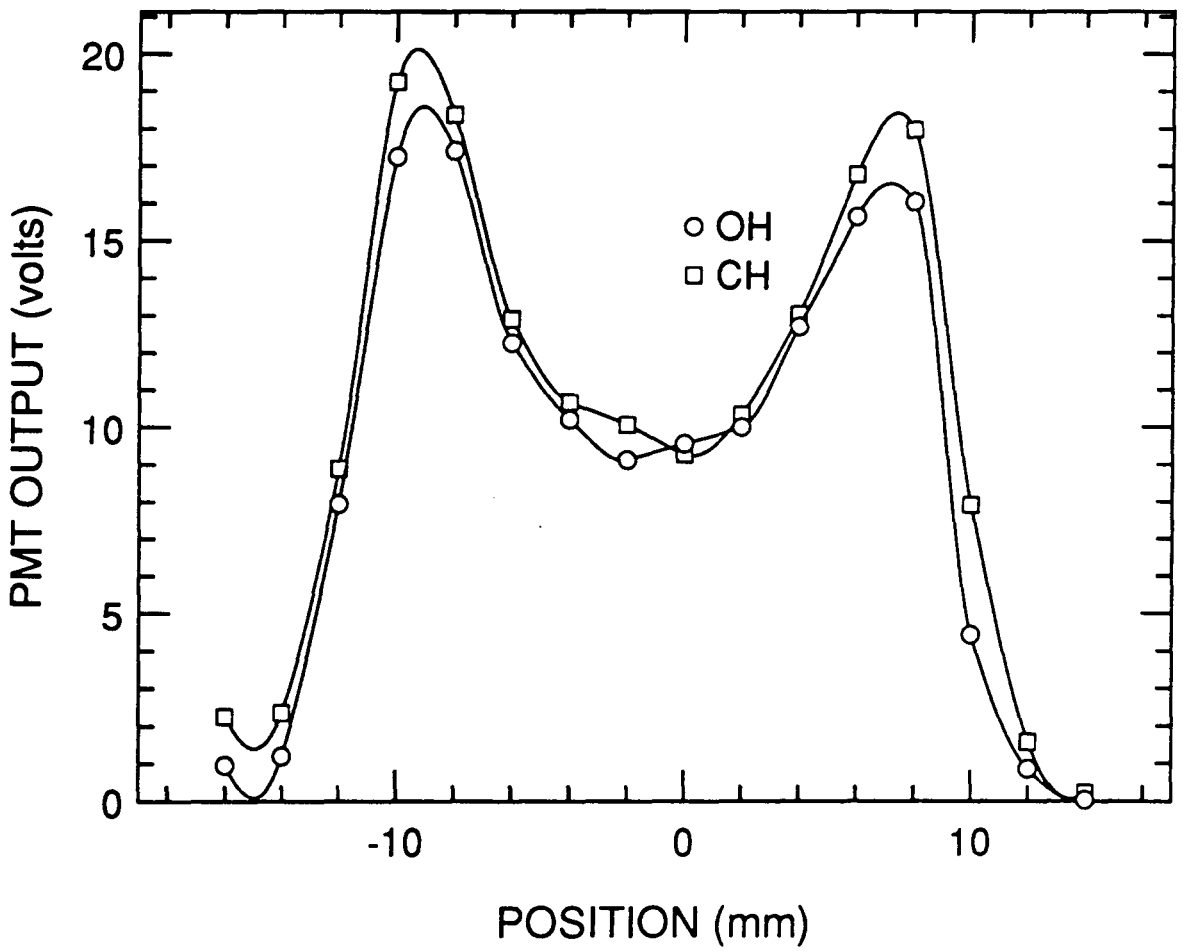

Figure 30. Radical measurements for the air atomized Jet-A, magnification = 2.0.

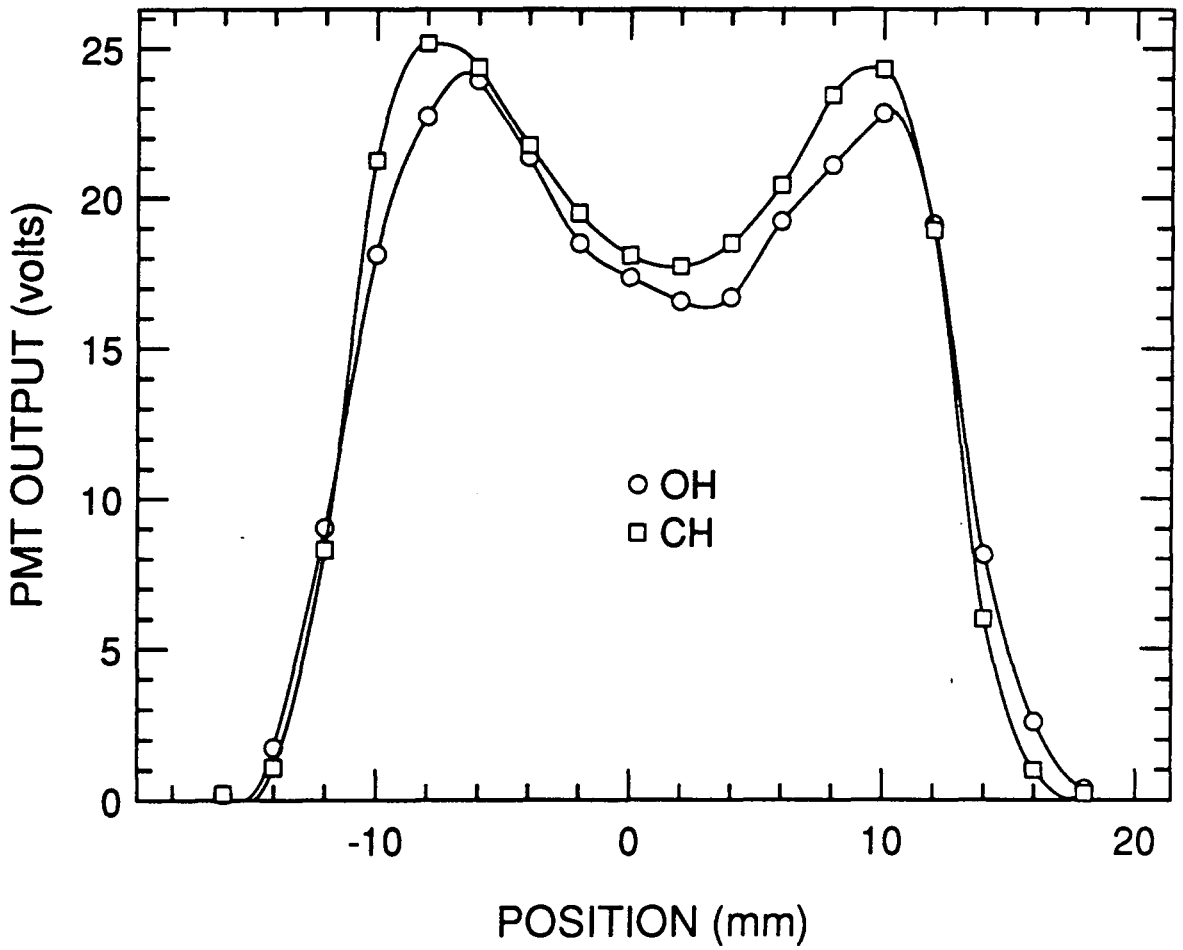

Figure 31. Radical measurements for the air atomized Jet-A, magnification = 1.0.

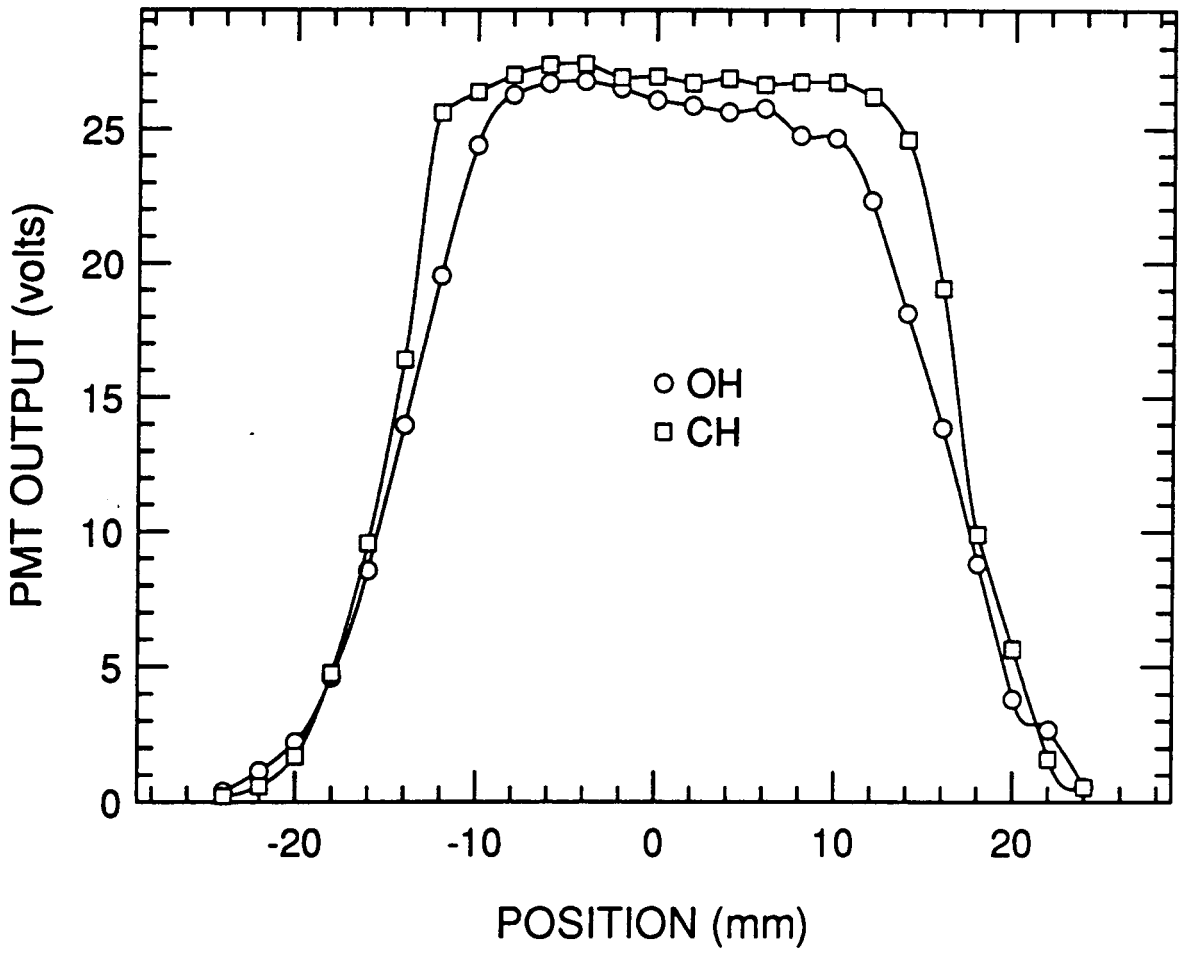

Figure 32. Radical measurements for the air atomized Jet-A, magnification = 0.33.

4. DISCUSSION

4.1 Introduction

In this chapter, the trends observed Chapter 3 are examined in more detail. In the first section, a discussion of rise times is given. Then, rise times are determined from the liquid fuel light-off ignition tests. The second section discusses the observed trend of increasing CH signal (as a percentage of OH signal) with decreasing Hydrogen to Carbon ratio (H/C). Finally, in the third section, magnification and position effects are discussed.

4.2 Determination of Rise Times

The original purpose of this work was to develop a fast response light-off detector for flame sensing. It was assumed that the initial combustion reactions that form OH and CH radicals occur on the time scale of a few hundred microseconds to a few milliseconds. Therefore, by monitoring the chemiluminescent emissions from these excited species, light-off of a flame could be detected in a matter of milliseconds.

However, the determination of rise times is ambiguous. What should be used for the initial time frame? When is time zero? What voltage level (10 %, 50 %, 90 % etc. of the average voltage) should be used as a signature of flame presence? These questions need to be answered before a working probe is to be built.

One possible event marking time zero would be when the tesla coil is turned on. This is similar to a pilot selecting the afterburner ignition switch. He needs to know as soon as possible if a successful ignition has occurred. A second possibility is to use the time when the PMT output voltage (indicative of the flame) becomes a continuous non-zero value.

The second method was chosen for this analysis because it is not believed that the tesla coil accurately simulates an afterburner ignition system. While the tesla coil does supply a large voltage, it does so at very low current.

To calculate a rise time, a reference voltage is needed. For the liquid fuel tests this value was calculated by averaging the steady-state values from the light-off ignition tests. Once the voltages became non-zero (and stayed non-zero) all voltages after that time were used to calculate the average voltage. Compared to a light-off ignition test, a steady-state OH or CH level is never obtained in the intermittent light-off ignition tests. This confirms that a steady-state level of OH or CH radical is a signature of a stable flame.

Rise times for the light-off ignition tests were calculated by determining how long it took for the PMT voltage to exceed certain percentages (10 %, 50 %, 90 %, and 100 %) of the calculated average value. Table 6 summarizes typical rise times for hexane and Jet-A fuels, while examining the OH and CH radicals.

If 100 % of the average voltage is used as the indicator of flame presence, the slowest rise time was 7.4 ms for the CH hexane test. The OH hexane test was the fastest, reaching its average level after only 1.9 ms.

If a level of 90 % of the average voltage is used as the indicator of flame presence, the slowest rise time was again for the CH hexane test at 6.53 ms. The OH hexane test again provided the fastest response, at 1.73 ms.

If a 50 % level of the average voltage is used as the indicator of flame presence, the slowest rise time was still due to the CH hexane test at 1.83 ms. The OH hexane test

Table 6. Typical rise times for various levels of the light-off ignition tests.

	Hexane OH	Hexane CH	Jet-A OH	Jet-A CH
File	D4R4	D4R8	D6R3	D6R7
Time for Start of Average (ms)	15.69	28.33	14.46	22.12
Time for End of Average (ms)	79.35	79.35	79.35	79.35
Total Average Time (ms)	63.66	51.02	64.89	57.23
Average Voltage (volts)	21.1	19.6	20.10	23.70
Standard Deviation of Average Voltage	5.39	4.55	4.98	8.00
First Time Average Voltage is Reached (ms)	17.59	35.73	16.75	24.27
100 % Rise Time (ms)	1.9	7.4	2.29	2.15
90 % of Average (volts)	19.0	17.6	18.1	21.30
First Time 90 % of Average is Reached (ms)	17.42	34.86	16.6	24.13
90 % Rise Time (ms)	1.73	6.53	2.14	2.01
50 % of Average (volts)	10.6	9.8	10.1	11.9
First Time 50 % of Average is Reached (ms)	16.91	30.16	16.1	23.67
50 % Rise Time (ms)	1.22	1.83	1.64	1.55
10 % OF Average (volts)	2.11	1.96	2.01	2.37
First Time 10 % of Average is Reached (ms)	16.81	29.38	15.24	23.01
10 % Rise Time (ms)	1.12	1.05	0.78	0.89

again had the fastest response, at 1.22 ms. However, the Jet-A OH and CH signals were not far behind at 1.64 ms and 1.55 ms, respectively.

If a level of 10 % of the average voltage was to be used as the indicator of flame presence, the slowest rise time was now due to the OH hexane signal at 1.12 ms. The CH hexane signal was faster with a response of 1.05 ms. The Jet-A OH signal was the fastest at 0.78 ms, and with the CH signal at 0.89 ms.

In Figure 33 these various levels (10 %, 50 %, 90 % and 100 %) of the Jet-A OH light-off ignition test were applied to the Jet-A light-off ignition and intermittent light-off ignition tests. Figure 34 shows the results of applying the CH levels to its respective tests.

It is obvious from these figures that a 100 % or 90 % level would not be ideal, due to the turbulent nature of the flame. Standard deviations were calculated to examine these turbulent effects. The standard deviations of the four tests shown in Table 6 were 20 % to 33 % of the average voltage level. By using such a high percentage of the average voltage, a signal indicating "No Flame" would be sent to the controller, even though a flame is present. The 50 % level would be a better choice, as it does a better job of compensating for the large fluctuations. It may be possible to use a smaller percentage to obtain a faster response, but this may not be necessary as the 50 % level provides an adequate response time. The 10 % level may be too low because of possible signal noise.

If the 50 % level is selected for flame presence sensing, at worst the signal would be four (4) times faster than a Geiger-Meuller Phototube. Because the phototubes require a 120 Hz signal to indicate a stable flame, at least 8.3 ms is required to fulfill this requirement. Using the 50 % level, all responses were less than 2 ms.

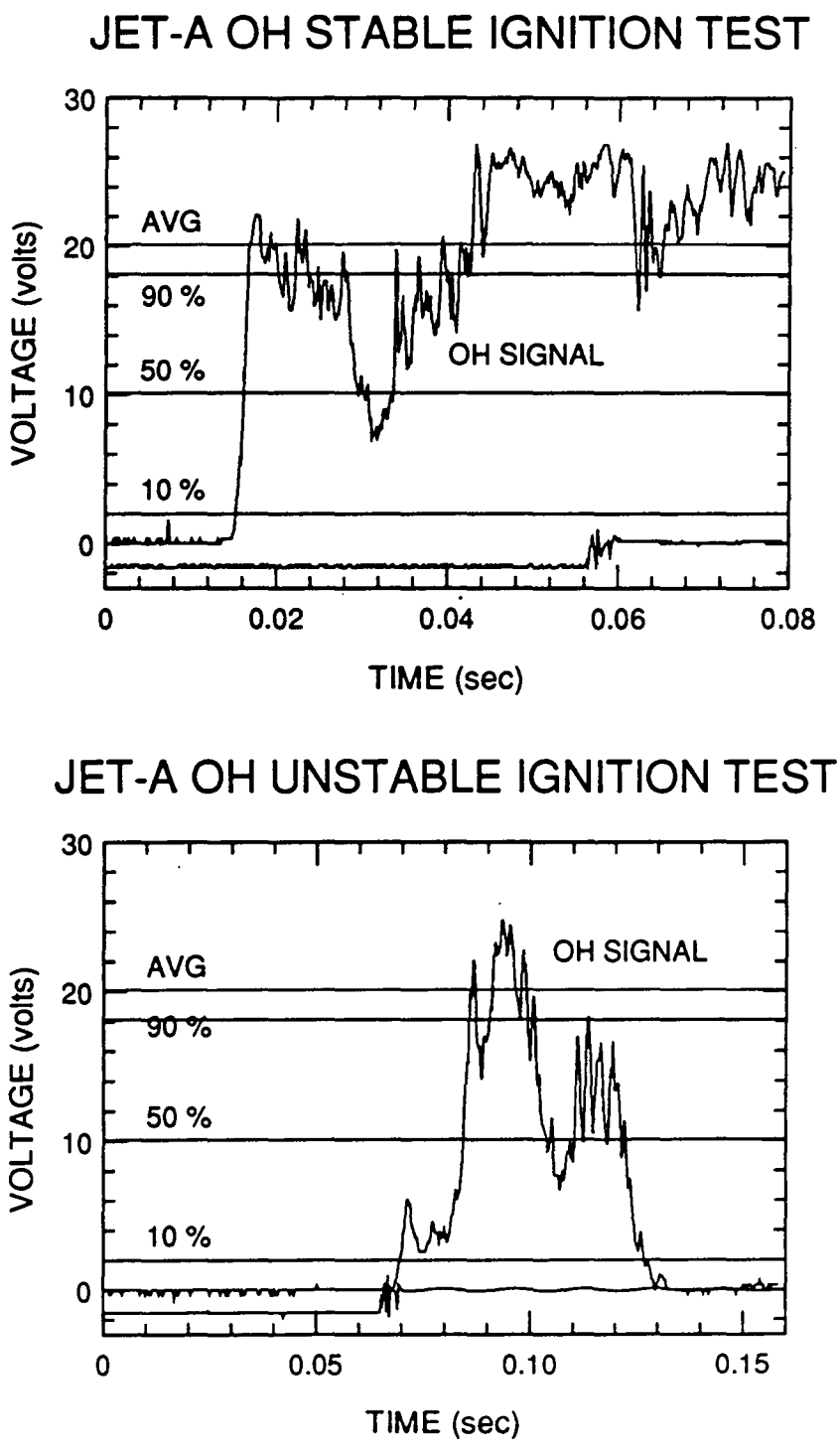

Figure 33. Different Average Levels for OH Jet-A Ignition Tests.

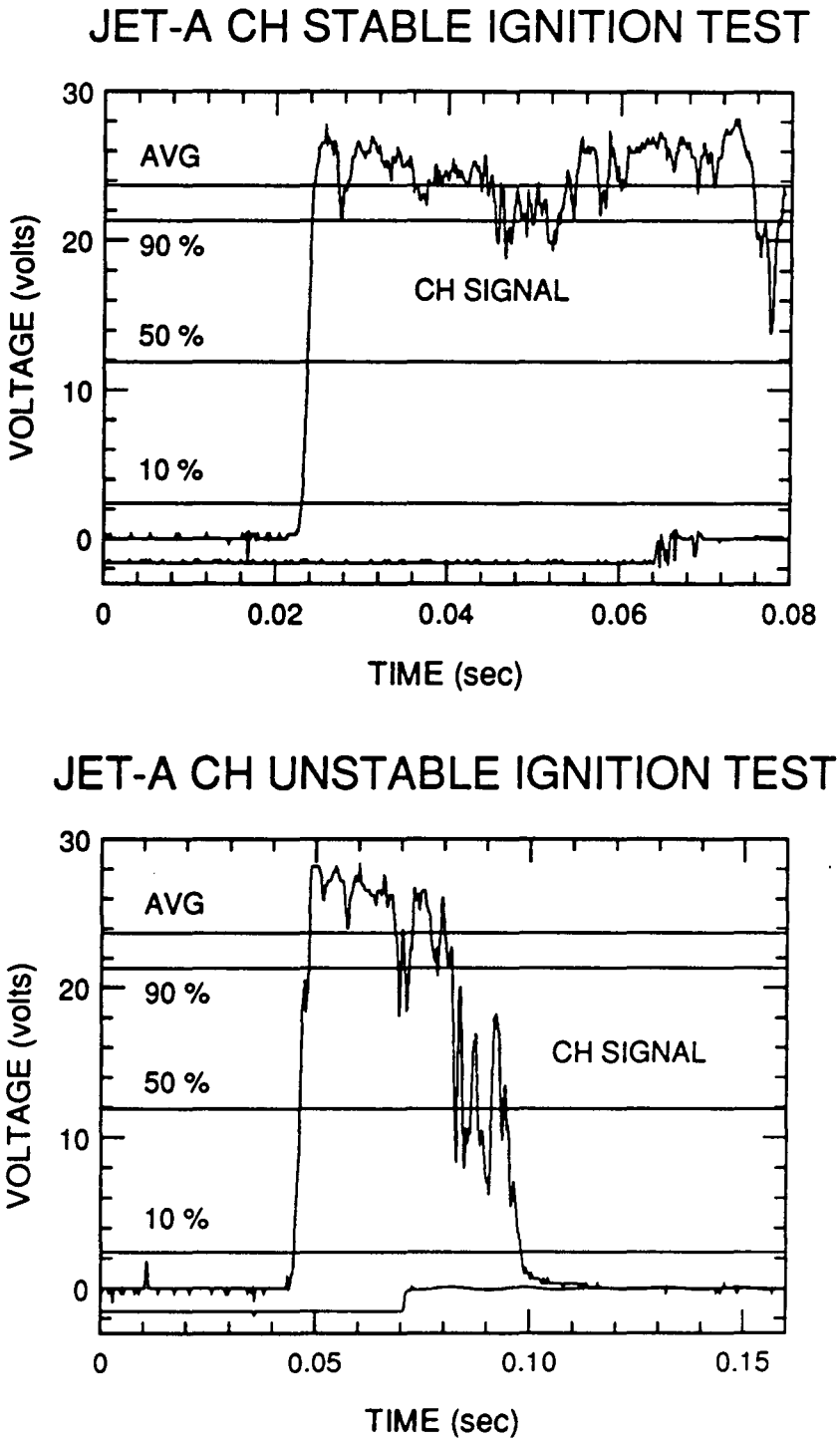

Figure 34. Different Average Levels for CH Jet-A Ignition Tests.

4.3 Repeatability of Tests

The light-off ignition and the intermittent light-off ignition tests produced similar results when multiple runs were performed. Appendix A has the results of sixteen runs of the light-off ignition tests: four hexane OH, four hexane CH, four Jet-A OH and four Jet-A CH. The rise times of these sixteen tests are averaged and summarized in Table 7.

As the table shows, the tests produced very similar results in all runs. The hexane CH tests had the fastest 50 % rise time at 1.05 milliseconds and a standard deviation of 0.47. The hexane OH response time was 1.11 milliseconds with the smallest standard deviation of 0.32. The Jet-A OH tests produced slightly slower response times of 1.44 milliseconds on the average, with a standard deviation of 0.48. Finally, the Jet-A CH produced the slowest response time of 2.61 milliseconds, and the largest standard deviation of 1.10.

4.4 Effect of Hydrogen to Carbon (H/C) Ratio

The full spectral scans performed to identify possible signatures of flame presence were in agreement with previously studied flames [23]. Qualitatively, the same scan was reproduced for different fuels, equivalence ratios, flame magnifications and flame positions.

Four possible signals of ignition were identified by these tests (an OH system, a CH system, and two C_2 systems). However, the OH peak at 309 nm and the CH peak at 430 nm were selected for continued investigation because their emission signals were the strongest observed in all of the flames tested. Also, their signals were deeper in the ultraviolet (UV) range than the C_2 systems where they would not be affected by background radiation in the high temperature environment of an afterburner. This should

Table 7. Average rise times of sixteen light-off ignition tests.

	Hexane OH	Hexane CH	Jet-A OH	Jet-A CH
Average of Four Tests				
100 % Rise Time (ms)	1.55	2.91	2.75	4.38
100 % Rise Time S.D.	0.33	2.61	1.33	2.24
Average of Four Tests				
90 % Rise Time (ms)	1.46	2.56	2.63	4.03
90 % Rise Time S.D.	0.32	2.30	1.30	2.31
Average of Four Tests				
50 % Rise Time (ms)	1.11	1.05	1.44	2.61
50 % Rise Time S.D.	0.32	0.47	0.48	1.10
Average of Four Tests				
10 % Rise Time (ms)	0.47	0.56	0.73	1.37
10 % Rise Time S.D.	0.38	0.30	0.36	0.65

provide a good signal-to-noise ratio since, in an afterburner, most of the broadband background emissions are in the infrared and visible wavelengths.

The results of the methane full spectral scan showed that the CH signal was about 40 % the intensity of the OH signal intensity. This led to an initial belief that the OH radical should be used as the signal to detect light-off as it was the stronger signal. However, it should be noted that the Hydrogen to Carbon ratio (H/C) of methane is 4:1. As liquid fuels are more realistic to those used in jet engines, they were investigated next. The results of the hexane full spectral scan showed that the CH signal had increased to about 82 % the intensity of the OH signal. The H/C ratio of hexane is 2.33:1. Finally, in the Jet-A full spectral scan test, the CH signal was about 13 % stronger than the intensity of the OH signal. The H/C ratio of Jet-A is about 1.8:1.

It appeared that as the H/C ratio of the fuel tested was decreased, the CH signal intensity (as a percentage of the OH signal intensity) increased. Therefore, for fuels used in actual jet engines, the CH radical may be just as valuable, if not more so, than the OH radical in detecting light-off.

After the next three tests were performed (light-off ignition, intermittent light-off ignition and magnification), the same pattern was evident. These results are summarized in Table 8. Burning methane produced average CH signals that were 36 % the intensity of the OH signals. Burning hexane produced average CH signals that were 87 % the intensity of the OH signals. Burning methane produced average CH signals that were 110 % the intensity of the OH signals.

In order to further investigate this trend, a computer simulation was performed to compare the experimental findings with a computational kinetics model of the flame reactions. Two models were investigated, methane (CH_4) and acetylene (C_2H_2). These

Table 8. Test results showing effect of H/C ratio on OH and CH concentrations.

Test	Methane H/C = 4:1			Hexane H/C = 2.33:1			Jet-A H/C = 1.8:1		
	OH (volts)	CH (volts)	CH/OH (%)	OH (volts)	CH (volts)	CH/OH (%)	OH (volts)	CH (volts)	CH/OH (%)
Air Scan	4.1	1.6	39	28	23	82	23	26	1.13
N2 Scan	---	---	---	22	15	68	23	27	1.17
Stable	---	---	—	21.1	19.6	93	20.1	23.7	1.18
M=2 peak	1.75	.55	31	16	14.5	91	17	18.5	1.09
M=2 plateau	.9	.3	33	9	8	89	9.5	10	1.05
M=1.5 peak	3.2	1.1	34	---	---	---	---	---	---
M=1.5 plateau	1.8	.6	33	---	---	---	---	---	---
M=1 peak	5	1.9	38	27	25	93	23	24.5	1.07
M=1 plateau	3	1.1	37	25	23	92	17	18.5	1.09
M=0.67 peak	6.8	2.6	38	---	---	---	---	---	---
M=0.67 plateau	5	1.8	36	---	---	---	---	---	---
M=0.33 peak	7.8	2.8	36	26	23	88	26	27	1.04
M=0.33 plateau	7.8	2.8	36	26	23	88	26	27	1.04
AVERAGE			36			87			1.10

models were chosen because their H/C ratio range (4:1 to 1:1) covered the experimental H/C ratio range (4:1 to 1.8:1). The model for burning methane contained 130 reactions and 28 species [35]. The model for burning acetylene contained 103 reactions and 26 species [36]. The code used for obtaining results from the kinetics models, CHEMKIN [37], is a shell program which provides the necessary thermochemical data and a reaction interpreter to utilize an ordinary differential equation solver. The CHEMKIN model requires as input: reaction pressure, flow rate, equivalence ratio, length of run, step size and flame temperature profile. For output, CHEMKIN provides species concentrations as a function of time. The code provides a way to examine the trends and time scales of complex chemically reacting systems.

Figure 35 shows OH and CH concentration versus time for stoichiometric mixtures of both fuels. Adiabatic flame temperatures, calculated from STANJAN [38], were used for isothermal flame temperature profiles. (Flame temperatures can be seen in Appendix B.) The figure shows that the maximum concentrations of OH are nearly equal for both fuels. However, the maximum acetylene CH concentration is nearly thirty (30) times greater than that produced by the methane. This computational model agrees with the experimental results; as the H/C ratio of the fuel decreases, CH concentration as a percentage of OH concentration increases. Figure 36 shows OH and CH maximum concentration versus equivalence ratios (Concentration versus time can be seen in Appendix C). The figure shows the same results were obtained for different equivalence ratios and flame temperatures. From this figure, the OH levels are of the same order of magnitude, while the CH level for acetylene is about thirty (30) to 1000 times greater than the methane produced CH concentration.

In both of the models, two factors were varied with each run, the type of fuel and the flame temperature profiles. Therefore, to see if the increase in CH production was

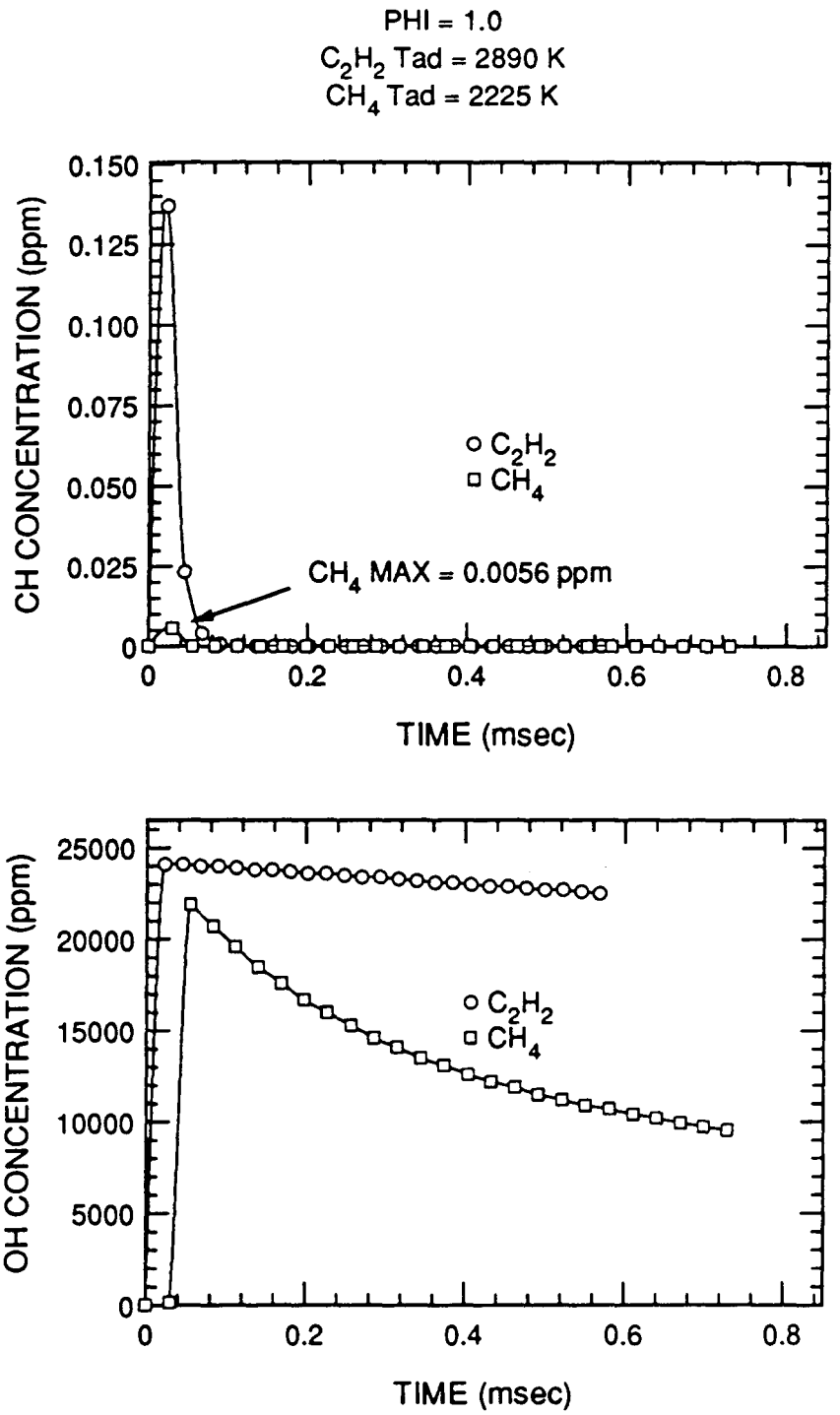

Figure 35. CHEMKIN OH and CH Concentrations Versus Time for Methane and Acetylene, PHI = 1.0.

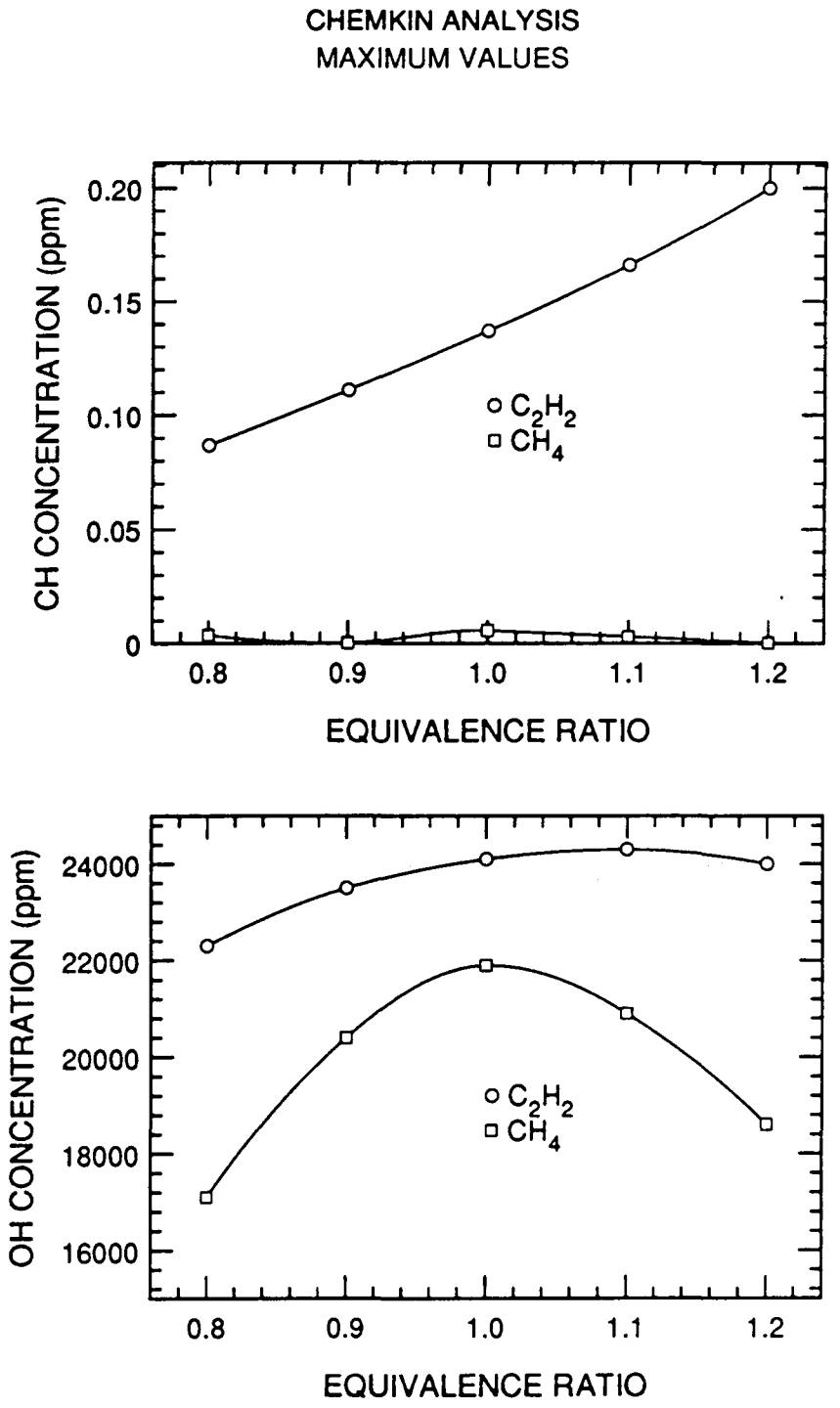

Figure 36. CHEMKIN OH and CH Concentrations Versus Equivalence Ratio for Methane and Acetylene, Maximum Values.

due to the higher adiabatic flame temperature of acetylene (T = 2600 K), the acetylene model was run again using the methane adiabatic flame temperature (T = 2225 K). Figure 37 shows that the acetylene OH production decreased 25 % with the lower flame temperature, while the CH production increased 20 %. However, the CH production is still thirty (30) times greater for the acetylene than the CH produced by methane at the same temperature. The OH production is still about the same for methane and acetylene. Therefore, it is believed that the increase in CH production (as a percentage of OH production) is due to the decreasing H/C ratio, and not the increased flame temperature.

Further tests must be performed to determine which signal, or both, should be monitored for light-off detection. However, OH has the advantage over CH in that its radiation is emitted from deeper in the UV spectrum where background radiation will not be a problem.

4.5 Magnification and Position Effects

As expected, the output signal voltages were found to be sensitive to the flame image magnification and the position of the flame under observation. The maximum voltages were found to occur at the position which corresponded to the edges of the flame. This is because a greater volume of the annular flame was being scanned. Figure 38 shows a top of view of the methane flame for two cases: A) when the volume to be imaged onto the monochromator entrance slit is in the middle of the flame, and B) when the volume to be imaged is on the edge of the flame. As expected, the Z position for Figure 38 B) corresponded to higher output voltages.

The smaller magnifications (0.33 and 0.67) were found to be broader than the larger magnifications (3/2 and 2.0). This means it took more Z positions to scan completely across the flame, because those changes in position (1 mm increments) had a

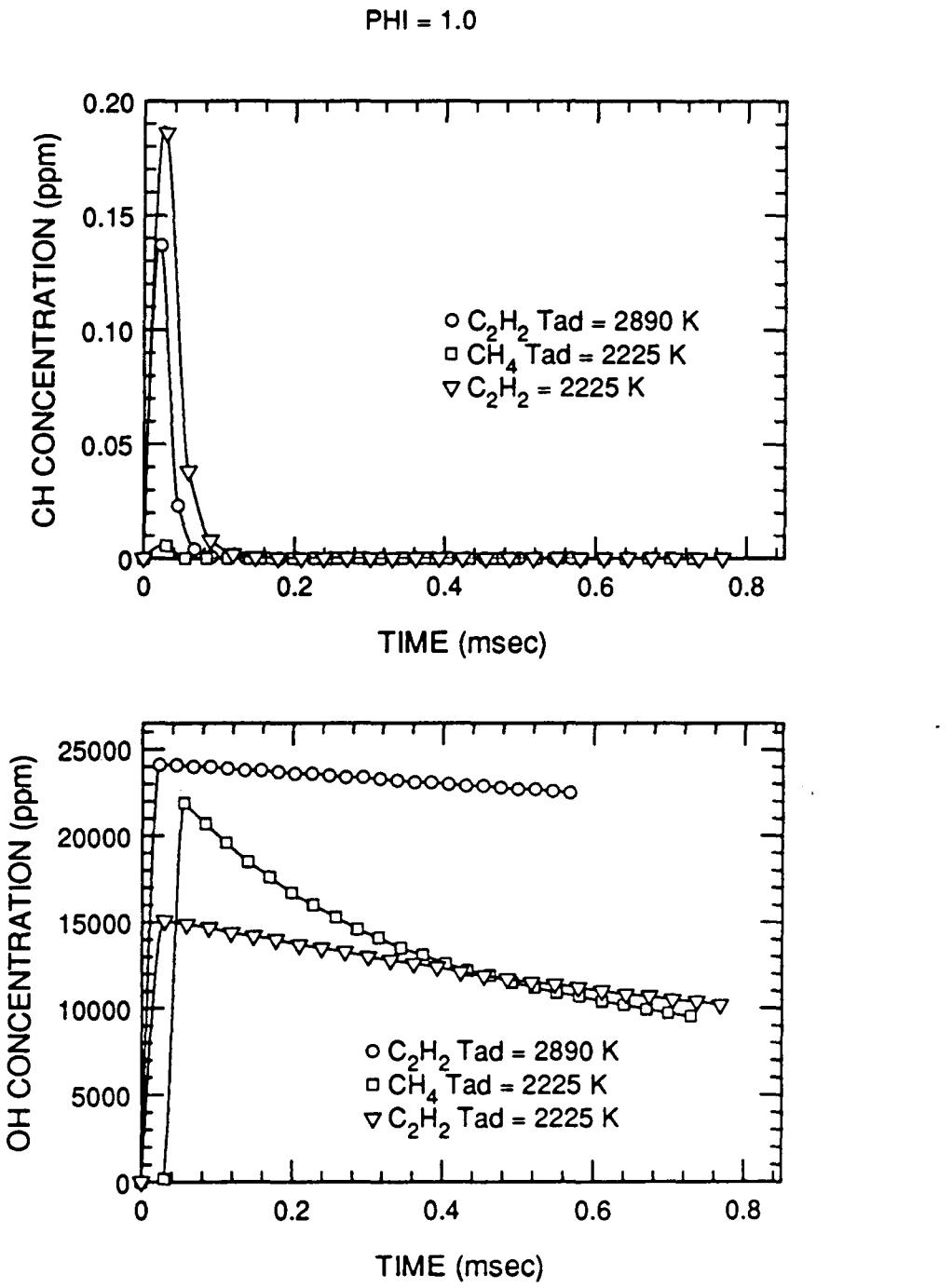

Figure 37. CHEMKIN OH and CH Concentrations Versus Time for Methane at 2225 K, Acetylene at 2225 K and 2890 K.

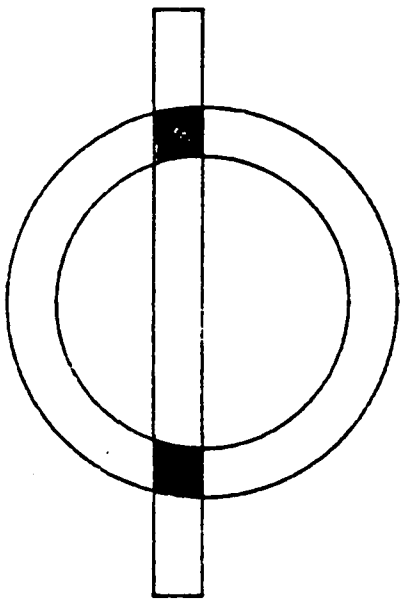

Volume to be
Imaged onto
Monochromator
Entrance Slit

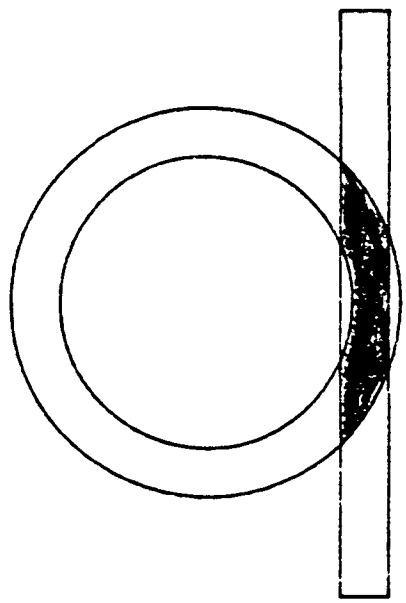

Volume to be
Imaged onto
Monochromator
Entrance Slit

Figure 38. Top View of an Annular Flame.

smaller effect on moving the flame image at the monochromator entrance slit. For example, the Jet-A magnification of 2.0 took twenty-eight (28) increments to completely scan across the flame, while the 0.33 magnification took forty-eight (48) increments.

Figure 39 shows how the PMT voltages for the methane magnification tests varied with magnification. The peak voltages correspond to the average voltage at the two luminous cones. The plateau voltage is the average of the points between the peaks. As the magnifications decreased from 2.0, the two luminous cone peaks grew closer together until at the 0.33 magnification, they disappeared completely. This is because the flame image resolution has been reduced.

The figure shows that the 0.33 magnification, compared to the 2.0 magnification, produced voltages about four (4) times greater for the OH peak voltage and about eight (8) times greater for the OH plateau voltage. The CH peak and plateau voltages were about three (3) times greater when comparing the two magnifications. The smaller magnifications have these greater PMT outputs because a greater amount of light is being imaged into the same input slit area.

However, it is not believed that as the magnification is decreased the voltage will continue to increase indefinitely. As was shown in Table 1, as the magnification was decreased, the distance between the flame and the lens (S_o) increased for a fixed focal length. As this happens a smaller volume of light (in steradians) is collected, and this will eventually over compensate for the greater amount of light being focused onto the same input slit area. Also, once the magnification is so small that the whole flame fits into the input slit, further flame image reductions will have little effect.

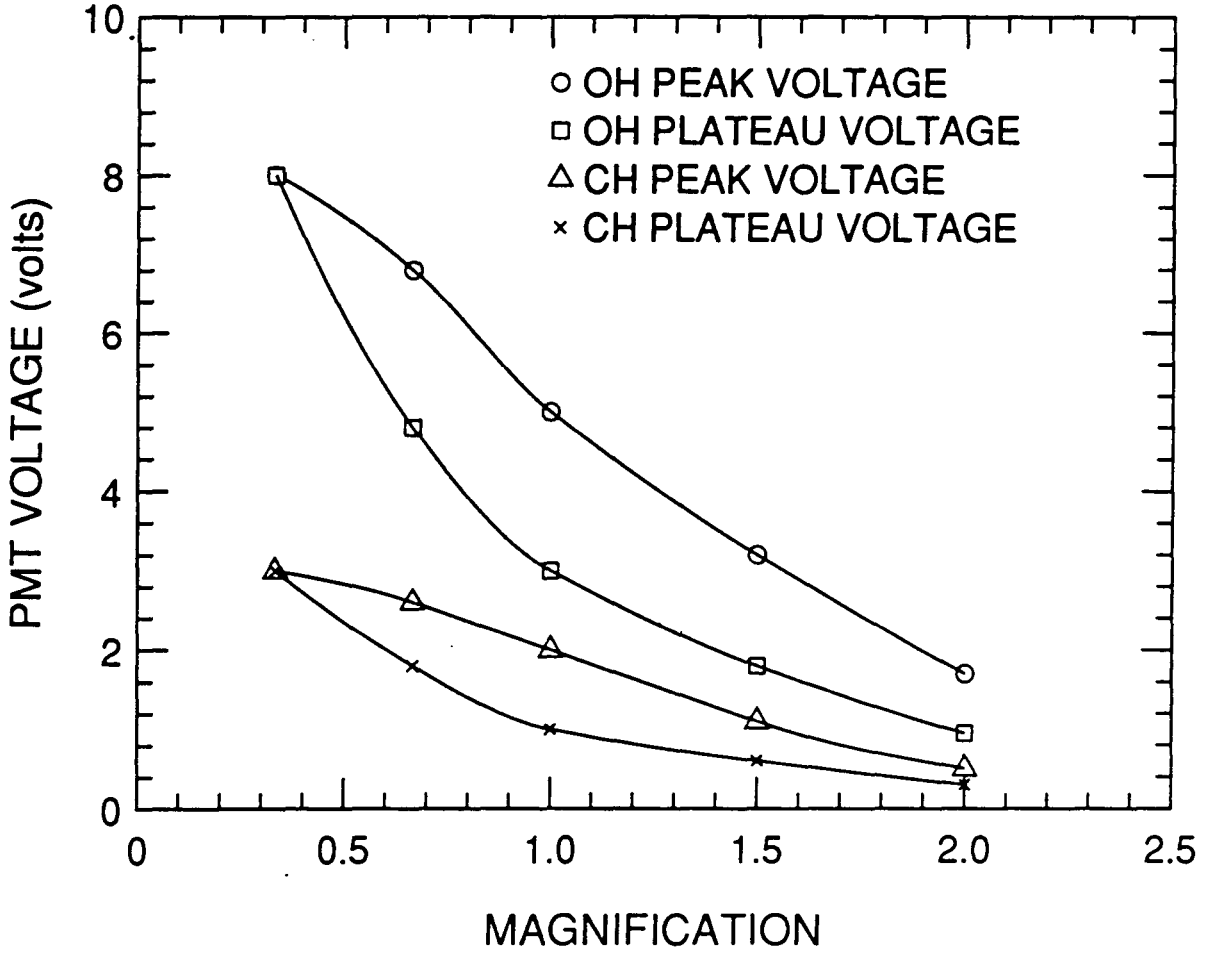

Figure 39. PMT Output Voltage Versus Magnification.

These results show the importance of observing the correct flame location and magnification to obtain the maximum signal possible. To obtain the maximum voltage possible, observations should on the peak location of a small flame image magnification.

5. SUMMARY AND CONCLUSIONS

5.1 Summary

In Chapter 1, a six (6) step process was given to develop a practical working probe. A summary of important results for each step is given below.

1) After performing spectral scans from 280 nm to 610 nm, three species were determined to be possible candidates for flame sensing, OH, CH and C_2. The head of the OH system at 309 nm and the head of the CH system at 430 nm were found to be much stronger signals than the heads of the C_2 systems at 470 nm and 515 nm.

2) Light-off ignition tests and intermittent light-off tests showed that both signals were good indicators of flame presence.

3) Signal intensity was found to be sensitive to flame image magnification and flame position under observation.

4) Probe weight, volume and system complexity may be reduced by replacing the photomultiplier tube with a narrow band interference filter and the monochromator with a photodiode. A possible experimental setup is discussed in Section 5.2.1.

5) Implement fiber optic cable to transport light to a remotely located detector. A possible experimental setup is discussed in Section 5.2.2.

6) Future experiments to optimize the probes effectiveness and practicality are given in Section 5.2.3.

5.2 Recommendations

5.2.1 Photodiode Experimental Setup

The next step in developing a working probe is do reduce the probe's weight, volume and system complexity by replacing the monochromator with a narrow band interference filter and the photomultiplier tube with a photodiode.

A possible schematic for a photodiode detector is shown in Figure 40. The figure shows the flame image being projected through the fused silica lens and onto a narrow

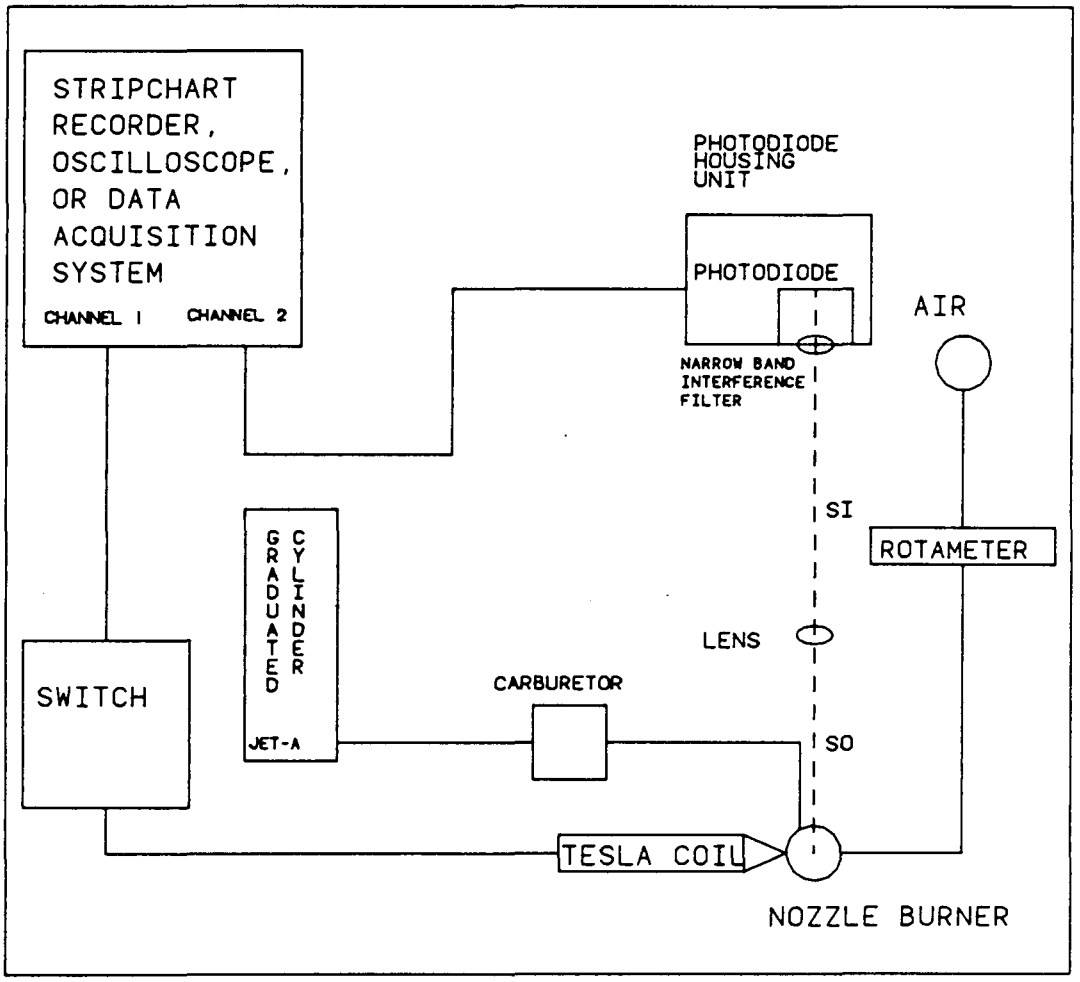

Figure 40 Photodiode Detector Experimental Apparatus.

band interference filter. These filters only allow light of a specific wavelength to pass through and reach the photodiode.

To investigate the OH radical at 310 nm an Oriel 53375 narrow band interference filter should be used. To investigate the CH radical at 430 nm an Oriel 53815 narrow band interference filter should be used. Figure 41 shows the transmission curves of these filters. For example, the figure shows that the CH filter is centered at the systems "head", or line, at 430 nm, however, this filter also allows other lines (from about 422 nm to about 438 nm) of the CH system to pass to the photodiode. These wavelengths are nearly exculsive to the CH system (there is a very weak O_2 system at 429 nm, and a weak O_2 system at 438 nm [22]).

To detect the amount of light present, an unbiased photovoltaic photodiode detector (Oriel model 7181) should be used. The photodiode, which is mounted in a housing (Oriel model 71920), has a spectral range of 200 nm to 1100 nm, a photosensitive area of 5 mm^2, and a rise time of 75 nanoseconds. The photodiode creates a voltage proportional to the intensity of the light present which may be measured by the Nicolet 4094C Digital Oscilloscope.

5.2.2 Fiber Optic Detector Experimental Setup

After the probes size has been reduced with the photodiode detector, a fiber-optic cable should be used to transport the light. For the fiber optic light-off detector, a collimating beam probe is used to collect radiant energy from the flame and focus it onto the entrance face of the fiber optic cable. The light travels through the fiber optic bundle, passes through a narrow band interference filter and onto a photodiode. The photodiode creates a voltage proportional to the intensity of the light present.

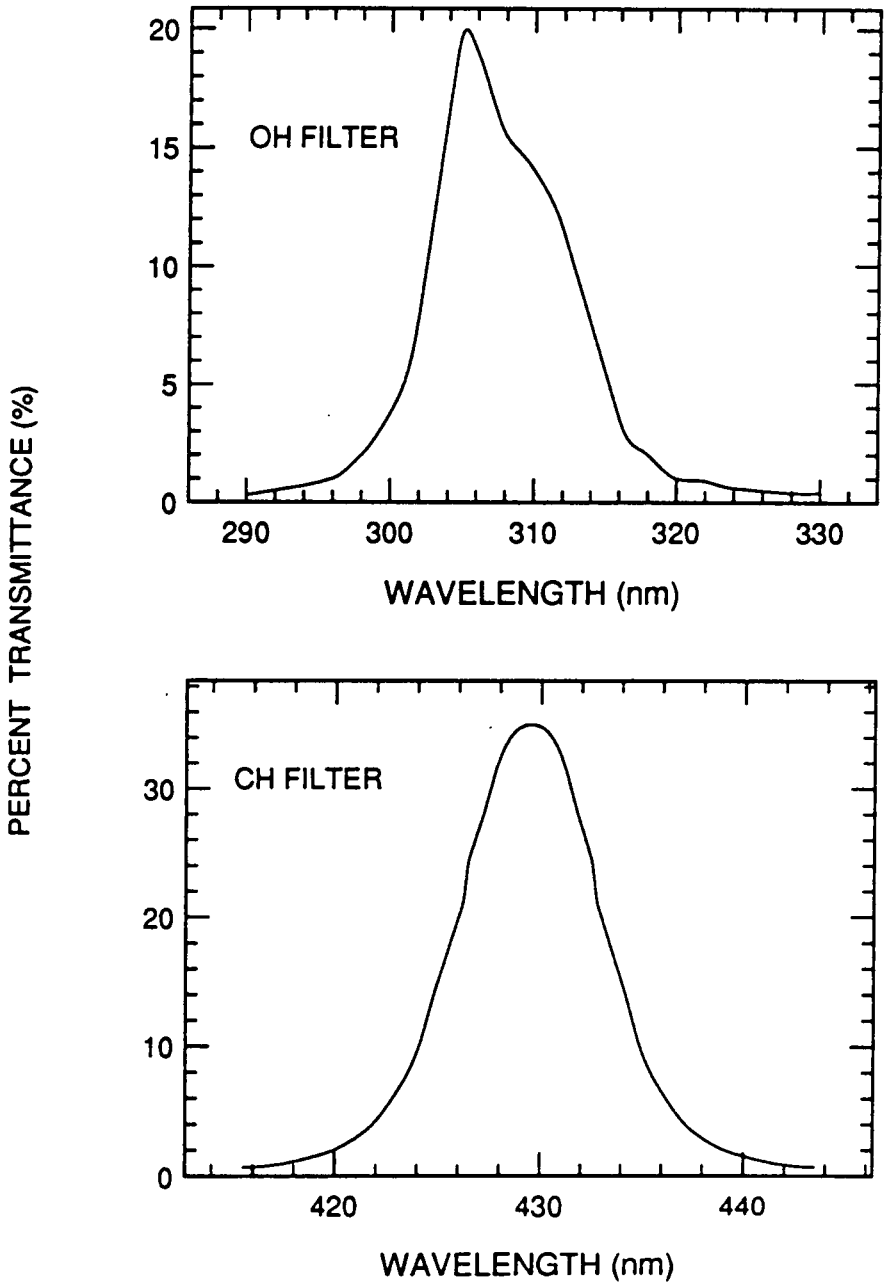

Figure 41 Transmission Curves for OH and CH Narrow Band Interference Filters.

To collect radiant energy from the spray flame, a collimating beam probe (Oriel model 77644) should be used to focus the radiant energy onto the entrance face of the fiber optic bundle. The collimating probe contains an 11 mm diameter, 19 mm focal length fused silica plano convex lens.

The fused silica fiber optic bundle (Oriel model 77562) has a numerical aperture (NA) of 0.27, an acceptance cone 2a of 31 degrees, and transmits light from 280 nm to 2200 nm.

Once the light passes through the fiber, it enters a second collimating probe before it is filtered by a 1 inch diameter narrow band interference filter. To investigate the OH radical at 310 nm an Oriel 53375 filter is used, while an Oriel 53815 filter is used to investigate the CH radical at 430 nm.

5.2.3 Future Experiments

1) One of the first experiments should be to use the fiber optic probe described in 5.2.1 to transport light to a remote detector. The stable and unstable ignition tests should be performed again to investigate light attenuation caused by the fiber optic cable. Next, the positioning of the first collimating beam probe should be varied to find the optimal position to obtain the maximum output signal.

2) The next step should be to use a bifuricated fiber optic cable to transport the same light to two different detectors. The first detector should use the OH narrow band interference filter for light selection, and the other should use the CH narrow band interference filter. By repeating the transient tests, it should be possible to determine which species gives the fastest response.

3) Next the bifuricated cable should be used to test the photomultiplier tube and photodiode for response times. By using the bifuricated cable you guarantee that the

same flame location is being observed. The PMT should provide the faster response time as it has a slightly shorter rise time.

4) For stationary gas turbines, minimizing space is not as critical as it is for aircraft. The possibility of using a narrow band interference filter with a photomultiplier tube for gas turbines should be examined. The photomultiplier tube is more responsive and has a faster rise time than a photodiode. Also, the filter costs about 1 % of the monochromator.

5) The probe should be tried on different fuels - diesel fuel, gasoline, various jet fuels. This is in order to test for radical presence, concentrations, and proportions.

6) Test the probe on a pressurized flame, as this is more realistic to a real combustion device, to investigate for radical presence, concentrations, and proportions.

7) A test of the probe should be run on an actual afterburner while positioned on a test stand. Murphey, Jones and Jones [21] developed a fiber optic based jet engine augmentor viewing system which would allow for convenient probe testing.

8) A GRIN lens (Graded Index of Refraction) should be tried at the entrance of the collimating beam probe to maximize signal.

10) A new plano-convex lens within the collimating probe should be investigated to maximize signal.

5.3 Conclusions

A method for detection of light-off in liquid spray flames has been developed. The method uses chemiluminescent signals from OH and CH radicals to indicate the presence of a flame. The method was successfully tested on methane, hexane and Jet-A. Light-off ignition tests and intermittent light-off tests showed that both signals (OH and CH) were good indicators of flame presence, showing a response time of less than 2 milliseconds.

The strength of the CH signal (as a percentage of the OH signal) was found to be a function of the H/C ratio of the fuel tested. As the H/C ratio of the fuel decreased, the CH signal intensity increased. This trend was also seen by the chemical kinetics code CHEMKIN when acetylene and methane were investigated.

Signal intensity was found to be sensitive to flame image magnification and flame position under observation. Small magnifications and the luminous cone peaks provided the highest output signal voltages.

REFERENCES

1) Yates, T. C., and Smith, T. S., "Pumping Systems and Flow Interfaces for Rapid Response Electronic Reheat Controls," AGARD Conference Proceedings No. 421, Advanced Technology for Aero Gas Turbine Components, Paris, France, 4-8 May 1987.

2) Vleghert, J. P. K., "Deterioriation in Service of Engine Transient Behavior," AGARD Conference Proceedings No. 324, Engine Handling, Marathon, Attika, Greece, 11-14 October 1982.

3) Bauerfeind, I. K., "Some General Topics in the Field of Engine Handling," AGARD Conference Proceedings No. 324, Engine Handling, Marathon, Attika, Greece, 11-14 October 1982.

4) Sotheran, A., "High Performance Turbofan Afterburner Systems," AGARD Conference Proceedings No. 422, Combustion and Fuels in Gas Turbine Engines, Chania, Crete, Greece, 19-23 October 1987.

5) Stetson, H. D., "Designing for Stability in Advanced Turbine Engines," AGARD Conference Proceedings No. 324, Engine Handling, Marathon, Attika, Greece, 11-14 October 1982.

6) Skirak, C. A., De Hoff, R. L., and Hall, W. E., "Design, Evaluation and Test of an Electronic, Multivariable Control for the F100 Turbofan Engine," AGARD Conference Proceedings No. 274, Advanced Control Systems for Aircraft Powerplants, DFVLR, Cologne, Germany, 1 & 2 October 1979.

7) Gothan, G., and Sievers, H., "Flight Test Experience on Military Aircraft Engine Handling," AGARD Conference Proceedings No. 324, Engine Handling, Marathon, Attika, Greece, 11-14 October 1982.

8) Bakker, J. T., and Huurman, C., "Operational and Maintenance Aspects of the Introduction of an Advanced Fighter Type," AGARD Conference Proceedings No. 324, Engine Handling, Marathon, Attika, Greece, 11-14 October 1982.

9) Patterson, G. T., "Techniques for Determining Engine Stall Recovery Characteristics," AGARD Conference Proceedings No. 324, Engine Handling, Marathon, Attika, Greece, 11-14 October 1982.

10) Porter, M. J., "A New Approach to Reheat Control," AGARD Conference Proceedings No. 324, Engine Handling, Marathon, Attika, Greece, 11-14 October 1982.

11) Kurkov, A. P., "Turbofan Compressor Dynamics During Afterburner Transients," AGARD Conference Proceedings No. 177, Unsteady Phenomena in Turbomachinery, 22-26 September 1975.

12) McAulay, J. E., and Abdelwahab, Mahmood, "Experimental Evaluation of a TF30-P-3 Turbofan Engine in an Altitude Facility: Afterburner Performance and Engine-Afterburner Operating Limits." NASA TN D-6839, 1972.

13) Treager, I. E. Aircraft Gas Turbine Engine Technology, Second Edition, New York, New York, McGraw-Hill Book Company, 1979.

14) Morey, W. W., "Investigation of Combustion Process using Fiber Optics," UTRC Final Report to Naval Air Systems Command R81-925172-4, 1981.

15) Morey, W. W., "Hot Section Viewing Systems," NASA CR-174773, 1984.

16) Morey, W. W. and Angello, L. C., "Diagnostics from Imaging Inside Gas Turbine Combustors," Proc. SPIE Vol. 665., 1986, pp. 306-313.

17) Morey, W. W., "Utility Gas Turbine Combustor Viewing System," Final Report EPRI AP5956, Vol. 1 and Vol. 2, 1988.

18) Morey, W. W., Quentin, G. H., and Angello, L. A., "Fiber Optic Probe for Flame Monitoring in Gas Turbine Combustors," American Society of Mechanical Engineers 89-GT-49, Gas Turbine and Aeroengine Congress and Exposition, Toronto, Ontario, Canada, June 4-8, 1989.

19) Cohen, L. M., Gat, N., and Witte, A. B., "Start-of-Ignition Sensor for a Diesel Engine," Combustion Science and Technololgy, vol. 42, pp. 211-216, 1985.

20) Zoia, D., and Inoue, M., "Combustion Sensors; Push for New Technology is Growing", WARD'S Auto World, 9-88 Detroit, Michigan.

21) Murphy, P. J., Jones, D. W., and Jones, R. R., "Fiber Optics Based Jet Engine Augmenter Viewing System," ASME, Gas Turbine and Aeroengine Congress and Exposition, Amsterdam, Netherlands, 6-9 June, 1988, ASME Paper 88-GT-320.

22) Gaydon, A. B., The Spectroscopy of Flames, Second Edition, Chapman and Hall, New York, (1974).

23) Beyler, C. L., Flame Structure and Stabilization in Premixed Swirl-Stabilized Combustion, M. S. Thesis, Cornell University, Ithaca, New York (1981)

24) Peeter, J., Lambert, J., Hertoghe, P. and Van Tiggelen, A., "Mechanism of C_2^* and CH^* Formation in a Hydrogen-Oxygen Flame Containing Hydrocarbon Traces," Thirteenth Symposium (International) on Combustion, The Combustion Institute, p. 321 (1971).

25) Heffington, W., Parks, G., Sulzman, K. and Penner, S., "Studies of Methane-Oxidation Kinetics, " Sixteenth Symposium (International) on Combustion, The Combustion Institute, p. 997 (1977).

26) Bowman, C. T. and Seery, D., "Chemiluminescence in the High-Temperature Oxidation of Methane," Combution and Flame, vol 12, p. 611 (1968).

27) Kaskan, W., "The Source of the Continuum in Carbon Monoxide-Hydroge-Air Flames," Combustion and Flame, Vol. 3, p. 39 (1959).

28) Gaydon, A., "The Use of Shock Tubes for Studying Fundamental Combustion Processes," Eleventh Symposium on Combustion, The Combustion Institute, p. 321 (1971).

29) Porter, R., Clarke, A., Kaskan, W., Brown, W., "A Study of Hydrocarbon Flames," Eleventh Symposium on Combustion, The Combustion Institute, p. 907 (1967).

30) Child, E., Wohl, K., "Spectrophotometric Studies of Laminar Flames - I, The Decay of Radical Radiation," Seventh Symposium on Combustion, The Combustion Institute, p. 215 (1959).

31) Kashida, R., Wohl, K., "Spectrophotometric Studies of Laminar Flames, The Flame Front," Seventh Symposium on Combustion, The Combustion Institute, p. 221 (1959).

32) Schott, G. L., Journal of Chemical Physics, Vol. 32, p. 710, 1960.

33) Lyon, R. K., and Kydd, P. H., Journal of Chemical Physics, Vol. 34, p. 1069, 1961.

34) Wirth, D. A., Soot Formation in Vitiated-Air Diffusion Flames, M. S. Thesis, Virginia Polytechnic Institute and State University, Blacksburg, VA (1989).

35) Kee, R. J., Miller, J. A., Evans, G. H., and Dixon-Lewis, G., Twenty-Second Symposium (International) on Combustion, The Combustion Institute, Pittsburgh, PA (1989).

36) Thorne, L. R., Branch, M. C., Chandler, D. W., Kee, R. J., and Miller, J. A., Twenty-First Symposium (International) on Combustion, The Combustion Institute, Pittsburgh, PA (1987).

37) Kee, R. J., Miller, J. A., and Jefferson, T. H., "CHEMKIN: A General-Purpose Problem-Independent, Transportable, Fortran Chemical Kinetics Code Package," Sandis Report SAND80-8003 (1980).

38) Reynolds, W. C., STANJAN Chemcal Equilibrium Solver, Version 2.38, Stanford University, Stanford, California, (1987).

Appendix A.

This Appendix contains the results of sixteen light-off ignition tests: four hexane OH, four hexane CH, four Jet-A OH and four Jet-A CH. Rise times for the four levels (10 %, 50 %, 90 % and 100 %) of the average voltage were calculated. Standard deviations of that average voltage was also calcualted.

HEXANE OH

File	D4R2	D4R3	D4R4	D4R5	Avg	S.D.
Time for Start of Average (ms) *	11.14	8.80	15.69	15.56		
Time for End of Average (ms)	79.35	79.35	79.35	79.35		
Total Average Time (ms)	68.21	70.55	63.66	63.79		
Average Voltage (volts) *	18.30	18.30	21.10	17.6	18.80	1.34
Standard Deviation ** of Average Voltage	8.05	8.17	5.39	5.39		
Number of Points for S.D. of Average Voltage	6728	6910	6194	6209		
First Time Average Voltage is Reached (ms)	12.16	10.32	17.59	17.30		
100 % Rise Time (ms)	1.02	1.52	1.90	1.74	1.55	0.33
90 % of Average (volts)	16.47	16.47	19.0	15.84		
First Time 90 % of Average is Reached (ms)	12.08	10.26	17.42	17.26		
90 % Rise Time (ms)	0.94	1.46	1.73	1.70	1.46	0.32
50 % of Average (volts)	9.15	9.15	10.6	8.80		
First Time 50 % of Average is Reached (ms)	11.82	9.78	16.91	17.12		
50 % Rise Time (ms)	0.68	0.98	1.22	1.56	1.11	0.32
10 % OF Average (volts)	1.83	1.83	2.11	1.76		
First Time 10 % of Average is Reached (ms)	11.40	9.10	16.81	15.74		
10 % Rise Time (ms)	0.26	0.30	1.12	0.18	0.47	0.38

* Average Voltage was calculated from the initial non-zero value (where no other zero values followed) to the end of the scan.

** Standard Deviation was calculated from the first time 90 percent of the average had been exceeded to the end of the scan.

Standard Deviations were calculated using σ_n points, not σ_{n-1}.

HEXANE CH

File	D4R6	D4R7	D4R8	D4R9	Avg	S.D.
Time for Start of Average (ms) *	12.98	7.92	28.33	17.26		
Time for End of Average (ms)	79.35	79.35	79.35	79.35		
Total Average Time (ms)	66.37	71.43	51.02	62.09		
Average Voltage (volts) *	14.28	13.60	19.60	16.49	16.0	2.34
Standard Deviation ** of Average Voltage	6.88	8.14	4.55	5.97		
Number of Points for S.D. of Average Voltage	6508	7051	4449	6077		
First Time Average Voltage is Reached (ms)	14.74	8.90	35.73	18.74		
100 % Rise Time (ms)	1.76	0.98	7.40	1.48	2.91	2.61
90 % of Average (volts)	12.85	12.24	17.60	14.84		
First Time 90 % of Average is Reached (ms)	14.28	8.84	34.86	18.58		
90 % Rise Time (ms)	1.48	0.92	6.53	1.32	2.56	2.30
50 % of Average (volts)	6.49	6.80	9.80	8.25		
First Time 50 % of Average is Reached (ms)	13.48	8.60	30.16	18.28		
50 % Rise Time (ms)	0.68	0.68	1.83	1.02	1.05	0.47
10 % OF Average (volts)	1.30	1.36	1.96	1.65		
First Time 10 % of Average is Reached (ms)	13.18	8.18	29.38	17.82		
10 % Rise Time (ms)	0.38	0.26	1.05	0.56	0.56	0.30

* Average Voltage was calculated from the initial non-zero value (where no other zero values followed) to the end of the scan.

** Standard Deviation was calculated from the first time 90 percent of the average had been exceeded to the end of the scan.

Standard Deviations were calculated using σ_n points, not σ_{n-1}.

JET-A OH

File	D6R1	D6R2	D6R3	D6R4	Avg	S.D.
Time for Start of Average (ms) *	39.98	15.50	14.46	29.25		
Time for End of Average (ms)	79.35	79.35	79.35	79.35		
Total Average Time (ms)	39.37	63.85	64.89	50.10		
Average Voltage (volts) *	16.29	19.01	20.10	13.20	17.15	2.67
Standard Deviation ** of Average Voltage	7.10	4.71	4.98	7.97		
Number of Points for S.D. of Average Voltage	3689	5912	6276	4894		
First Time Average Voltage is Reached (ms)	42.52	20.40	16.75	30.51		
100 % Rise Time (ms)	2.54	4.90	2.29	1.26	2.75	1.33
90 % of Average (volts)	14.66	17.11	18.1	11.88		
First Time 90 % of Average is Reached (ms)	42.47	20.23	16.6	30.42		
90 % Rise Time (ms)	2.49	4.73	2.14	1.17	2.63	1.30
50 % of Average (volts)	8.15	9.51	10.1	6.60		
First Time 50 % of Average is Reached (ms)	42.09	16.70	16.1	30.07		
50 % Rise Time (ms)	2.11	1.20	1.64	0.82	1.44	0.48
10 % OF Average (volts)	1.63	1.90	2.01	1.32		
First Time 10 % of Average is Reached (ms)	41.28	15.97	15.24	29.61		
10 % Rise Time (ms)	1.30	0.47	0.78	0.36	0.73	0.36

* Average Voltage was calculated from the initial non-zero value (where no other zero values followed) to the end of the scan.

** Standard Deviation was calculated from the first time 90 percent of the average had been exceeded to the end of the scan.

Standard Deviations were calculated using σ_n points, not σ_{n-1}.

JET-A CH

File	D6R5	D6R6	D6R7	D6R8	Avg	S.D.
Time for Start of Average (ms) *	21.05	29.31	22.12	19.03		
Time for End of Average (ms)	79.35	79.35	79.35	79.35		
Total Average Time (ms)	58.30	50.04	57.23	60.32		
Average Voltage (volts) *	23.14	23.51	23.70	22.45	23.2	0.23
Standard Deviation ** of Average Voltage	3.24	13.09	8.00	4.38		
Number of Points for S.D. of Averge Voltage	5497	4211	5523	5750		
First Time Average Voltage is Reached (ms)	27.24	37.38	24.27	22.23		
100 % Rise Time (ms)	4.10	8.07	2.15	3.20	4.38	2.24
90 % of Average (volts)	20.83	21.16	21.30	20.21		
First Time 90 % of Average is Reached (ms)	24.38	37.25	24.13	21.86		
90 % Rise Time (ms)	3.33	7.94	2.01	2.83	4.03	2.31
50 % of Average (volts)	11.57	11.78	11.9	11.23		
First Time 50 % of Average is Reached (ms)	23.14	33.76	23.67	21.39		
50 % Rise Time (ms)	2.09	4.45	1.55	2.36	2.61	1.10
10 % OF Average (volts)	2.31	2.35	2.37	2.25		
First Time 10 % of Average is Reached (ms)	22.08	31.54	23.01	20.33		
10 % Rise Time (ms)	1.03	2.23	0.89	1.31	1.37	0.52

* Average Voltage was calculated from the initial non-zero value (where no other zero values followed) to the end of the scan.

** Standard Deviation was calculated from the first time 90 percent of the average had been exceeded to the end of the scan.

Standard Deviations were calculated using σ_n points, not σ_{n-1}.

Appendix B.

This Appendix contains the products and reactants considered when calculating adiabatic flame temperatures using the computer code STANJAN. Calculated adiabatic flame temperatures are given for all three fuels and all five equivalence ratios.

Stanjan Adiabatic Flame Temperature Calculations

Reactants: Fuel, O_2, N_2

Fuels: Methane CH_4
Acetylene C_2H_2
Ethene C_2H_4

Products Considered

Fuel, CO, CO_2, H, HO, H_2O, N, NO, N_2, O, O_2

PHI	Methane TAD (K)	Acetylene TAD (K)	Ethene TAD (K)
0.8	1996	2780	2160
0.9	2134	2845	2290
1.0	2225	2890	2370
1.1	2211	2930	2390
1.2	2136	2960	2370

Appendix C.

This Appendix contains the results of the CHEMKIN kinetics model for methane and acetylene. Various equivalence ratios were investigated.

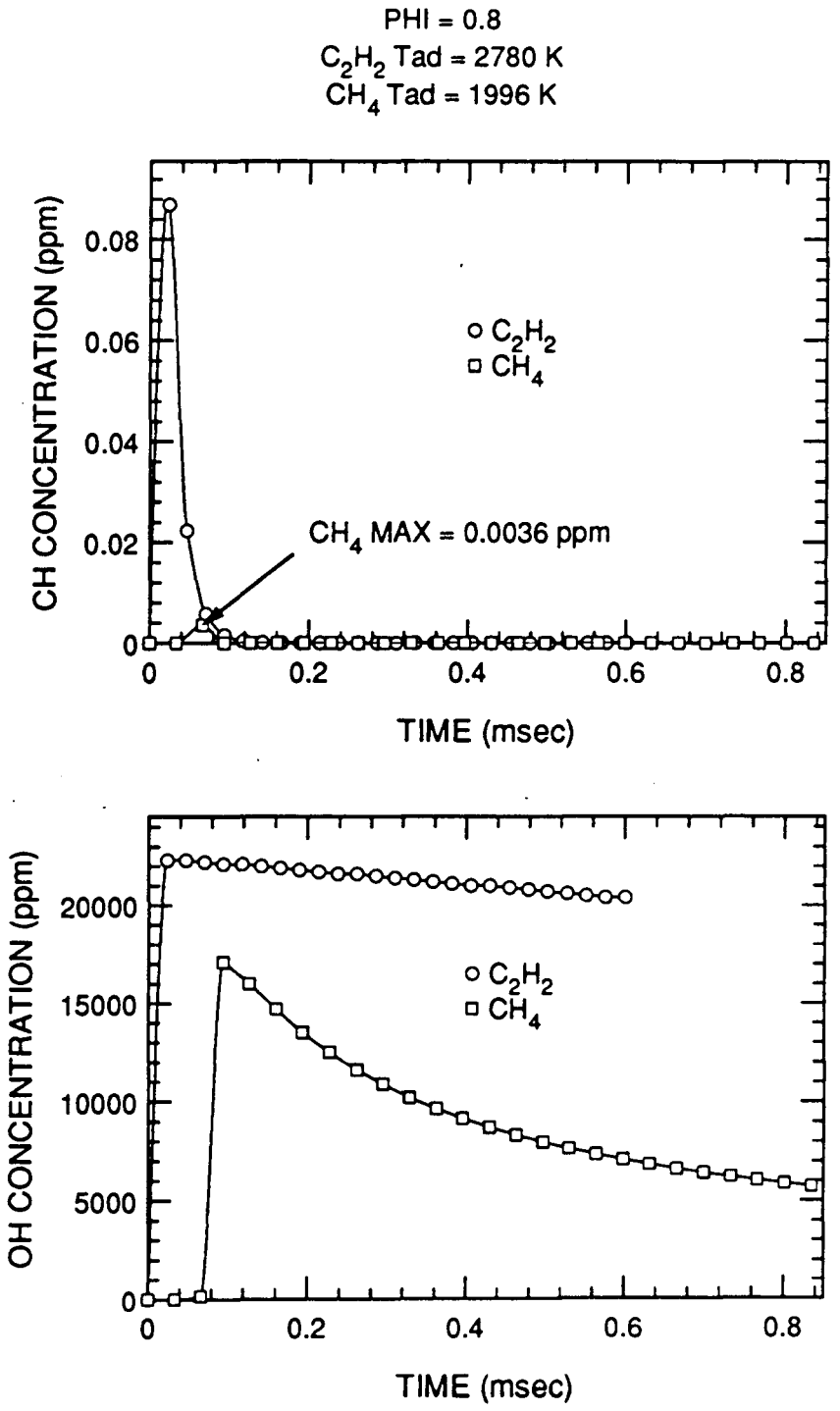

CHEMKIN OH and CH Concentrations Versus Time for Methane and Acetylene, PHI = 0.8.

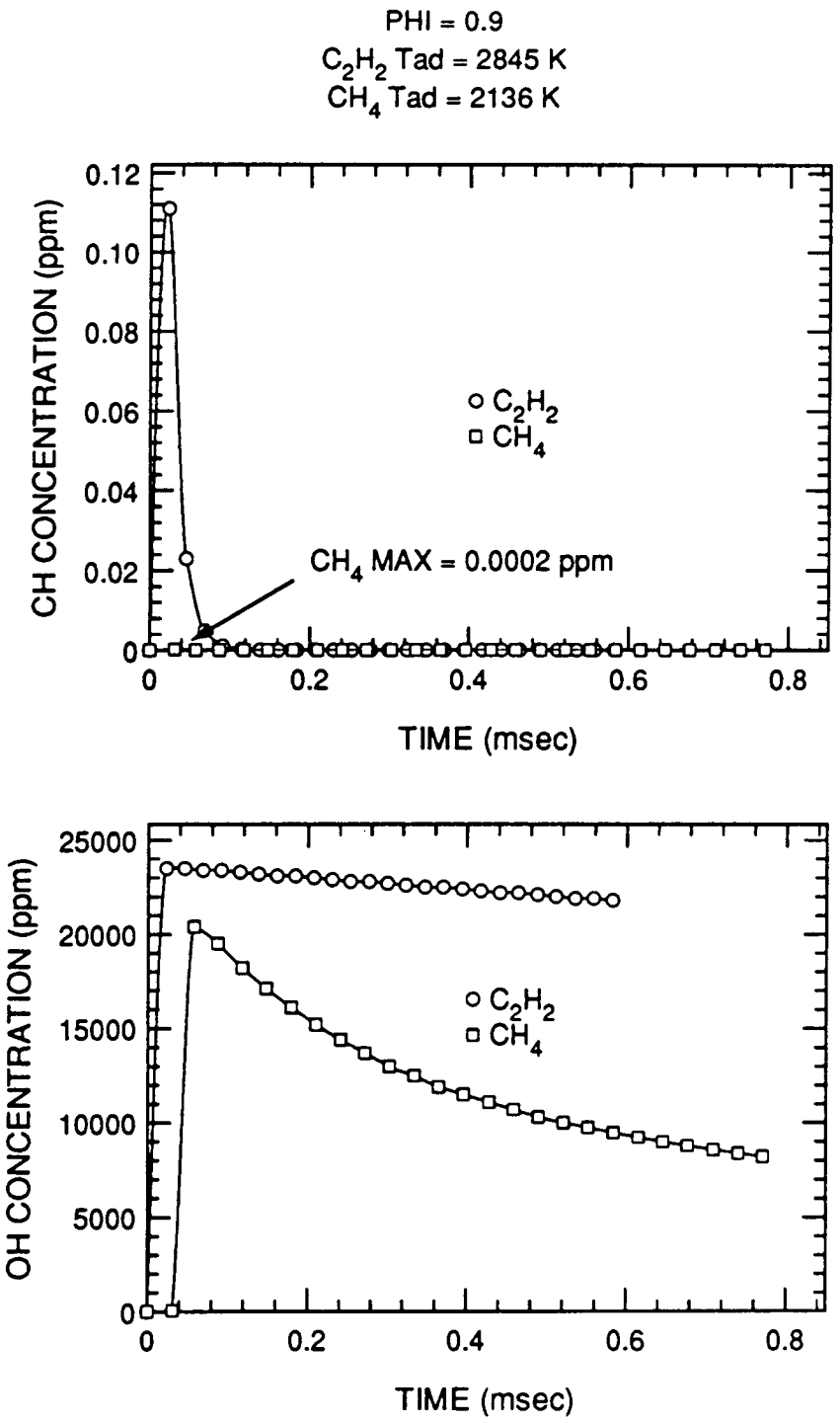

CHEMKIN OH and CH Concentrations Versus Time for Methane and Acetylene, PHI = 0.9.

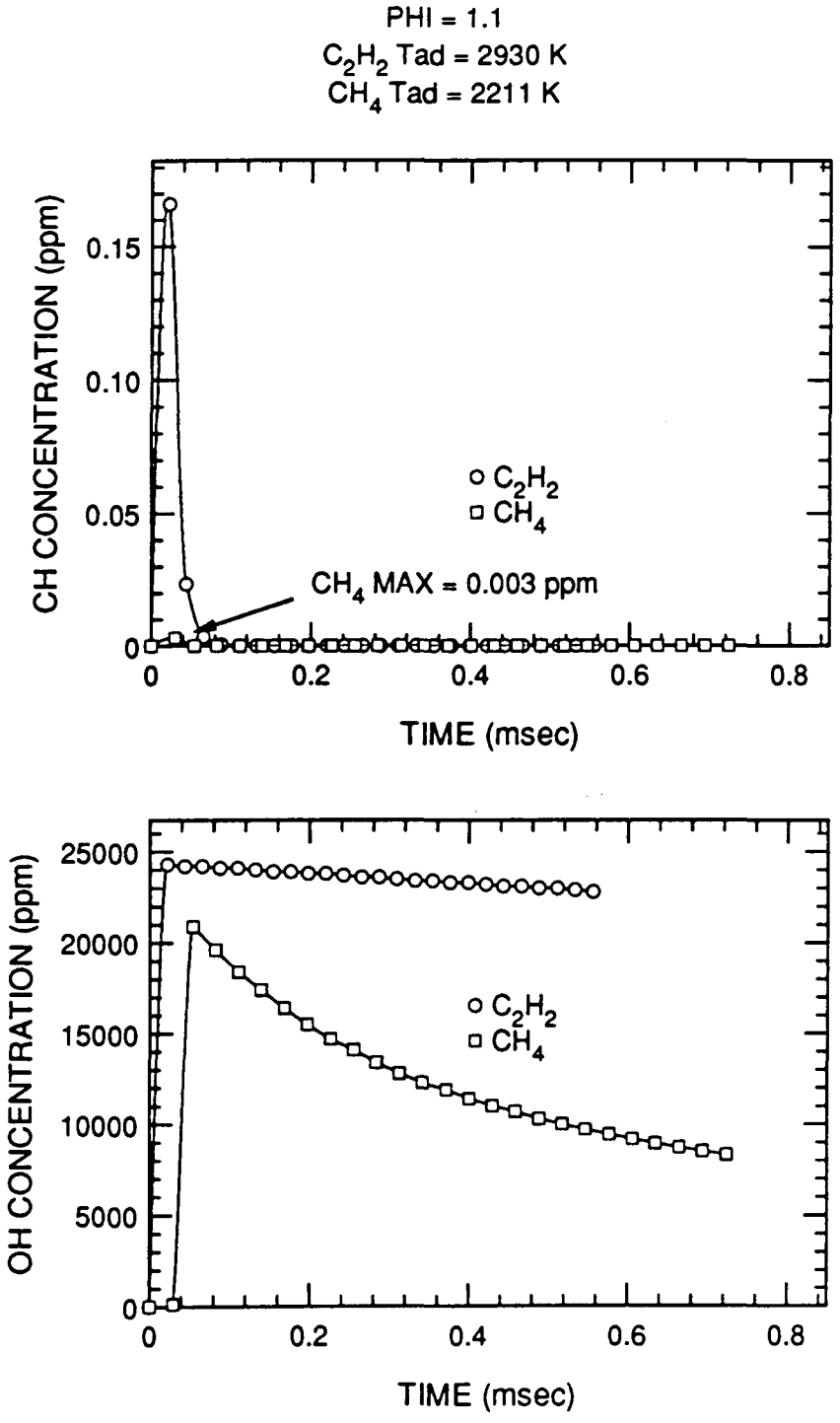

CHEMKIN OH and CH Concentrations Versus Time for Methane and Acetylene, PHI = 1.1.

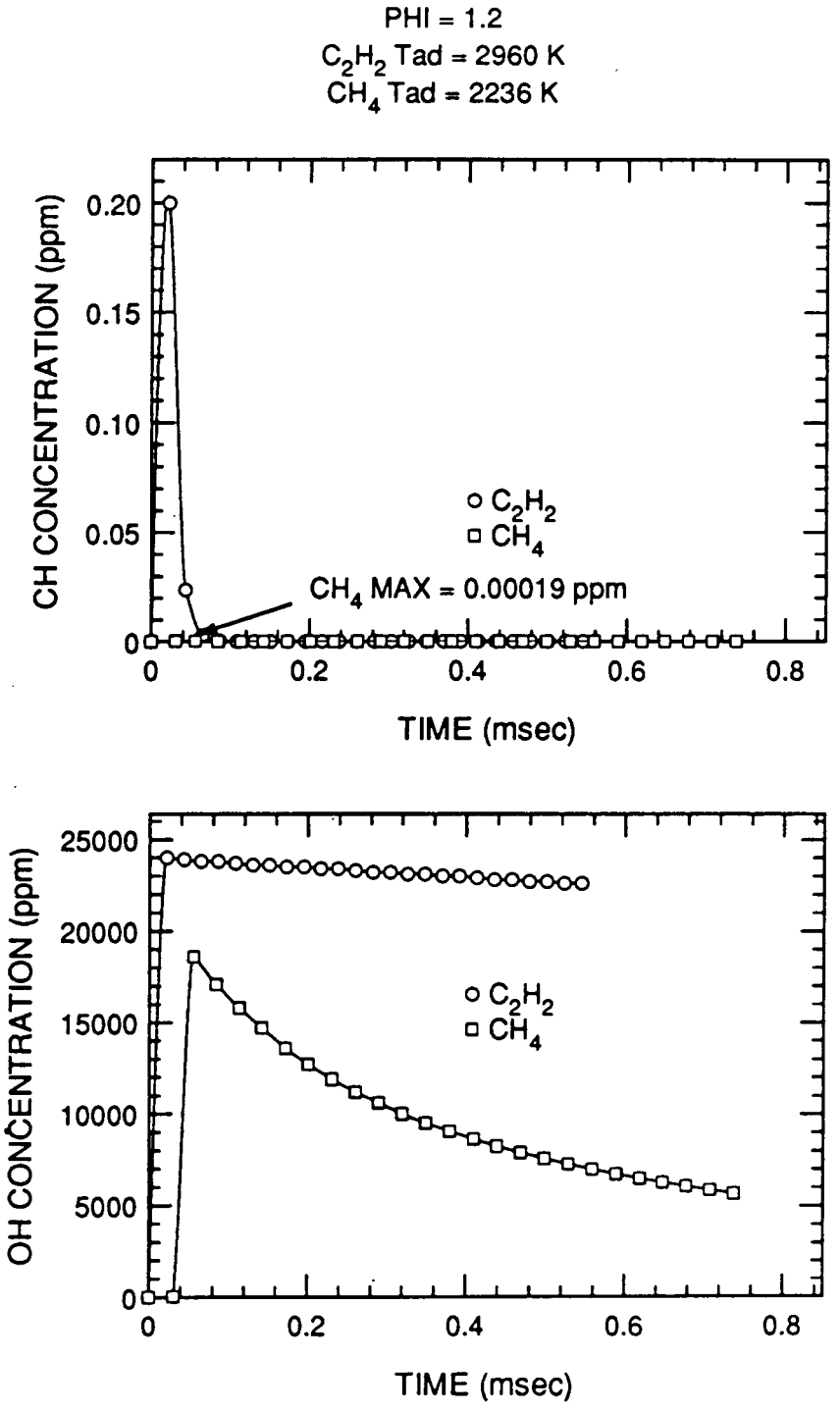

CHEMKIN OH and CH Concentrations Versus Time for Methane and Acetylene, PHI = 1.2.

The vita has been removed from the scanned document